J.M. CHEMPALATHRA

The Free Streamline Theory to a Right Angled Duct.

APPLICATION OF THE FREE STREAMLINE THEORY TO A RIGHT ANGLED DUCT

by

John Mohan Chempalathra

A thesis submitted to the FACULTY OF GRADUATE STUDIES and RESEARCH in partial fulfilment for the degree of MASTER OF ENGINEERING

Department of Civil Engineering
McGill University
Montreal Quebec

January 1971

© John Mohan Chempalathra 1971

APPLICATION OF THE FREE STREAMLINE THEORY TO A RIGHT ANGLED DUCT

by

John Mohan Chempalathra

A thesis submitted to the FACULTY OF GRADUATE STUDIES and RESEARCH in partial fulfilment for the degree of MASTER OF ENGINEERING

Department of Civil Engineering
McGill University
Montreal Quebec

January 1971

© John Mohan Chempalathra 1971

SUMMARY

On the assumptions of incompressible ideal fluid flow theory this work is directed towards investigating the design of a right-angled bend in a rectangular (or square) conduit incorporating one curved surface only (the 'intrados'). Experiments were conducted to ascertain the utility of guide vanes intended to prevent loss of energy due to separation and subsequent eddy formation. In the present instance, the boundary layer formation, as well as turbulence, was kept to a minimum by the use of a large constant level tank at the inlet to the test section. The uniform velocity distribution thus obtained was, however, modified in testing, and by the use of mesh, trapezoidal distributions simulating possible disturbances met with in practice were also investigated.

The design of the inner curved wall and internal guide vanes was carried out for the case in which both legs of the elbow have the same cross sectional area, viz., there is no change of section in the main duct before and after the bend. But the method of analysis is applicable to a whole family of possible designs depending on the values of x_o/b (x_o = horizontal projection of the inner curved wall, b = width of inlet).

The mathematical analysis for obtaining the shape of the internal guide vanes was verified by an electrical

analogy. Experimental investigations on the selected shape was carried out on a lucite conduit having a square inlet section. The measurement of head loss and velocity had been conducted with and without internal guide vanes and also with a sharp mitre bend, in order to evaluate the possible advantages of both the inside guide vanes and the inner curved wall.

For the uniform inlet velocity distribution, pressure measurements showed that with guide vanes the loss of head was reduced almost to zero under suitable conditions (after deducting skin friction losses) and the velocity measurements confirmed that the separation and eddy formation had diminished considerably with the introduction of guide vanes.

John Chempalathra
M.Eng.
Civil Engineering

ACKNOWLEDGEMENTS

The author is indebted to Professor G.D. Ransford for his guidance and advice throughout the course of this work.

The author also wishes to express his gratitude to Professors S.B. Savage and J. Nemec for their suggestions and comments in the course of setting up of the equipment. The author is grateful to Mr. G. Neveu for his assistance during the analysis of the problem and building of the apparatus.

Thanks are also due to Miss M. Solomon for careful typing of the manuscript. The work was supported by the National Research Council under Grant No. 245 - 57.

TABLE OF CONTENTS

Page No.

Page No.

LIST OF TABLES,PLATES AND FIGURES

LIST OF SYMBOLS

a	-	The breadth of the issuing jet at infinity
a_1, a_2, a_3	-	Indicates different guide vanes(Ref.fig.20).
A	-	Wetted area in the duct over which the frictional forces acts.
A_1, A_2	-	Area of cross section of the constant level tank at section (1) & (2) respectively in Fig.6
A', A''	-	Indicates different guide vanes (Refer fig.19).
b	-	The breadth of the test section at $A_\infty H_\infty$ in the z-plane, fig.9.
b_1, b_2	-	The breadth of the constant level tank at section (1) & (2) respectively in fig.6.
B	-	A constant, varies between 1.1 and 1.5
B_1	-	An arbitrary constant
c	-	The width from the extrados of the duct to the guide vane under consideration.
c'	-	Horizontal projection of the guide vane(fig.12).
C_c	-	Ratio of the contracted area to the fully expanded area of flow in the duct.
d	-	Diameter of circular pipe, or side of square pipe in the plane of bend.
D	-	Depth of rectangular duct in the plane of curvature.
ds	-	Differential length along the free stream line.
g	-	The acceleration due to gravity.
h_L	-	Estimated total loss.
ΔH	-	Head loss due to the bend.

LIST OF SYMBOLS(CONTINUED)

K	-	Head-loss coefficient. $K = \Delta H/(V_2^2/2g)$
K^*	-	A secondary flow parameter. $K^* = R_n(2d/R)^{\frac{1}{2}}$
ℓ	-	Length of the guide vane (Fig.16b).
L	-	Overall length of the surface subjected to laminar boundary layer.
m_1, m_2	-	Constants
n_1, n_2	-	Constants
p	-	Pressure
P_1, P_2	-	Perimeter of the constant level tank at section (1) & (2) respectively in fig.6.
q	-	Magnitude of the resultant velocity. $q=\sqrt{u^2+v^2}$
Q	-	$\log_e(V\ dz/dw)$
r	-	Radius of the semi-circle representing the complex line BF in fig.3.
r_1, r_2	-	Constants
R	-	Mean radius of curvature of the bend.
R_n	-	Reynolds number.
S_1, S_2	-	Constants.
t	-	An auxillary variable used in the analysis.
t'	-	Spacing between guide vanes(Refer fig.16).
u, v	-	The component of the velocity in the x and y directions respectively.
U'	-	The incoming and outflowing uniform velocity at infinity.
V	-	The constant velocity along the free streamline.

LIST OF SYMBOLS(CONTD.)

V_{*}, V_{**}	-	The velocity of water inside the constant level tank at section (1) & (2) respectively in fig.6.
V_1	-	The velocity in the contracted area.
V_2	-	Average velocity in the fully expanded area.
w	=	$\phi + i\psi$
w_i	-	The density of the manometer liquid.
w'	-	The density of the metered fluid.
x_o	-	The horizontal projection of the inner curved wall in fig.1(or $\int_G^E dx$)
x_*	-	The distance from the origin of the momentum thickness(or boundary layer thickness) to section (1) in fig.6.
x_{**}	-	The distance from the origin of the momentum thickness to section (2) in fig.6.
$x_1=x_4$	=	$(\lambda+1) + 2\cos\beta + (1-\lambda)\cos 2\beta$
$x_2=x_3$	=	$(1-\lambda) + 2\cos\beta + (1+\lambda)\cos 2\beta$
x_5	=	$(\lambda+1) - 2r\cos\beta + r^2(1-\lambda)\cos 2\beta$
x_6	=	$(\lambda+1)\cos 2\beta - 2r\cos\beta + r^2(1-\lambda)$
x_7	=	$(1-\lambda) - 2r\cos\beta + r^2(1+\lambda)\cos 2\beta$
x_8	=	$(1-\lambda)\cos 2\beta - 2r\cos\beta + r^2(1+\lambda)$
$y_1=-y_4$	=	$-2\sin\beta - (1-\lambda)\sin 2\beta$
$y_2=-y_3$	=	$2\sin\beta + (\lambda+1)\sin 2\beta$
y_5	=	$2r\sin\beta - r^2(1-\lambda)\sin 2\beta$

LIST OF SYMBOLS(CONTD.)

y_6	-	$(\lambda + 1)\sin\beta - 2r\sin\beta$
y_7	-	$2r\sin\beta - r^2(1 + \lambda)\sin 2\beta$
y_8	-	$(1 - \lambda)\sin 2\beta - 2r\sin\beta$
z	=	$x + iy$

GREEK SYMBOLS

α	-	Angle of impact of the streamline with the guide vane(Refer fig.16a)
β	-	Angle taken along the semi-circle representing the complex line BF(Refer fig.3)
γ	-	The specific gravity of the manometer liquid.
δ	-	Boundary layer thickness.
$\delta_2^{*}, \delta_2^{**}$	-	Momentum thickness at section (1) & (2) respectively in fig.6.
ζ	-	Reciprocal of the complex velocity. $\zeta = 1/\sigma$
θ	-	Inclination of the resultant velocity with the x-axis.
θ'	-	$(5\pi/2 - \theta)$
θ_i	-	Arc tan (y_i/x_i), $i = 1,2,3,\ldots.8$
λ	-	A dimensionless parameter in the analysis.
ν	-	Kinematic viscosity.
ξ	-	$\mathrm{Exp}(w\pi/aU)$
π	-	3.14159
ρ	-	The density.

LIST OF SYBOLS(CONTD.)

ρ_i	-	$\sqrt{x_i^2 + y_i^2}$, i = 1,2,3,.....8
σ	-	complex velocity. $\sigma = -dw/dz$
ϕ	-	velocity potential
ψ	-	stream function.

INTRODUCTION

Many two-dimensional flow patterns which include the formation or deflection of jets,flows over bends or steps or flows past cavities,involve separation of the fluid from the solid surface with a corresponding loss of energy with or without the occurrence of cavitation.Problems of this type are particularly difficult to analyze and predict when the distribution of the velocity of the incoming fluid is not uniform.

A bend in a pipe line causes local disturbance of the velocity distribution with a corresponding loss of mechanical energy.From momentum considerations,owing to the change in flow direction,there must be an increase in pressure(and hence a decrease in velocity) around the outside of the bend,or the extrados,and a decrease in pressure around the inside of the bend.

It may be of interest to know what happens and how head losses occur when a bend(the centre line of which is a circular arc) is introduced in a circular pipe with the usual type of non-uniform velocity distribution. As the flow enters such a bend,the inertia effect(so-called centrifugal forces) acting on the upstream velocity profile produces an oscillatory secondary flow,transverse to the main flow.After some oscillations in the transition region of the bend,the secondary flow is damped by viscosity and, if the bend is sufficiently long,fully developed curved flow is reached.In the outlet pipe of the bend the disturbances attenuate gradually over a distance of up to 50 pipe diameters.Hawthorne(Ref.23) has shown that fully developed curved flow is not established in most bends of practical interest.Large head losses occur when high energy fluid spreads from the centre to the wall of the pipe on account of the secondary flow.He states that the losses in the bend itself are probably least when the bend deflection does not exceed $B(\pi/2)\sqrt{d/R}$ radians, where R represents the mean radius of curvature of the bend,d the pipe diameter and B,a constant,varies between 1.1 and 1.5.This loss is a maximum in the outlet transition region when the bend deflection is once or 3 times the above value.The loss in the outlet transition region is a minimum when the bend deflection is twice the above value and fully developed curved flow has been established.

Owing to viscous effects,the inlet velocity will generally be non-uniform with zero velocity at the wall of the circular pipe.The inertia effects usually predominate over the viscous ones at the initial portion of the bend for most of the cross section.

In the bend transition region the secondary flow exhibits the characteristics of a damped vibration. For low Reynolds numbers,no oscillation occurs.At large

Reynolds numbers,the secondary flow is oscillatory and fully developed curved flow is never reached.Hence the flow enters the outlet transition region downstream from a bend at a phase of the damped oscillation depending both on the bend geometry and the inlet conditions.The possible conditions at the inlet to the downstream pipe are hence numerous and experimental results are difficult to interpret.

The major loss in a pipe bend is the increased viscous dissipation due to the large gradient of axial velocity created on the outer wall of the pipe when the high velocity fluid initially in the centre of the pipe is displaced outwards by the secondary flow.

The foregoing discussion has been concerned with bends in pipes of circular cross section.Analyzing bends following circular arcs in pipes of square or rectangular cross section,Cuming(1955) has stated that the dynamical parameter on which the secondary flow in a pipe of rectangular cross section depends is

$$K^* = R_n(2d/R)^{\frac{1}{2}} \qquad (1)$$

where d is the axis of the rectangle in the plane of the bend.R is the radius of curvature of the axis of the pipe and R_n is the Reynolds number based on the mean velocity and the dimension d. When the value of K^* is large,the viscous effects tend to become confined to a boundary layer on the wall of the pipe.

In a square pipe, the secondary velocity at the axis is more than twice the value in a circular pipe of diameter equal to the side of the square pipe. The comparison is made at flows giving the same pressure loss per unit length of straight pipe.

Squire and Winter (1951) have shown experimentally that in the case of a rectangular channel bent to the form of a circular arc, the secondary vorticity in a right angled bend can be easily three times the initial vorticity at right angles to the flow. Since large velocity gradients can occur near the wall of the duct, this explains the pronounced secondary flows which are frequently observed.

Several methods have been tried in the past to reduce this loss of energy, oscillatory flow and possibilities of cavitation damage at high velocities. The most recent line of approach has been to introduce a series of deflecting vanes in a simple mitre joint, and several empirical designs have been tried to get the maximum efficiency.

A theoretical approach to this type of problem was lacking until the development of the Helmholtz-Kirchhoff theory of free streamlines. The purpose of the present work is to investigate theoretically and experimentally the possibilities of solving this problem by adopting a suitable curve along the inner side of the bend with necessary guide vanes inside,all designed using the Kirchhoff theory of free streamlines.

For experimental purposes,the problem was was studied by allowing the water to flow through a lucite right angled duct having a square cross section with removable casing of the bend on the inner side, inclined at 45° to the horizontal.Guide vanes could be introduced or removed at will through this wall (Fig.7).A uniform velocity distribution at the inlet to the lucite bend was achieved by bolting it to a constant level tank having a funnel type bottom with a square opening at the end.With a constant outflow the velocity and head losses were measured before and after the bend with a sharp right angled mitre bend and also with the designed curved intrados with and without internal guide vanes.The experimental study was extended to two different trapezoidal velocity distributions(one with maximum along the intrados and one minimum) at the entrance to the bend.The flow follows the path of the streamlines and it was noted that in the absence of internal guide vanes, separation occurs from the curved intrados with eddies forming; this was reduced considerably by the introduction of internal guide vanes.Similarly,it was observed that the head losses and variation in velocity distribution were reduced appreciably.

In the theoretical study, the free streamline along which pressure and velocity were constant, was used for the determination of the profile of the curved intrados of the right angled duct.

The analysis of this problem is extended to the determination of the shape of the internal guide vanes also. The method consists of the definition of successive conformal transformations including a hodograph plane and the application of the Schwarz-Christoffel transformation. This type of transformation for the two-dimensional flow was amenable to the free streamline analysis, since the boundaries upstream and downstream from the constant pressure section were made of straight lines along which the direction of flow was constant.

2. DETAILS OF PREVIOUS INVESTIGATIONS

2.1. PREVIOUS STUDIES FOR MINIMIZING BEND LOSSES

Several investigations have previously been carried out with a view to reducing the loss of energy in bends, which really involves reduction in both the secondary flow and the separation effects, either through proper changes in the bend geometry or by introducing suitable deflecting vanes.

Such sets of vanes have been experimented and proposed by Kröber (Ref. 3) in particular for rectangular ducts (ventilation shafts for example). These may be computed like turbine cascades. The absolute values of pitch and depth (Fig. 16a) should be optimised considering the thrust on these vanes, Kröber gave the shape of practical profiles, obtained experimentally for angles of 90°, 60° and 45°. These profiles can be built out of thin metal sheets (Fig. 16b). The separation occurring on the inner curved wall for right angled bends may be reduced by using thick profiles (Fig. 17), made up of two metal sheets, but this adds of course to the difficulty of construction. Fig. 18 shows a design prepared by Rateau Pump Company, France.

The head-loss coefficient with Krober guide vanes (Ref. 3) is claimed to be as low as $0.15 \dfrac{V_2^2}{2g}$, whatever the bend angle may be, i.e., 45° or 90°, in turbulent flow conditions, providing that the vanes are very carefully built. In this formula, V_2 represents the average velocity in the fully expanded area, downstream of the bend. These vanes could be used for circular ducts but head losses would be greater owing to separation occurring at the junction of these vanes with the circular boundary.

Another method is to round off the inner corner with a radius R as large as possible. Such a design may also call for vanes like A' and A" in Fig.19. Still another method inspired by the slotted wing principle is to make use of a series of vanes like a_1, a_2, a_3 (Fig.20) of convenient shape and suitably placed with respect to each other(Ref.3). This is of course the approach studied in the present thesis.

Wirt (described in Ref.2) tried to reduce the intensity of the secondary flow* by increasing the width and decreasing the depth for different aspect ratios of a 90° bend in a rectangular duct of width b_2 and depth D in the plane of curvature and having a centre line radius R. The results obtained by him are described in Ref.2 and reproduced in the following table:

TABLE I

LOSS COEFFICIENTS FOR RECTANGULAR DUCTS

b_2/D	6	6	6	3	3	3
R/D	5/3	1	2/3	5/3	1	2/3
K	0.09	0.16	0.38	0.15	0.22	0.55

* Refer page 1

Here K is the head-loss coefficient and is defined as the ratio of the head loss to velocity head. The results show some success in lowering the intensity of the secondary flow and also it indicates that separation losses decreases as the curvature ratio increases.. This was used for circular cross section for quite sometime. Hofmann's results suitable for cases in which the inner surface is properly finished,as in pipes or tunnels,are described in Ref.2 and reproduced in fig.11 as functions of Reynolds number.

It was found later that far better results could be obtained by introducing a series of deflecting vanes(described in Ref.2) in a simple mitre bend (fig.13). For example,the head-loss coefficient K for a plain mitre bend was approximately 1.1 and that for a normal long radius elbow could be of the order of 0.5,in either case,a properly designed set of vanes could reduce K to as little as 0.15,and beyond the bend would restore the same velocity distribution across the section as in the incoming flow. Typical vanes used had short leading and trailing tangents as shown in fig.12.by the investigation of Wirt,Klein,Tupper and Green as described in Ref.2. The latter investigators found that vanes without tangents (fig.13) perform equally well.

2.2. DEVELOPMENT OF THE FREE STREAMLINE THEORY

During the period of over 100 years which has elapsed since the original development of the method of Helmholtz and Kirchhoff, numerous contributions to this theory have been made primarily by mathematicians. The concept of the discontinuous surface, or free streamline separating the flow into two regions and thus permitting more realistic analysis of flow situations, was introduced by Helmholtz (1868). The only prior classical theory was for flow which doubled back on the boundary in such a way as to give infinite velocities and negatively infinite pressures at the end of the channel (point A in Fig. 14a). Helmholtz's fundamental contribution was the concept of a free boundary which was defined in the kinematic, rather than in the geometric sense (Fig. 14b). He reasoned that the bounding streamline would separate from the solid boundary and that the free streamline thus formed could be characterized by a constant pressure and hence by a constant velocity. He visualized a quiescent wake of constant pressure and a velocity discontinuity at the free streamline. In 1869 his colleague, G. Kirchhoff, solved the problem of an efflux from an opening in an infinite reservoir having plane boundaries, and also that of the effect of a plate in an otherwise uniform field of flow extending to infinity in all directions. Lord Rayleigh (1876) systematized these results and extended free streamline analysis to the case of an inclined plate, found the value of 0.611 for the plane orifice contraction coefficient from

Kirchhoff's solution, and studied intersecting jets or currents. The approach employed by these pioneers was indirect, to the extent that they tried out various functions and adjusted constants until useful results were obtained.

Development of a direct method of solving any of a large class of free streamline flows awaited definition of the hodograph planes and certain complementary transformations. In 1884, Max Planck introduced the use of logarithmic hodographs in the solution of free streamline problems.

Considerable work has since been carried out on the extension and application of this type of analysis. A brief outline of some of the most important work is described below:- N.E. Joukowsky greatly extended Planck's indirect analysis technique in 1890, and worked on the theory of jets and wakes. His method allowed for the solution of problems with a large number of stagnation points and free surfaces.

J.H. Michell (1890) showed how to use the Schwarz-Christoffel transformation and the auxiliary t-plane between the logarithmic and complex potential planes. In his extension and formalization of Michell's method, A.E. Love (1891) indicated the limits of the flow field in the Q, ζ, w and t planes, using locations of important points along the real axis of the t-plane for identification. M. Rethy (1894) found solutions for a number of jet discharge cases in the style of Joukowski (i.e., without using the Schwarz-Christoffel transformation). T. Levi-Civita

(1901) indicated that free streamlines could start from rounded bodies as well as from sharp cornered ones. Further extension of the free streamline analysis was presented by A.G.Greenhill(1910).

R.von Mises (1917) studied extensive efflux problems. In 1920, G.Colonetti and Riabouchinsky studied the case of flow past inclined plates held perpendicularly to the middle of an infinite jet and flows past symmetric pairs of wedges at suitable angles. Later, A.Betz and E.Petersohn (1931) studied multiple orifices and grids. Lavrentieff, in 1938 simplified the theory of the uniqueness and qualitative behavior of free streamlines. Gurevich, in 1947 considered the problem of a two dimensional jet issuing from a vertical wall taking into account surface tension of the jet. Birkhoff and Zarantonello, in 1953 (Ref.18), made extensive studies of ideal steady flows moving under the influence of inertia, mainly the behavior liquid jets in air, cavities behind obstacles in high speed flows, cavitation behind cascades of airfoils, and also ideal plane flows with free boundaries past curved obstacles and gave a qualitative description of the geometry of free streamlines. The work of J.S.McNown and C.S.Yih (1953) represents a relatively recent contribution and includes a wide range of free streamline problems. Comparisons of the results of theory and of experiment indicate a correspondence which is usually close and sometimes astonishingly so.

3. FREE STREAMLINE THEORY

Many plane irrotational flow patterns which include the formation or deflection of jets can be analyzed completely by the Helmholtz - Kirchhoff theory of free streamlines. Patterns of flow through well streamlined bends have been found to be defined at least moderately well by potential flow theory. The particular type of transition to be considered herein was characterized by a constant pressure (and therefore by a constant magnitude of the velocity) around the curved portion of the boundary.

Consider a plane steady flow of an ideal, incompressible fluid. The equations of motion are:

$$u \frac{\partial u}{\partial x} + v \frac{\partial u}{\partial y} = \frac{-1}{\rho} \frac{\partial p}{\partial x} \tag{2}$$

$$u \frac{\partial v}{\partial x} + v \frac{\partial v}{\partial y} = \frac{-1}{\rho} \frac{\partial p}{\partial y} \tag{3}$$

where

u, v = Components of velocity in the x, y directions, respectively

ρ = the density

p = the pressure

g = the acceleration due to gravity.

The equation of continuity is:

$$\frac{\partial u}{\partial x} + \frac{\partial v}{\partial y} = 0 \tag{4}$$

Since the motion is irrotational, one can introduce a velocity potential ϕ, such that

$$u = \frac{\partial \phi}{\partial x} \quad , \quad v = \frac{\partial \phi}{\partial y} \tag{5}$$

The equation (4) reduces to

$$\frac{\partial^2 \phi}{\partial x^2} + \frac{\partial^2 \phi}{\partial y^2} = 0 \tag{6}$$

and the equations (2) and (3) can be integrated to give

$$\frac{p}{\rho} + \frac{1}{2}(u^2 + v^2) + gy = B_1 \tag{7}$$

where B_1 is an arbitrary constant.

In plane motion one can introduce a stream function ψ, such that

$$u = \frac{\partial \psi}{\partial y} \quad , \quad v = \frac{-\partial \psi}{\partial x} \tag{8}$$

From (5) and (8), one obtains

$$\left.\begin{aligned} \frac{\partial \phi}{\partial x} &= \frac{\partial \psi}{\partial y} \\ \frac{\partial \phi}{\partial y} &= \frac{-\partial \psi}{\partial x} \end{aligned}\right\} \tag{9}$$

These are the Cauchy-Riemann equations which indicate that the complex potential $w = \phi + i\psi$ is an analytic function of the complex variable $z = x + iy$, i.e.,

$$w = f(z) \tag{10}$$

Now

$$\sigma = \frac{1}{\zeta} = - \frac{dw}{dz} = - q\, e^{-i\theta} \qquad (11)$$

in which σ and ζ are the complex velocity and its reciprocal respectively. q,the magnitude of the resultant velocity, and θ its inclination measured from the x-axis.

Thus $$q = \sqrt{u^2 + v^2} \qquad \theta = \mathrm{Tan}^{-1} \frac{v}{u} \qquad (12)$$

3.1. <u>FIXED AND FREE BOUNDARIES</u>

The boundaries of a moving fluid may consist partly of free streamlines and partly of fixed rigid walls. A rigid wall acting as a boundary is of course a streamline along which ψ = constant, but it is not necessarily either an isobar or an isotachic line. The Kirchhoff theory can be applied to cases in which the rigid boundaries are straight, and which depend on the function

$$Q = \log(V \frac{dz}{dw}) \qquad (13)$$

where V represents the constant velocity along the free streamline. If to simplify the terminology, ζ is substituted for $-dz/dw$ the two kinds of hodographs commonly used are representations of ζ and of Q. The second is also expressible in the form

$$Q = \log (\frac{V}{q}) + i\, \theta \qquad (14)$$

Since the pressure is constant, the speed 'q' along a free streamline is constant and hence log(V/q) is constant. Along a straight rigid boundary the flow direction θ is constant since it follows the direction of the boundary.

Hence as a general rule, straight solid boundaries in the z-plane (Fig.9.) transform in to radial lines in the ζ-plane (U/V = constant) and into straight lines parallel to the real axis (θ = constant) in the Q-plane. Furthermore, free streamlines along which the pressure and velocity are constant in the z-plane, become circular arcs with centres at the origin ($u^2 + v^2$ = constant) in the ζ-plane and straight lines parallel to the imaginary axis (q = constant) in the Q-plane. It is thus evident that the original boundary transforms into either a circular sector or a rectangle. Hence when the boundary is transformed into the Q-plane, the diagram will be a polygon, the interior of which can be mapped by the Schwarz-Christoffel transformation on the upper half of the t-plane. A relation between Q and t can be obtained, i.e., between dw/dz and t.

Similarly, when the boundary is transformed into the w-plane, the diagram will consist of straight lines constituting a polygon, the interior of which can be mapped on the upper half of the t-plane. From this a relation between w and t can be obtained. If t is eliminated from the two relations, one obtains a relation between dw/dz and w, which on integration gives a relation between w and z, characterizing the motion. Alternatively, instead of eliminating t , w and z can be expressed in terms of t .

3.2. PROPERTIES OF FREE STREAMLINES

Along a free streamline the pressure is constant, and hence the speed of flow is too (Bernoulli's theorem). Also the stream function ψ is constant along a free streamline just as on any other streamline.

3.3. MAIN ASSUMPTIONS AND LIMITATIONS IN THE THEORY

(i) The influence of gravity is negligible.

(ii) The influence of viscous friction along solid boundaries is negligible.

(iii) The flow approaching the section has essentially a uniform velocity distribution, or, in practice that the non-uniformity of the velocity distribution is not significant.

The first assumption does not, of course, affect the flow pattern studied here, since the flow takes place in a closed conduit. As far as the third assumption was concerned, the shaping of the lower portion of the tank gives one a uniform velocity distribution. The problem was thus reduced to a two-dimensional potential flow problem to which classical hydrodynamics can be applied.

4. THEORETICAL DESIGN OF INTERNAL GUIDE VANES AND THE INNER CURVED WALL

4.1. GENERAL CONSIDERATIONS

A general analysis based on free streamline theory is described for determining the flow characteristics in a two dimensional pipe bend. Expressions for velocity and pressure at any point in the flow field are also obtained. The z-plane diagram represents (Fig. 9 .) the right angled duct, whose walls are $A_\infty BC_\infty$ and $H_\infty GFED_\infty$. The wall $H_\infty G$, is part of a streamline. The fluid flows along $H_\infty G$, turns at G and flows out of the duct along GED_∞. At the section $C_\infty D_\infty$, there is uniform parallel flow with velocity U say. Let the breadth $C_\infty D_\infty$ be 'a' and the flux out of the duct be aU.

If one takes $\psi=0$ on $A_\infty BC_\infty$, then $\psi=$ aU on the streamline $H_\infty FD_\infty$. Again one may also assume that $\phi = 0$ at B and F, which can always be arranged, since an arbitrary constant can be added to the velocity potential. Thus at $A_\infty H_\infty$, i.e., at all points in the tank at a great distance from BF, $\phi = +\infty$, while $\phi = -\infty$ at C_∞ , D_∞.

According to the principles explained in Chapter 3, the z-plane is transformed into the w-plane. The diagram obtained in the w-plane is a polygon having the boundary $H_\infty D_\infty C_\infty A_\infty$, having the vertices CD and AH at infinity. The interior of this polygon is next mapped on the upper half of the t-plane using the Schwarz-Christoffel transformation, making G and E correspond to $t = -1$ and $t = +1$ respectively. B and F are regarded as coincident at $t = 0$.

The following transformation relation is thus obtained:

$$\frac{dw}{dt} = \frac{r_1}{(t + \lambda)(t - \lambda)} \qquad (15)$$

λ represents a parameter, to be evaluated later and r_1 is a constant. The next step is to draw the polygon described by

$$Q = \log \left(V \frac{dz}{dw}\right)$$

$$= \log \left(\frac{V}{q}\right) + i\theta$$

In order to map this polygon on the t-plane, the plane showing

$$V \frac{dz}{dw} = -V\zeta \qquad (16)$$

is drawn. On the free streamline $q = V$ and therefore $-V\zeta = e^{i\theta}$. Therefore along GFED in the $-V\zeta$ plane (Fig.9.) $-V\zeta$ describes a quarter circle having a unit radius. Along HG one has $\theta = i\frac{\pi}{2}$, while q increases from 0 to V at G. Hence $-V\zeta$ changes to $e^{i\pi/2} = i$, at G. Again at the point E, $\theta = 0$ and $q = V$ and $-V\zeta = e^0 = 1$. Similarly, in the ζ-plane, one has

$$\zeta = -dz/dw = \frac{-1}{V} e^{Q} \qquad (17)$$

At the point E, $Q = 0$ and $\zeta = -1/V$ and at G, $Q = i\pi/2$ and $\zeta = -i/V$. The Q plane diagram is also similarly drawn. A polygon is obtained having a vertex B at infinity. Now this polygon is mapped on to the upper half of the t-plane by using the Schwarz-Christoffel transformation, and the following transformation relations are obtained:

$$\frac{dQ}{dt} = \frac{m_1}{i\sqrt{(1-t)(t+1)}} \quad \text{for } -1 < t < 1 \quad (18)$$

m_1 positive and real

$$\frac{dQ}{dt} = \frac{m_1}{\sqrt{(t-1)(t+1)}} \quad \text{for } t > 1 \quad (19)$$

$$\frac{dQ}{dt} = \frac{-m_1}{\sqrt{(t-1)(t+1)}} \quad \text{for } t < -1 \quad (20)$$

Since $Q = \log_e \left(V \frac{dz}{dw}\right)$

$$\frac{dz}{dw} = \frac{1}{V} \exp (Q) \quad (17)$$

Now the above equations are integrated and the constants evaluated.

From equation (15) $\frac{dw}{dt} = \frac{r_1}{(t+\lambda)(t-\lambda)}$ where r_1 is a constant.

Solving by partial fractions:

$$dw = r_1 \left\{ \frac{-1}{2\lambda\,(t+\lambda)} + \frac{1}{2\lambda\,(t-\lambda)} \right\} dt$$

$$\therefore \quad w = \frac{r_1}{2\lambda} \log_e \frac{(t-\lambda)}{(t+\lambda)} + S_1, \text{ where } S_1 \text{ is a constant.}$$

$$\left.\begin{array}{ll} \text{When } t = 0 & w = iaU \\ t = \infty & w \to 0 \end{array}\right\} \text{giving} \quad S_1 = 0, \; r_1 = \frac{2\lambda aU}{\pi}$$

Hence,

$$w = \frac{aU}{\pi} \log_e \frac{(t-\lambda)}{(t+\lambda)} \qquad (21)$$

$$\frac{dw}{dt} = \frac{aU}{\pi} \left(\frac{1}{(t-\lambda)} - \frac{1}{(t+\lambda)} \right)$$

$$= \frac{2\lambda aU}{\pi (t-\lambda) \; (t+\lambda)} \qquad (22)$$

From equation (21)

$$\frac{(t-\lambda)}{(t+\lambda)} = e^{w\pi/aU}$$

i.e.

$$\frac{2\lambda}{(t+\lambda)} = 1 - e^{w\pi/aU}$$

$$t = \lambda \left[\frac{1+\text{Exp}\,\frac{w\pi}{aU}}{1-\text{Exp}\,\frac{w\pi}{aU}} \right] \qquad (23)$$

Now equation (18) was integrated

$$Q = m_1 \log_e \left(2t + 2i \sqrt{(1-t)\,(t+1)}\right) + n_1$$

where n_1 is a constant

for $-1 \leqslant t \leqslant 1$ and t - complex.

This may be re-written as follows:

$$Q = 2m_1 \log_e \left(\sqrt{t+1} + i\sqrt{1-t} \right) + n_1 \qquad (24)$$

For $t > 1$

$$Q = m_1 \log_e \left(2t + 2\sqrt{(t-1)(t+1)} \right) + n_1 \qquad (25)$$

For $t < -1$

$$Q = m_1 \log_e \left| 2t - 2\sqrt{(t-1)(t+1)} \right| + n_1 \qquad (26)$$

Substituting the boundary conditions

$$Q = 0 \quad \text{for} \quad t = +1$$

and $$Q = i\pi/2 \quad \text{for} \quad t = -1$$

hence $$m_1 = \tfrac{1}{2}$$

$$n_1 = -\tfrac{1}{2} \log_e(2)$$

$$\therefore \; Q = \tfrac{1}{2} \log_e\left(t + i\sqrt{(1 - t)(t + 1)}\right) \qquad (27)$$

From equation (24), one obtains:

$$Q = \log_e \left[\frac{\sqrt{t + 1} + i\sqrt{1 - t}}{\sqrt{2}} \right] \qquad (28)$$

and

$$\frac{dQ}{dt} = \frac{1}{2\, i \sqrt{(1 - t)(1 + t)}} \qquad (29)$$

From equation (17)

$$\frac{dz}{dw} = \frac{1}{V} e^{Q}$$

$$= \frac{1}{V} \sqrt{t + i\sqrt{(1 - t)(t + 1)}} \qquad (30)$$

$$= \frac{1}{V\sqrt{2}} \left(\sqrt{t + 1} + i\sqrt{1 - t}\right) \qquad (31)$$

valid for t-complex or

$$-1 < t \text{ real} < 1$$

Determination of λ as a function of V/U

From the definition of ζ and Q,

For $t = +\lambda$

$$e^{Q} = V\frac{dz}{dw} = \frac{V}{U} \quad \text{and hence}$$

$$Q = \log_e \frac{V}{U} \tag{32}$$

Therefore:

$$\log_e \frac{V}{U} = 1/2 \log_e \left(\lambda + i\sqrt{(1-\lambda)(1+\lambda)}\right) \tag{33}$$

$$\therefore \frac{V}{U} = \left(\lambda + i\sqrt{(1-\lambda)(1+\lambda)}\right)^{1/2} \tag{34}$$

$$\left(\frac{V}{U}\right)^2 - \lambda = +\sqrt{\lambda^2 - 1}$$

$$\lambda = \frac{V^4 + U^4}{2V^2U^2} \tag{35}$$

or

$$\frac{V}{U} = \mathrm{Exp}\ (1/2 \operatorname{arcosh} \lambda) \tag{36}$$

and

$$(\lambda+1) = \frac{1}{2V^2U^2} (V^2 + U^2)^2 \tag{37}$$

$$(\lambda-1) = \frac{1}{2V^2U^2} (V^2 - U^2)^2 \tag{38}$$

Equation (30), together with equations (21), (23) and (35) constitute the solution of the problem. t could be eliminated from the above equations and the relation between w and z, obtained by integration.

4.2. THE SHAPE OF THE FREE STREAMLINE

From the projections of the length of the free streamline on the x-axis, for instance, one may find the precise location of point E with respect to B (or, alternatively, of G with respect to B, considering the y-axis) in fig.9. Thus, one of the major parameters of the bend was found.

The general observations were:

1. On a free streamline $Q = i\theta$ and $dz = ds.e^{i\theta}$, where ds is an element of the curve and θ is the inclination of the tangent.
2. Again, along a free streamline t is real, since it is mapped on the real axis of the t-plane.
3. If a point on the free streamline be designated as (x,y) then

$$dx/ds = \cos\theta \quad ; \quad dy/ds = \sin\theta \qquad (39)$$

4. Also $\left|V\, dz/dw\right| = e^{i\theta} = 1$

   Where V represents the constant speed along the free streamline.

   From the above, on a free streamline

$$1 = \left|V\, dz/dw\right| = \left|V\, e^{i\theta}\, \frac{ds}{dt}\, \frac{dt}{dw}\right|$$

$$= \pm \frac{ds}{dt} \left|V \frac{dt}{dw}\right| \qquad (40)$$

$\frac{ds}{dt}$ being negative.

the upper or lower sign being taken according as 's' increases with t or not. In the present problem, the origin in the z-plane was taken at F and the free streamline GE was considered. As one goes along that line from F in the z-plane to E, t increases from 0 to +1. Therefore, along FE, $\frac{ds}{dt}$ was positive, whereas, if one goes along FG, t decreases from 0 to -1, ds/dt was negative along FG.

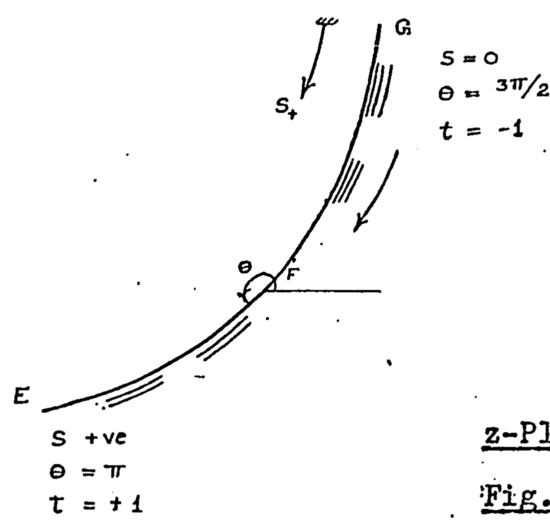

z-Plane

Fig.1

From equation (22), one has:

$$\frac{dt}{dw} = \frac{\pi(t-\lambda)\ (t+\lambda)}{2\lambda aU}$$

Substituting in equation (40)

$$1 = \frac{-\pi V\ (t-\lambda)\ (t+\lambda)}{2\lambda aU} \quad \frac{ds}{dt}$$

$$\therefore \quad \frac{ds}{dt} = \frac{-2\lambda aU}{V\pi} \quad \frac{1}{(t^2 - \lambda^2)} \qquad (41)$$

with the sign conventions shown.

And

$$Q = i\,\Theta - i\pi = \tfrac{1}{2} \text{ arc cos } t \tag{42}$$

from the property of the free streamline. Also this result could be deduced by integrating

$$\frac{dQ}{dt} = \frac{1}{2i\,\sqrt{(1-t)\,(t+1)}} \quad (\text{ for } -1 < t < 1, t \text{ real})$$

Hence

$$t = \cos 2\Theta$$

$$dt = -2 \sin 2\Theta \, d\Theta \tag{43}$$

Also

$$dx/ds = \cos\Theta \;; \quad dy/ds = \sin\Theta \tag{39}$$

Taking the projection GE on the x-axis

$$\int_G^E dx = \int_{3\pi/2}^{\pi} \cos\Theta \; \frac{-2\lambda a U}{\pi V} \; \frac{1 \quad d\Theta}{(\cos^2 2\Theta - \lambda^2)} (-2 \sin 2\Theta)$$

$$= \frac{-2\lambda a U}{V \pi} \int_0^{-1} \frac{4u^2 \, du}{4u^4 - 4u^2 - (\lambda^2 - 1)} \tag{44}$$

where $u = \cos\Theta$

$du = -\sin\Theta \, d\Theta$

$$\frac{-\pi V}{2\lambda a U} \int_G^E dx = \left(1 - \frac{1}{\lambda}\right) \frac{1}{\sqrt{2}\,(\sqrt{\lambda} - 1)} \text{ arc tan } \frac{\sqrt{2}\,u}{\sqrt{\lambda} - 1} \Bigg|_0^{-1}$$

$$- \left(1 + \frac{1}{\lambda}\right) \frac{1}{2\sqrt{2}\;(\sqrt{\lambda} + 1)} \log_e \frac{\sqrt{\lambda+1} + \sqrt{2}\,u}{\sqrt{\lambda+1} - \sqrt{2}\,u} \Bigg|_0^{-1} \tag{45}$$

$$\frac{\pi V}{2\lambda a U} \int_E^G dx = \frac{\sqrt{\lambda - 1}}{\sqrt{2}\,\lambda} \quad \text{arc tan } \frac{\sqrt{2} \cos\Theta}{\sqrt{\lambda - 1}} \Bigg|_{3\pi/2}^{\pi}$$

$$- \frac{\sqrt{\lambda + 1}}{2\sqrt{2}\,\lambda} \log_e \frac{\sqrt{\lambda + 1} \quad + \sqrt{2} \cos \theta}{\sqrt{\lambda + 1} \quad - \sqrt{2} \cos \theta} \Bigg|_{3\pi/2}^{\pi} \qquad (46)$$

Evidently, as

$$\lambda \rightarrow 1 \qquad (V \rightarrow U) \qquad \int_G^E dx \rightarrow \infty$$

$$\lambda \rightarrow \infty \qquad (V \rightarrow \infty) \qquad \int_G^E dx \rightarrow 0$$

The position of F in the middle of the curve is found by putting $\cos \theta = 5\pi/4$ in the upper limit. The expression for $\int_G dy$ is, of course, similar to that for $\int_G dx$, except that $\cos \theta$ replaces $\sin \theta$.

The value of λ is obtained from equation (45) by putting $x_o = a$, giving the V/U ratio for the desired geometry, where x_o represents $\int_G^E dx$.

Hence

$$x_o = \frac{2 \lambda a U}{\pi V} \left[\frac{\sqrt{\lambda + 1}}{2\sqrt{2}\lambda} \log_e \frac{\sqrt{\lambda + 1} \quad + \sqrt{2}}{\sqrt{\lambda + 1} \quad - \sqrt{2}} \right.$$

$$\left. - \frac{\sqrt{\lambda - 1}}{\lambda\sqrt{2}} \arctan \frac{\sqrt{2}}{\sqrt{\lambda - 1}} \right] \qquad (47)$$

with

$$\frac{V}{U} = \frac{\sqrt{\lambda + 1} \quad + \sqrt{\lambda - 1}}{\sqrt{2}} \qquad \text{from equation (33)}$$

hence

$$\frac{\sqrt{\lambda+1}+\sqrt{\lambda-1}}{\sqrt{2}} = \frac{2\lambda}{\pi}\left[\frac{\sqrt{\lambda+1}}{2\sqrt{2}\,\lambda}\log_e\left\{\frac{\sqrt{\lambda+1}+\sqrt{2}}{\sqrt{\lambda+1}-\sqrt{2}}\right\} - \frac{\sqrt{\lambda-1}}{\sqrt{2}\,\lambda}\arctan\frac{\sqrt{2}}{\sqrt{\lambda-1}}\right] \qquad (48)$$

Solving the above expression, one gets the value of $\lambda = 1.099$. The computer programme is shown in Appendix 1.

The x co-ordinate of the free streamline is obtained from equation (41) by substituting the values of $\frac{V}{U}$ and λ for different values of θ between π and $^{3\pi}/_{2}$. Similarly, the y-co-ordinate of the free streamline is obtained by replacing Cos θ by Sin θ and substituting different values for θ, between $^{3\pi}/_{2}$ and π. The shape of the inner curved wall obtained is plotted in figure 21.

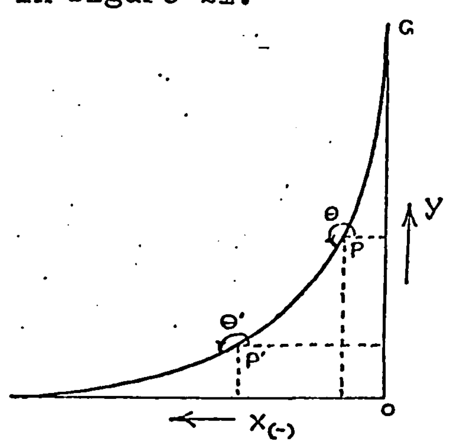

Figure 2

Of course, the value of y can be found by symmetry.

$\therefore y_{(+)} = -x_{(-)}$ for point with $\theta' = \frac{5\pi}{2} - \theta$ with θ as shown above. $(\pi < \theta < {}^{3\pi}/_{2})$.

4.3. FORM OF THE STREAMLINES AND EQUIPOTENTIALS

This involves the integration of dz along a complex plane.

First $\int_B^F$ dz will be evaluated.

as $t = \lambda \left[\dfrac{(1+\exp^{w\pi}/aU)}{(1-\exp^{w\pi}/aU)} \right]$ from equation (23).

$$(t+1) = \frac{(\lambda+1) + (\lambda-1) \quad e^{w\pi/aU}}{(1 - e^{w\pi/aU})} \qquad (49)$$

$$(t-1) = \frac{(\lambda-1) + (\lambda+1) \quad e^{w\pi/aU}}{(1 - e^{w\pi/aU})} \qquad (50)$$

$$\frac{dz}{dw} = \frac{1}{V} \exp (Q) \qquad (17)$$

$$= \frac{1}{V} \sqrt{t + i \sqrt{(1-t)(t+1)}} \qquad (30)$$

$$= \frac{1}{V} \left[\frac{\sqrt{t+1} + i\sqrt{(1-t)}}{\sqrt{2}} \right] \qquad (31)$$

Substituting the values of t, (t+1) and (t-1) etc., one obtains

$$\frac{dz}{dw} = \frac{1}{\sqrt{2}\, V} \left\{ \sqrt{\frac{(\lambda+1) + (\lambda-1) \; e^{w\pi/aU}}{1 - e^{w\pi/aU}}} + i \sqrt{- \frac{(\lambda-1) + (\lambda+1) e^{w\pi/aU}}{1 - e^{w\pi/aU}}} \right\}$$

(51)

As one moves from B to F, the function $e^{w\pi/aU}$ varies as $(\cos\theta + i \sin\theta)$ with θ ranging from 0 to π. The above equation was integrated by putting

$$\zeta = e^{w\pi/aU} \tag{52}$$

$$d\zeta = \frac{\pi}{aU}\,\zeta\;dw \tag{53}$$

$$\frac{dz}{dw} = \frac{dz}{d\zeta}\;\frac{d\zeta}{dw}$$

$$= \frac{dz}{d\zeta}\;\frac{\pi\zeta}{aU} \tag{54}$$

therefore,

$$\frac{dz}{d\zeta} = \frac{aU}{\pi\zeta}\;\frac{1}{\sqrt{2}\,V}\left\{\sqrt{\frac{(\lambda+1)\;+\;(\lambda-1)\zeta}{(1-\zeta)}}\right.$$

$$\left. + \, i\sqrt{\frac{-(\lambda-1)\;-\;(\lambda+1)\zeta}{(1-\zeta)}}\right\} \tag{55}$$

Multiplying the numerator and the denominator by the numerator, one obtains

$$\frac{dz}{d\zeta} = \frac{aU}{\pi V\sqrt{2}}\left\{\frac{(\lambda+1)\;+\;(\lambda-1)\zeta}{\zeta\sqrt{(1-\zeta)}\;\left[(\lambda+1)+(\lambda-1)\zeta\right]}\right.$$

$$\left. + \, i\;\frac{-(\lambda-1)\;-\;(\lambda+1)\zeta}{\zeta\sqrt{(1-\zeta)}\;\left[-(\lambda-1)-(\lambda+1)\zeta\right]}\right\} \tag{56}$$

4.4. THE SHAPE OF THE INTERNAL STREAMLINES

One has to integrate the above expression, for ζ varying from -1 to $-e^{-i\beta}$ to get the point along the line BF and also from $\zeta = -e^{-i\beta}$ to $= -\gamma e^{-i\beta}$, for the case $r > 1$ and r real to get the x and y co-ordinates of the internal streamlines.

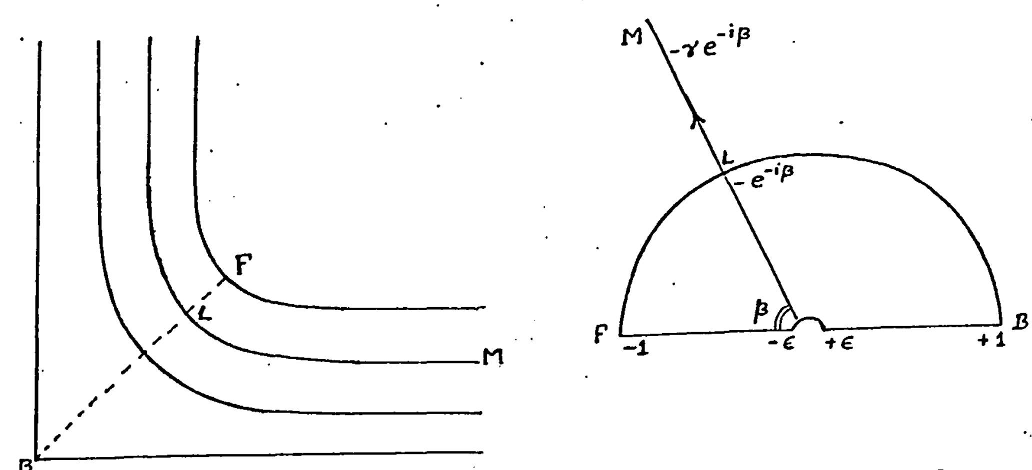

Fig.3

Numerical integration of equation (56) for the range of ζ from -1 to $-e^{-i\beta}$ yields (as per appendix 3 part I)

$$\int dz = \frac{aU}{\sqrt{2}\,\pi V}\Bigg[-(\lambda+1)\left\{ i\int_0^\beta \frac{\cos(\theta_1/2)}{\rho_1^{1/2}}\,d\beta + \int_0^\beta \frac{\sin(\theta_1/2)}{\rho_1^{1/2}}\,d\beta \right\}$$

$$+ (\lambda-1)\left\{ i\int_0^\beta \frac{\cos(\theta_2/2)}{\rho_2^{1/2}}\,d\beta + \int_0^\beta \frac{\sin(\theta_2/2)}{\rho_2^{1/2}}\,d\beta \right\}$$

$$+ (\lambda-1)\left\{ -\int_0^\beta \frac{\cos(\theta_3/2)}{\rho_3^{1/2}}\,d\beta + i\int_0^\beta \frac{\sin(\theta_3/2)}{\rho_3^{1/2}}\,d\beta \right\}$$

$$+ (\lambda+1)\left\{ \int_0^\beta \frac{\cos(\theta_4/2)}{\rho_4^{1/2}}\,d\beta - i\int_0^\beta \frac{\sin(\theta_4/2)}{\rho_4^{1/2}}\,d\beta \right\}\Bigg] \qquad (57)$$

INNER CURVED WALL ALONE

VISUALIZATION OF FLOW BREAKAWAY USING CONDENSED MILK

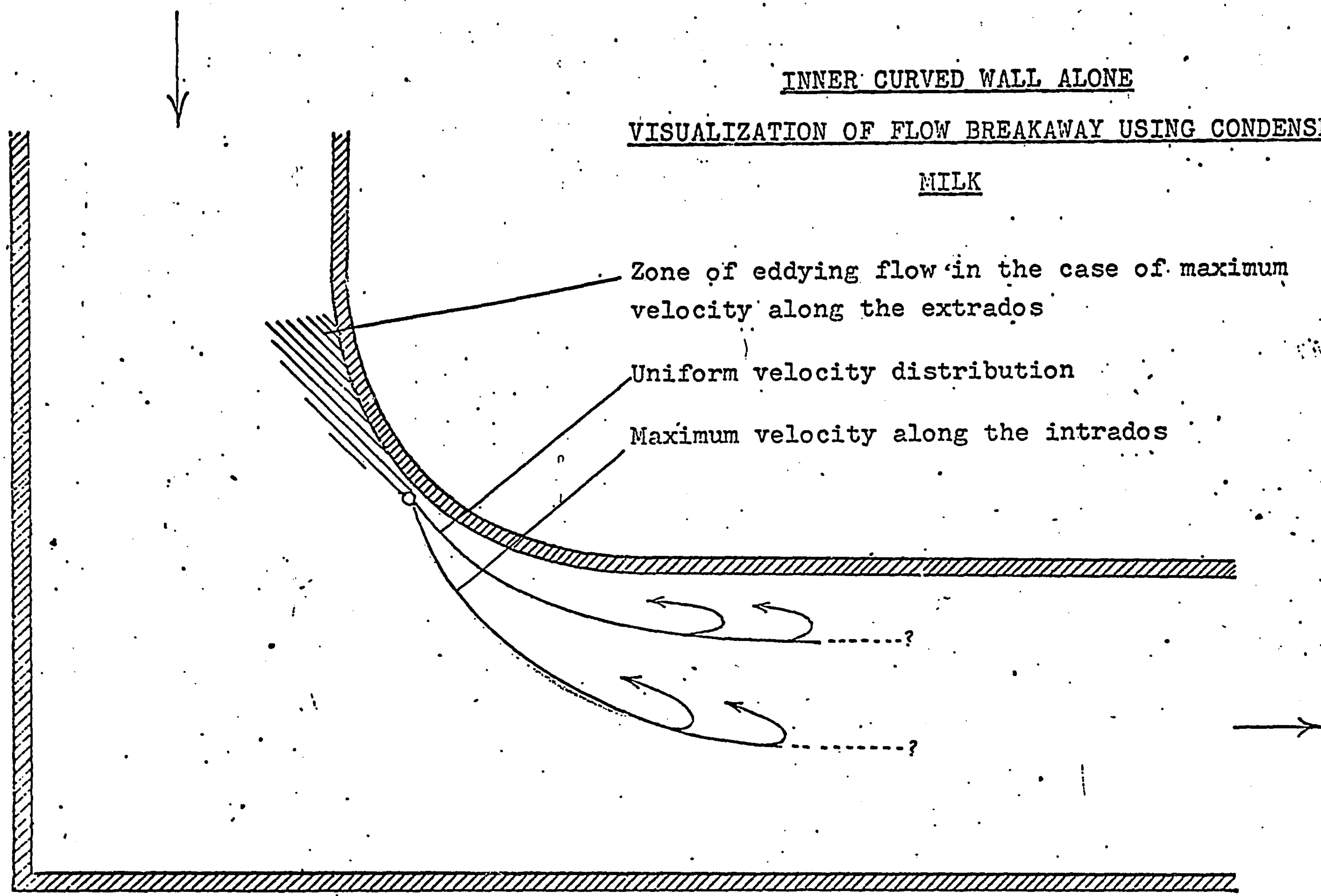

Fig. 24.

$$y_2 = -y_3 = 2 \sin\beta + (1+\lambda) \sin 2\beta \tag{67}$$

$$y_5 = 2r \sin\beta - r^2(1-\lambda) \sin 2\beta \tag{68}$$

$$y_6 = (\lambda+1) \sin 2\beta - 2r \sin 2\beta \tag{69}$$

$$y_7 = 2r \sin\beta - r^2(1+\lambda) \sin 2\beta \tag{70}$$

$$y_8 = (1-\lambda) \sin 2\beta - 2r \sin\beta \tag{71}$$

From the definition of $\mathfrak{z}$

$$\mathfrak{z} = -r\, e^{-i\beta} \tag{72}$$

$$= -r \cos\beta + ir \sin\beta$$

$$= e^{w\pi/aU}$$

$$= e^{(\phi + i\psi)\,\pi/aU} \tag{73}$$

$$-r\,(\cos\beta - i \sin\beta) = e^{\frac{\phi\pi}{aU}} \left[\cos\frac{\psi\pi}{aU} + i \sin\frac{\psi\pi}{aU} \right] \tag{74}$$

Hence $$r = e^{\frac{\phi\pi}{aU}} \tag{75}$$

The mirror image of the real diagram was taken for computations. Hence

$$r = e^{-\phi\pi/aU} \tag{76}$$

$$-\cos\beta = \cos\frac{\psi\pi}{aU} \tag{77}$$

$$\sin\beta = \sin\frac{\psi\pi}{aU} \tag{78}$$

$$y_2 = -y_3 = 2 \operatorname{Sin} \beta + (1+\lambda) \operatorname{Sin} 2\beta \tag{67}$$

$$y_5 = 2r \operatorname{Sin}\beta - r^2(1-\lambda) \operatorname{Sin} 2\beta \tag{68}$$

$$y_6 = (\lambda+1) \operatorname{Sin} 2\beta - 2r \operatorname{Sin} 2\beta \tag{69}$$

$$y_7 = 2r \operatorname{Sin}\beta - r^2(1+\lambda) \operatorname{Sin} 2\beta \tag{70}$$

$$y_8 = (1-\lambda) \operatorname{Sin} 2\beta - 2r \operatorname{Sin}\beta \tag{71}$$

From the definition of $\mathfrak{z}$

$$\mathfrak{z} = -r\, e^{-i\beta} \tag{72}$$

$$= -r \operatorname{Cos}\beta + ir \operatorname{Sin}\beta$$

$$= e^{w\pi/aU}$$

$$= e^{(\phi + i\psi)\pi/aU} \tag{73}$$

$$-r\,(\operatorname{Cos}\beta - i \operatorname{Sin}\beta) = e^{\frac{\phi\pi}{aU}} \left[\operatorname{Cos} \frac{\psi\pi}{aU} + i \operatorname{Sin} \frac{\psi\pi}{aU} \right] \tag{74}$$

Hence $$r = e^{\frac{\phi\pi}{aU}} \tag{75}$$

The mirror image of the real diagram was taken for computations. Hence

$$r = e^{-\phi\pi/aU} \tag{76}$$

$$-\operatorname{Cos}\beta = \operatorname{Cos} \frac{\psi\pi}{aU} \tag{77}$$

$$\operatorname{Sin}\beta = \operatorname{Sin} \frac{\psi\pi}{aU} \tag{78}$$

$$\pi - \beta = \frac{\psi\pi}{aU} \tag{79}$$

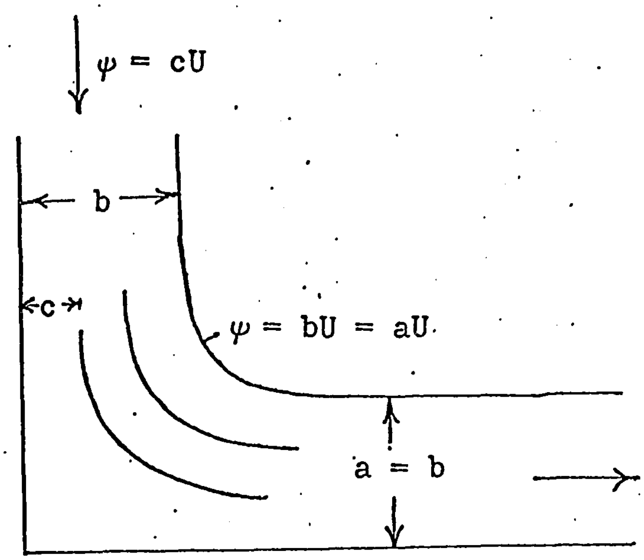

Figure 4

for,
$$\psi = cU$$

$$\pi - \beta = \frac{c}{a}\pi$$

$$\beta = \pi(1 - c/a) \tag{80}$$

Hence, suppose one wants a guide vane at 1/3 point, c/a = 2/3, taking the vane nearest the curved boundary. Hence $\beta = \pi/3$. Similarly for other guide vanes.

The integration was done by using Simpson's rule. The computer programme is shown in Appendix 1 and 2, and the results were tabulated in tables 4 - 9. The shape of the inner curved wall and internal guide vanes at $\frac{1}{4}$, $\frac{1}{2}$ and 3/4 positions have been plotted in figure (22), for values of $\beta = 45^\circ, 90^\circ$, and 135° respectively. The shape of the internal streamlines were checked by electrical analogy and excellent agreement was found.

5. FREE STREAMLINE ANALYSIS OF RIGHT ANGLED MITRE BENDS

5.1 GENERAL CONSIDERATIONS

The sudden deflection of flow produced by a mitre bend in a pipe line causes separation of the fluid from the solid boundary at the inner edge of the bend. The resulting contraction and subsequent expansion of the flow downstream from the bend produce a dissipation of energy which is primarily attributable to eddy diffusion. As a first approximation to this loss,one may endeavor to use the well known Borda formula

$$h_L = \frac{(V_1 - V_2)^2}{2g} \qquad (81)$$

or in dimensionless form

$$\frac{h_L}{V_2^2/2g} = \left(\frac{1}{C_c} - 1\right)^2 \qquad (82)$$

Here, h_L represents the loss in head, $V_2^2/2g$ and $V_1^2/2g$, respectively represent the velocity head in the pipe in the fully expanded area and the contracted area. C_c denotes the ratio of the contracted area to the area of the pipe. A schematic representation of the flow is shown in fig.15.

Determination of the velocity measurements before and after the bend suffices for an estimate of the head loss and also a check on the direct measurement of pressure difference.

In this chapter, a theoretical study has been described to determine to what degree the contraction coefficient of the mitre bend in a pipeline can be approximated to by an analysis of its free streamline counterpart.

5.2. THEORETICAL

The free streamline flow is bounded by 3 semi-infinite planes, the remainder of the boundary of flow being a curved surface of separation upon which a constant pressure is presumed to act. The planes $A_\infty B$ and BC_∞ form the outer boundary intersecting at the deflection angle of 90^o at the point B (Fig. 10). The inner solid boundary $F_\infty E$ is parallel to BA_∞ and separated from it by a distance 'b'. The free surface ED_∞ is a curve and becomes parallel to BC_∞ asymptotically, the ultimate thickness of the jet being 'a'. Since the pressure is assumed to be constant along the free surface, it follows that the velocity along the surface varies in direction only. The method of analysis is quite similar to that outlined in Chapter 4, and hence only a resumé is given here.

The flow pattern is first transformed to the ordinary hodograph by the basic relationship

$$\zeta = -dz/dw = \frac{-1}{q} e^{i\theta} \qquad (11)$$

Since the velocity along the free streamline has the constant magnitude V, ED_∞ appears as a circular arc in the ζ-plane and the solid boundaries become radial lines. The z-plane is plotted on the w-plane and the diagram in the w-plane is a polygon having the vertices CD and AF at infinity. The interior of this polygon is transformed on the upper half of the t-plane using the Schwarz-Christoffel transformation making CD and AF correspond to $t = +1$ and $t = +\lambda$, with B and E coincident at $t = 0$. The following transformation relation is obtained:

$$\frac{dw}{dt} = \frac{m_2}{(t-1)\ (t-\lambda)} \quad \text{, where } m_2 \text{ is a constant} \tag{83}$$

Similarly, the polygon described by $Q = \log_e \left(V \frac{dz}{dw}\right) = \text{Log}\ \frac{V}{q} + i\theta$ is drawn, having the vertex B at infinity. Now this polygon is plotted on the upper half of the t-plane using the Schwarz-Christoffel transformation giving the following relation:

$$\frac{dQ}{dt} = \frac{r_2}{\sqrt{t}\ (t-1)} \quad \text{, where } r_2 \text{ is a constant} \tag{84}$$

r_2 is positive for $t > 1$ (for t real)

$$\frac{dQ}{dt} = \frac{-ir_2}{\sqrt{t}\ (1-t)} \qquad 0 < t < 1 \tag{85}$$

$$\frac{dQ}{dt} = \frac{-r_2}{\sqrt{t}\ (1-t)} \qquad t < 0,\ t \text{ real} \tag{86}$$

$$\left(- \frac{ir_2}{\sqrt{t}\ (1-t)} = \frac{-ir_2}{i\sqrt{-t}\ (1-t)} \right)$$

Since $Q = \log_e \left(V \frac{dz}{dw} \right)$

$$\frac{dz}{dw} = \frac{1}{V}\ \text{Exp}\ (Q) \tag{13}$$

5.2.1. SOLUTION OF THE DIFFERENTIAL EQUATIONS AND DETERMINATION OF THE CONSTANTS

From equation (83)

$$dw = \frac{m_2 \, dt}{(t-1)\,(t-\lambda)}$$

Solving by partial fractions

$$w = \frac{m_2}{(1-\lambda)} \log_e \frac{(t-1)}{(t-\lambda)} + n_2 \text{ , where } n_2 \text{ is a constant} \qquad (87)$$

$$dw = m_2 \left[\frac{1}{(1-\lambda)(t-1)} - \frac{1}{(1-\lambda)(t-\lambda)} \right] dt \qquad (88)$$

Now where $t = o$, $w = iaV$

$$\therefore \; iaV = \frac{m_2}{(1-\lambda)} \log_e (i\pi) - \frac{m_2}{(1-\lambda)} \log_e (-\lambda) + n_2 \qquad (89)$$

When $t > o$, the imaginary part of $(w) = 0$

and the imaginary part $(n_2) = 0$

Therefore, $$m_2 = \frac{(1-\lambda)}{\pi} aV$$

and $$n_2 = \frac{aV}{\pi} \log_e (-\lambda) \qquad (90)$$

$$\frac{dw}{dt} = \frac{aV}{\pi} \frac{(1-\lambda)}{(t-1)(t-\lambda)} \qquad (91)$$

Now integrating equation (84)

$$\frac{dQ}{dt} = \frac{-ir_2}{\sqrt{t(1-t)}}$$

$$= \frac{-ir_2}{\sqrt{\frac{1}{4} - (\frac{1}{2}-t)^2}} \qquad (92)$$

$$\therefore Q = r_2 \log_e \left\{ (t-\tfrac{1}{2}) + i\sqrt{\tfrac{1}{4} - (\tfrac{1}{2}-t)^2} \right\} + S_2 \qquad (93)$$

where S_2 is a constant.

For $t = 1$ $\quad Q = o$

$t = 0$ $\quad Q = \frac{i\pi}{2}$

It follows, therefore, that

$$Q = \tfrac{1}{2} \log_e \left[(2t-1) + 2i\sqrt{t(1-t)} \right] \qquad (94)$$

for $o < t < 1$ $\qquad$ t real, and t complex

$Q = \frac{1}{2} \log_e \left(2t - 1 + 2\sqrt{t(t-1)} \right)$ for t real, $t > 1$

$$= \log_e \left\{ \sqrt{t} + \sqrt{t-1} \right\} \qquad (95)$$

and $\quad Q = \frac{1}{2} \log_e \left[1 - 2t + 2\sqrt{t(t-1)} \right] + \frac{i\pi}{2}$ $\qquad (96)$

for t real, $t < o$

The value of λ may now be obtained in terms of 'a' and 'b'.

$$Q = \log_e (-V\delta) \longrightarrow \log_e \left(i\frac{b}{a}\right)$$

$$= \log_e \left(\frac{b}{a}\right) + \frac{i\pi}{2} \qquad \text{for } t = \lambda \qquad (97)$$

Hence, $\log_e \frac{b}{a} = \frac{1}{2} \log_e \left(1 - 2\lambda + 2\sqrt{\lambda(\lambda-1)}\right)$, $t < o$, t real

$$\frac{b}{a} = \left\{ \sqrt{1-\lambda} + \sqrt{-\lambda+1} \right\} \qquad (98)$$

Finally, it is found that

$$-\lambda = +\frac{(b^2 - a^2)^2}{4a^2b^2} \tag{99}$$

$$-\lambda + 1 = \frac{(b^2 + a^2)^2}{4a^2b^2} \tag{100}$$

<u>Free streamline</u>

On the free streamline ($o < t < 1$) $Q = i\theta$, with the sign convention shown

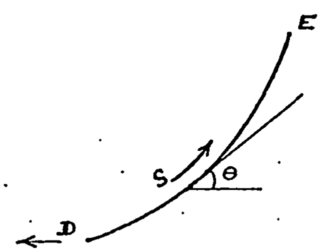

<u>Fig. 5</u>

also $\frac{dy}{ds} = \sin\theta \qquad \frac{dx}{ds} = \cos\theta$

On the streamline

$$1 = \left| V \frac{dz}{dw} \right| = \left| V \frac{e^{i\theta}\, ds}{dt} \frac{dt}{dw} \right| \tag{40}$$

hence,

$$\frac{ds}{dt} = \frac{a}{\pi} \frac{(1-\lambda)}{(t-1)(t-\lambda)} \tag{101}$$

($\frac{ds}{dt}$ is actually negative with the sign convention for s.)

On the other hand

$$Q = \tfrac{1}{2} \log_e \left[(2t-1) + 2i\sqrt{t(1-t)} \right] \tag{94}$$

$$= \tfrac{1}{2}\, i \,\text{arc cos}\, (2t-1)$$

$$= i\theta \tag{102}$$

Whence

$$(2t-1) = \cos 2\theta$$

$$t = \cos^2\theta$$

$$(1-t) = \sin^2\theta$$

$$dt = -\sin 2\theta \, d\theta \tag{103}$$

5.2.2 <u>DETERMINATION OF THE COEFFICIENT OF CONTRACTION</u>

$$\int_D^E dy = \int_{t=1}^{t=o} \frac{dy}{ds} \frac{ds}{dt} \left(\frac{dt}{d\theta} d\theta \right) \tag{104}$$

$$= \int_{\theta=0}^{\theta=\pi/2} \sin\theta \left\{ \frac{a}{\pi} \frac{(1-\lambda)}{(\cos^2\theta-1)(\cos^2\theta-\lambda)} (-\sin 2\theta) \right\} d\theta \tag{105}$$

$$= \int_0^{\pi/2} \frac{2a(1-\lambda)}{\pi} \frac{\cos\theta}{(\cos^2\theta-\lambda)} d\theta \tag{106}$$

$$= a \frac{\sqrt{1-\lambda}}{\pi} \log_e \frac{\sqrt{1-\lambda} + \sin\theta}{\sqrt{1-\lambda} - \sin\theta} \Bigg|_0^{\pi/2} \tag{107}$$

$$= \frac{a}{\pi} \sqrt{1-\lambda} \log_e \frac{\sqrt{1-\lambda} + 1}{\sqrt{1-\lambda} - 1} \tag{108}$$

$$= \frac{a}{\pi} \frac{(b^2+a^2)}{2ab} \log_e \left[\frac{\frac{(b^2+a^2)}{2ab} + 1}{\frac{(b^2+a^2)}{2ab} - 1} \right] \tag{109}$$

$$= \frac{(b^2 + a^2)}{\pi b} \log_e \frac{(b + a)}{(b - a)} \tag{110}$$

The coefficient of contraction is given by

$$\frac{a}{\left\{ a + \frac{(b^2 + a^2)}{\pi b} \log_e \frac{(b + a)}{(b - a)} \right\}}$$

In practice, for any given geometry, i.e., for b and

$\left(a + \frac{(b^2 + a^2)}{\pi b} \log_e \frac{b + a}{b - a} \right)$ known, 'a' must be determined numerically.

For the case of a right-angled duct

$$b = a + \frac{(b^2 + a^2)}{\pi b} \log_e \frac{(b + a)}{(b - a)} \qquad (111)$$

and hence

$\frac{b}{a} = 1.9$ (or the coefficient of contraction is 0.526.)

It may be of interest to note the important limiting case of $b \rightarrow \infty$

$$\ln \frac{b + a}{b - a} \simeq \ln \left(1 + \frac{2a}{b} \right) \longrightarrow \frac{2a}{b} \qquad (112)$$

$$\frac{b^2 + a^2}{\pi b} \ln \frac{b + a}{b - a} \rightarrow \frac{b}{\pi} \frac{2a}{b} = \frac{2a}{\pi} \qquad (113)$$

The contraction coefficient is therefore equal to

$$\frac{a}{a + \frac{2}{\pi} a} = \frac{\pi}{\pi + 2} \qquad (114)$$

as is well known.

5.2.3. EXPRESSIONS FOR THE STREAMLINES AND EQUIPOTENTIALS

In general

$$Q = \tfrac{1}{2} \log_e \left[(2t-1) + 2i\sqrt{t(1-t)}\right]$$

$$= \log_e \left(\sqrt{t} + i\sqrt{1-t}\right) \qquad (94)$$

$$\frac{dz}{dw} = \frac{1}{V}\,\mathrm{Exp}(Q)$$

$$= \frac{1}{V}\left\{\sqrt{t} + i\sqrt{1-t}\right\} \qquad (115)$$

On the other hand

$$\mathrm{Exp}\left(\frac{w\pi}{aV}\right) = \frac{(t-1)}{(t-\lambda)}(-\lambda) \qquad (116)$$

$$t = \frac{1 + \exp(w\pi/aV)}{1 - \dfrac{\exp(w\pi/aV)}{(-\lambda)}} \qquad (117)$$

Writing $\mathfrak{z} = \mathrm{Exp}(w\pi/aV)$ for simplicity's sake and $d\mathfrak{z} = \frac{\pi}{aV}\mathfrak{z}\,dw$,

One has

$$\frac{dz}{d\mathfrak{z}} = \frac{a}{\pi\mathfrak{z}}\left\{\sqrt{\frac{1+\mathfrak{z}}{1-\frac{\mathfrak{z}}{-\lambda}}} + i\sqrt{\frac{1}{-\lambda}+1}\;\sqrt{\frac{-\mathfrak{z}}{1-\frac{\mathfrak{z}}{-\lambda}}}\right\} \qquad (118)$$

whence

$$\frac{\pi}{a}\int dz = -\log_e\left[\frac{\sqrt{(1-\mathfrak{z})(1-\frac{\mathfrak{z}}{-\lambda})}+1}{\mathfrak{z}} + \frac{(1-\frac{1}{-\lambda})}{2}\right]$$

$$+ \frac{1}{\sqrt{\frac{1}{-\lambda}}}\arcsin\left[\frac{2(\frac{1}{-\lambda})\mathfrak{z} - (1-\frac{1}{-\lambda})}{(1+\frac{1}{-\lambda})}\right]$$

$$+ i\sqrt{-\lambda}\sqrt{\frac{1}{-\lambda}+1}\;\log_e\left[-\mathfrak{z} + \frac{(-\lambda)}{2} + \sqrt{\mathfrak{z}^2-(-\lambda)\mathfrak{z}}\right]$$

$$+ \text{constant} \qquad (119)$$

After slight simplification

$$\frac{\pi}{a}\int dz = -\log_e\left[\frac{\sqrt{(1+\zeta)(-\lambda-\zeta)}+\sqrt{-\lambda}}{\zeta\sqrt{-\lambda}} + \frac{(-\lambda)-1}{2(-\lambda)}\right]$$

$$+\sqrt{-\lambda}\ \text{arc sin}\left[\frac{2\zeta+1-(-\lambda)}{(-\lambda)+1}\right]$$

$$+ i\sqrt{(1-\lambda)}\ \log_e\left[-\zeta+\frac{(-\lambda)}{2}+\sqrt{\zeta^2-(-\lambda)\zeta}\right]$$

$$+ \text{constant} \qquad (120)$$

If B is chosen as the origin of the (x,y) co-ordinate system, the constant of integration may be determined by putting

$$w = \frac{aV}{\pi}\log_e(-\lambda) \quad \text{and} \qquad (121)$$

hence $\zeta = -\lambda$, the appropriate value at B

$$\text{Constant} = \log_e\frac{(\lambda-1)}{2\lambda} - \frac{\pi}{2}\sqrt{-\lambda} - i\sqrt{1-\lambda}\ \log_e\frac{\lambda}{2}$$

$$= \log_e\left[\frac{1+(-\lambda)}{2(-\lambda)} - \frac{\pi}{2}\sqrt{-\lambda}\right]$$

$$- i\sqrt{1-\lambda}\ \log_e\frac{(-\lambda)}{2} + \pi\sqrt{1-\lambda} \qquad (122)$$

---

6. EXPERIMENTAL PROCEDURE

6.1. DESCRIPTION OF THE EQUIPMENT USED

The experiments were performed in a lucite right-angled elbow having a 12" square cross-section at the inlet, the inner part of the bend being housed within a 45^{o} removable casing for introducing and removing the guide vanes. The layout is shown in Fig. 7 .

The lucite duct was supported on two I-sections welded together which in turn could be jacked up or down for fixing or removing the lucite bend. The jacks were supported on a concrete platform made to suit the requirements. A platform was constructed around the upper part of the tank (Fig. 7) for operation of the supply line and also for access inside the tank.

The lucite test elbow was bolted to a constant level tank which provided a constant head of 14'0" above the base of the test section. A constant level was maintained by a long overflow weir running around the upper edge of the tank. The flow from the weir went through an outlet pipe which led the surplus water to the sump. The lower part of the tank was designed so as to get a square velocity distribution and also minimum turbulence at the opening of the duct. An aluminum frame was built to cover the corners of the lucite bend, so as to prevent the lucite joints from separating under pressure. The tail end of the lucite duct was connected to a cast-iron reducer pipe which in turn was connected to two cast-iron valves on the outlet pipe. One of the valves served the purpose of keeping the flow adjusted to any desired value and the other one was a shut-off valve.

To reduce turbulence inside the test section to the lowest possible value, the main supply to the tank passed through a perforated barrel filled with a filter material.

The inner curved wall and internal guide vanes were made by moulding thin fibreglass supports to the shape of the computed streamlines. Aluminum plates 1/16" thick were fixed to these fibreglass supports, which were fixed in turn to thin lucite plates cut to suitable shapes in order to facilitate fixing of the guide vanes at the proper location inside the lucite bend (Plate 13). The right-angle mitre bend was constructed by fixing two plates of lucite at 90° at the proper location. The velocity measurements were done by dye injections (Fig. 8). Two liquids, one of specific gravity greater than water and one less, were mixed together and proportioned in such a way as to give a mixture of specific gravity equal to that of water, so that drops of the mixture, when injected in water, would follow the precise motion of water particles. The liquids used were dibutyl phthalate (Specific gravity 1.047) and petrolium ether (specific gravity 0.68) both insoluble in water; they mix quite well and do not cause damage to lucite by crazing.

When the tank was full of water and flowing at a constant discharge, the dye was allowed to fall freely through a glass tube 8" above the beginning of the bend at the central axis of the test section. The head of supply of dye was kept only slightly greater than that of water level in the tank, so that the velocity of injection relative to the main flow was low. The supply of dye to the test section was regulated by a valve, so as to get small droplets. A thin black metal plate ruled with a grid of lines painted bright yellow was fixed inside the lucite bend vertically close to the glass tube, which supplied the dye, so that measurements were not affected by parallax. The plate was illuminated from the sides. An identical plate was fixed in the horizontal portion of the lucite duct at the central axis adjacent to the tail end of the bend with similar facilities for dye injection.

The travel distance was measured by photography. A black disc having a V-shaped opening was attached to a steel rod revolving at a constant speed by a motor (Fig. 8.). The speed of revolution was reduced to 4 revolutions/second by a belt and speed reducer. A revolution counter was also attached to measure the exact time of travel of the droplets with the help of a stopwatch. A camera supported on a stand was fixed behind the disc and positioned in such a way that it could take pictures of the illuminated plate and the droplets, when the V-shaped opening of the disc passed in front of the shutter.

The experimental part of this work was rendered difficult for a variety of reasons. Since the lucite walls of the test section suffered deflection beyond permissible limits even under low heads, operation under a high head necessitated putting additional frames all around the duct. Since good visibility through the duct was a necessity for the experiments, either glass or lucite had to be used for construction of this bend, but both have their own serious disadvantages. Water-proofing the duct was a difficult task. Also since part of the duct had to be removable, in order to facilitate fixing of the guide vanes, it proved difficult to make the duct watertight under the operating head. Hence each setup involved considerable labour and time. After each set of tests (3 or 4 runs) it became essential to refurbish the lucite joints, since they tended to separate under high pressure. Fixing the lucite duct to the reducer pipe at the outlet was much more difficult than would appear, owing to both the heavy weight of the reducer pipe and the considerable difficulty in making the joint watertight.

Obtaining successive positions of the droplets in the same photograph involved considerable effort and time, by experimenting various trials. Each experimental run therefore required lengthy preparation and this restricted the actual number of experiments that could be carried out. Further tests that could have been carried out would include trying the effect of various lengths of the guide vanes, and possibly a different number of guide vanes instead of 3 used here, and also various discharges through the duct instead of only one used here.

6.2. MEASUREMENT OF VELOCITY

When the tank was full of water, the regulating valve was opened to get a constant maximum possible discharge. The opening was kept constant throughout all tests, and it was such that the surplus water from the weir was kept to a minimum. Next, the dye was allowed to fall in droplets. Since it had a specific gravity equal to that of water, each droplet followed the pattern of the streamlines. The disc was set in rotation at constant speed and the camera shutter was opened while the particular droplet in view passed the boundaries of the grid on the illuminated plate. Hence, in the same photograph, successive well-defined positions of the droplets were obtained along with the relevant portion of the illuminated grid - this enabled the travel distance of the droplet to be measured quite accurately within a limited interval of time. Several specimen photographs are shown in Plates 5-7. The travel time was obtained from the revolution counter of the rotating disc with the help of a stop watch, by noting the number of revolutions for a specific interval of time. The distance between successive positions of the droplet in the photograph represents one revolution, which could be measured accurately by comparing with the lines on the grid. Hence one obtains the velocity of the dye droplets, i.e., the velocity of the water particles at that particular location. By moving the inlet of the dye to different positions on the centreline of the test section, the velocities of the water particles upstream from the bend across a horizontal section of the test rig (Fig. 7) were obtained. Similarly, the velocity distribution was obtained downstream from the bend at another section. In the experiments, the velocity measurements were conducted at 8" before and after the bend down the middle of the test section. The droplets of dye were injected at 2", 4", 6", 8" and 10" from the side walls at the extrados or intrados. The ruled plate for measuring the travel distance was kept at a distance of $1\frac{1}{2}$" behind the place of injection of the dye, so as to prevent the dye gliding along the plate and also keeping the droplets away from the boundary layer of the plate. One may assume that no appreciable wake existed behind the vanes. This enables one to measure the velocity without disturbing effects. From the plot of the velocity distribution, the discharge could be estimated (unfortunately, laboratory facilities did not allow the discharge to be measured directly).

In subsequent tests, the square velocity distribution at the entrance to the lucite duct was modified by introducing a wire mesh, with layers of mesh increasing as uniformly as possible from one side to the other. With the help of the mesh, two more types of velocity distribution were introduced, one with maximum velocity and another with minimum velocity along the intrados. The velocity distribution obtained for different cases have been plotted (figures 26-34).

6.3. HEAD-LOSS MEASUREMENTS

Since the difference in pressures before and after the bend was small, a differential manometer was set up using a liquid having a specific gravity slightly greater than that of water (dibutyl phthalate, specific gravity 1.047) so as to give an amplified difference in level. The difference in pressures between points before and after the bend was measured on all the four central points of the sides. (Refer page 62).

The measurement of head-loss was carried out for the three different types of velocity distribution, and the readings obtained have been tabulated in Tables 2-3.

7. DISCUSSION OF EXPERIMENTAL RESULTS AND COMPARISON WITH THE THEORY

The main purpose of the experiments was to study the efficiency of internal guide vanes and the inner-curved wall in reducing head losses, for three different velocity distributions at the inlet. Even though the theory holds only for uniform velocity distribution, the merits of the internal guide vanes and the inner-curved bend were checked for all three velocity conditions.

(a) Uniform Velocity Distribution at Inlet

In the case of a sharp right-angled mitre bend, by injecting a mixture of condensed milk and water on the side of the lucite duct at the corner of the right angle, it was noted that the free streamline reaches as low as the centre line of the horizontal leg of the test section, leaving the upper half of the conduit downstream from the bend in eddying motion (fig.25). Replacing the mitre bend with the inner-curved wall designed for constant velocity and pressure, it was noted that droplets of condensed milk follows a spiralling path, as in the above case, leaving the top 20% of the conduit just downstream of the elbow bend in eddying motion. Separation from the solid surface occurred over a height of $2\frac{1}{4}$" only, compared with about 6" for the mitre bend (figure 23-25). With separation, a concentrated jet was formed along the extrados of the duct, with an accompanying loss of energy due to eddying motion. With guide vanes, separation and eddy formation were repressed completely in all intents and purposes. The velocity measurements by injecting the dye droplets in the horizontal portion of the bend in all three cases substantiated the above observations. With the right-angled mitre bend in position, a head-loss coefficient of the order of 0.52 was found. This was reduced to 0.47 when the inner-curved wall was substituted for the mitre bend. When the internal guide vanes were also introduced along with the inner curved wall, the head-loss coefficient was reduced to a very much lower figure of 0.04.

(b) Trapezoidal Velocity Distributions at the Inlet

With the maximum velocity along the extrados, it was observed that for all three cases, viz., with the right-angled mitre bend, with the inner-curved wall alone, and also with internal guide vanes, the droplets of condensed milk injected on the inner side of the bend moved back upstream and most of the horizontal portion of the test section was affected by eddying. The velocity measurements also gave evidence of this. The inner-curved wall, when compared with the mitre bend, helped to reduce the head-loss coefficient considerably (from 3.3 to 2.3). The use of the internal guide vanes further helped to reduce the head-loss coefficient from 2.3 to 1.5; this figure is, however, substantially higher than that achieved for a uniform velocity at the inlet.

With the maximum velocity along the intrados, it was observed in all three cases that the upper half of the horizontal test section was in turbulent motion and there was swirling of the fluid particles intermittently, which was also evidenced by the path taken by the dye droplets. It was noted that the incoming water separated from the solid boundary at approximately the midpoint of the inner-curved wall (or, of course, at the corner of the right angle in the case of the mitre bend) and issued as a sharp jet through the bottom of the horizontal portion, leaving the area above in eddying motion. This was also clear from the condensed milk test (figures 23,24 & 25). The pressure tests indicated that the inner-curved wall showed surprising efficiency in reducing the head-loss coefficient (from 2.1 to 0.64). But the internal guide vanes showed only a marginal improvement (0.64 to 0.57). The results shown on figures(23-25) indicate that in the case of uniform inlet velocity distribution (the only case for which the theory holds), the internal guide vanes were effective in reducing the separation and uniformizing the velocity after the bend. In other cases, particularly with high velocities at the intrados, the guide vanes did not conserve the original distribution past the bend.

It is quite possible that, in spite of every effort to prevent turbulence inside the test section, some turbulence did in fact subsist. Photographs of the streamline pattern throughout the duct would have helped to investigate flow conditions, but this could not be done owing to the necessity of having the large frame at the middle of the bend. Improved results would no doubt have been obtained if the experiments had been conducted with air, because no such frame would have been required. It should be noted that the results of downstream points were improved considerably with the curved intrados, and still better with the internal guide vanes, With the mitre bend in position the velocity at the downstream points could not be measured accurately owing to the irregular paths taken by the droplets. These measurements were introduced here particularly to illustrate the efficiency of the curved intrados and internal guide vanes. It would have been better to measure the velocities in the lateral locations to verify that the flow was in fact two-dimensional. However, owing to considerable difficulties and time involved in the experiments, the work is limited to its present form.

It seems reasonable at this point to show that the boundary layer is in fact laminar inside the test section. In the present experiments, a laminar boundary layer starts forming in theory from the top water level of the constant level tank and grows approximately to a thickness* of 3.5" at a horizontal

---

* The laminar boundary layer thickness is given by the well known formula $\delta \simeq 4.91 \sqrt{\frac{\nu x_*}{U_o}} = 4.91 \sqrt{\frac{10^{-5} \times 7}{0.01}} = 3.5''$

section, just before the converging funnel is reached at the bottom. A major parameter associated with the boundary layer is the momentum thickness, which at this section is

$$\begin{aligned} \delta_2^* &= 0.664 \sqrt{\frac{\nu x_*}{V_*}} \quad \text{(laminar case)} \\ &= 0.664 \sqrt{\frac{10^{-5} \times 7}{0.01}} \quad \text{feet} \\ &= 0.666'' \end{aligned} \tag{123}$$

where x_* = The distance from the top water level to section(1) where the momentum thickness or boundary layer thickness is measured.

V_* = The velocity inside the tank at section (1).

Owing to the funnel shape, the flow accelerates (the velocity increases from 0.01 to 0.38 ft/sec.) at the inlet of the test section.

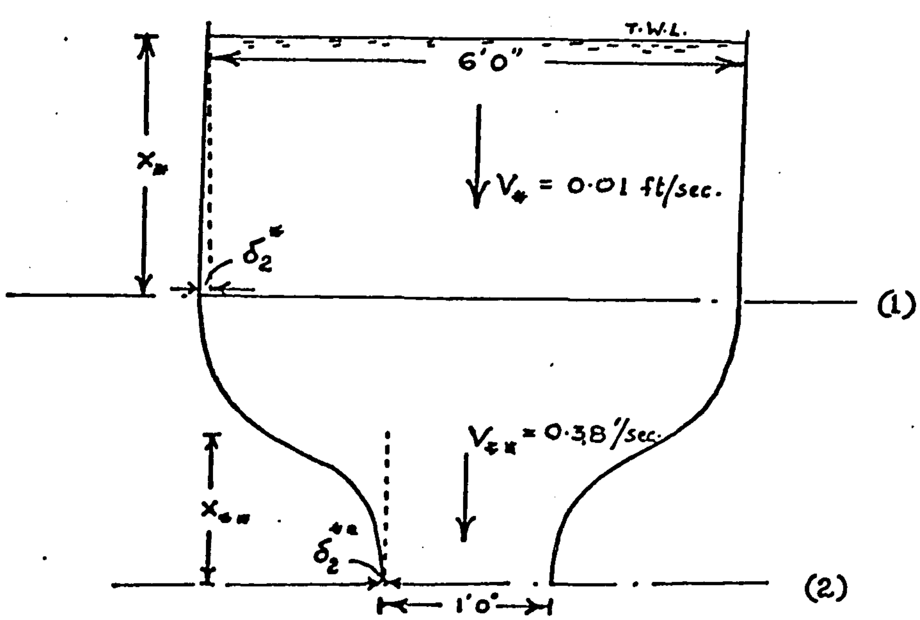

Fig.6

As a rough approximation, it seems logical to assume that the momentum thickness at sections just before and after the conical funnel type bottom are equal (of course, here one neglects the friction losses and the boundary layer growth along the curved bottom). Hence

Momentum defect at section (1) = Momentum defect at section (2)

$$\delta_2^{*} \; V_*^2 \, P_1 = \delta_2^{**} \, V_{**}^2 \, P_2 \tag{124}$$

$$\delta_2^{**} = \delta_2^{*} \left(\frac{V_*^2}{V_{**}^2} \right) \frac{P_1}{P_2} \quad \text{since} \quad \frac{V_*}{V_{**}} = \frac{A_2}{A_1}$$

$$= \delta_2^{*} \left(\frac{A_2}{A_1} \right)^2 \left(\frac{A_1}{A_2} \right)^{\frac{1}{2}} \qquad P_2/P_1 = b_1/b_2$$

Where P_1 and P_2 are the perimeters, A_1, A_2 are the areas and b_1, b_2 are the breadths at section (1) and (2) respectively, and δ_2^{**} is the momentum thickness at section (2).

$$\delta_2^{**} = \delta_2^{*} \left(A_2/A_1 \right)^{3/2} \tag{125}$$

$$= \delta_2^{*} \left(1/6 \right)^3$$

i.e. $\delta_2^{**} = \dfrac{0.666}{216} = 0.03''$

but $\delta_2^{**} = 0.664 \sqrt{\dfrac{x_{**} \nu}{V_{**}}}$

where x_{**} = The distance from the origin of the momentum thickness to section (2) in fig.6.

V_{**} = The velocity at the inlet to the test section(section 2 in fig.6)

i.e. $x_{**} = \left[\frac{0.03}{12 \times 0.664}\right]^2 \frac{0.38}{10^{-5}} = 0.0054''$

Hence it may be assumed for all practical purposes that a new boundary layer is in effect brought into existence at the start of the test section.

7.1. DISCUSSION OF HEAD LOSS MEASUREMENTS

(a) Right angled Mitre bend

The coefficient of contraction corresponding to theory outlined in Chapter 4 is 0.526. Hence the height of the issuing jet at the vena contracta should be 0.526' whereas fully expanded flow spreads, of course to 1'. The actual measurement of velocity by dye injection and also the test with condensed milk in the case of a mitre bend with uniform velocity distribution showed that the vena contracta occupied a height of 0.5' approximately, indicating a coefficient of contraction of nearly 0.5, closely agreeing with theory. The loss of head due to sudden contraction can be estimated in terms of the velocity head by the familiar formula $(V_1 - V_2)^2/2g$ (81)

where V_1 and V_2 are respectively the velocities at the contracted area and at the fully expanded region.

(i) From table 2.3 for uniform velocity distribution in the case of the mitre bend,

V_1 = 0.544 ft/sec. (Average velocity interpolated from the graph-figure 28)

V_2 = 0.344 ft/sec.

Estimated head loss = $(V_1 - V_2)^2/2g$

= 0.0006'

(of course, this formula is only quoted here as an approximate check)

Weighted average head loss as per table 2.3

= 0.275" of the manometer liquid.

$\therefore$ Measured head loss in the differential manometer

$$= \frac{0.275}{12}\left(\frac{w_i}{w'} - 1\right)$$

$$= \frac{0.275}{12}(1.047 - 1)$$

$$= 0.00108'$$

where w_i = density of the manometer liquid

w' = density of the metered fluid

Using the Blasius theory of the laminar boundary layer for a flat plate (admittedly only an approximation in the present case), one may get a rough idea of the loss due to the laminar boundary layer acting on the walls of the test section* (on the assumptions of no breakaway, of course, and neglecting the effect of pressure gradients). Though this approach is very approximate indeed, it is perhaps better than making no such estimate at all.

According to Blasius, frictional force $= \dfrac{V_2^{\,2}}{2g} \dfrac{1.328A}{\sqrt{\dfrac{V_2 L}{\nu}}}$ (126)

and the head-loss is obtained by dividing this by the area of the wetted cross section (1 sq.ft.) at the measuring point.

where ν = Kinematic viscosity

L = Overall length of plate subjected to laminar boundary layer

A = Wetted area over which the frictional force acts.

$$\therefore \text{Head-loss} = \frac{(0.344)^2}{64.4} \frac{1.328}{\sqrt{\dfrac{0.344 \cdot 4.817}{10^{-5}}}} \cdot 19.2$$

$$= 0.000115'$$

Net head-loss due to the bend alone $\Delta H = 0.00108 - 0.000115$

$$= 0.00096'$$

$$\frac{V_2^{\,2}}{2g} = \frac{(0.344)^2}{64.4} = 0.00184$$

---

*Note that in applying this theory, any change in wetted cross section through the bend is neglected, too. The theory is approximate indeed!

Let K be the head-loss coefficient, then $K\,V_2^2/2g = \Delta H$, i.e.

$$0.00184K = 0.00096$$

$$K = 0.52$$

Similarly, the values of K for non-uniform velocity distributions have been tabulated in Table 10.

(b) Inner-Curved Wall in Place of the Mitre Bend (Uniform Velocity Distribution)

From Table 3.3

$V_1 = 0.544$ ft/sec (Average velocity interpolated from the graph, Fig. 31)

$V_2 = 0.344$ ft/sec

Estimated head-loss $= \dfrac{(V_1 - V_2)^2}{2g} = 0.00062'$

(Once again, this value is included as a rough indication only).

Measured head-loss in the differential manometer $= \dfrac{0.25}{12}(0.047)$

$= 0.00098'$

Loss due to laminar boundary (cf. previous section)

$$= \frac{V_2^2}{2g} \frac{1.328A}{\sqrt{\frac{V_2 L}{\nu}}} = 0.000115'$$

Loss due to the bend alone $\Delta H = 0.00098' - 0.000115'$

$= 0.00086'$

$$\therefore \quad 0.00184K = 0.00086$$

(where 0.00184 as previously is the value of $\dfrac{V_2^2}{2g}$)

$$K = 0.47$$

(c) Inner-Curved Wall With Internal Guide Vanes (Uniform Velocity Distribution)

Loss due to laminar boundary layer acting on the sides = 0.000115'.

Loss due to laminar boundary layer acting on both sides of the guide vanes =

$$\frac{2 \times (0.344)^2 \times 1.328}{64.4} \left\{ \frac{1.943^*}{\sqrt{\frac{0.344 \times 1.943}{10^{-5}}}} + \frac{2.135^*}{\sqrt{\frac{0.344 \times 2.135}{10^{-5}}}} + \frac{2.057^*}{\sqrt{\frac{0.344 \times 2.057}{10^{-5}}}} \right\}$$

$$\fallingdotseq 0.000113'$$

(as if these were plane plates with zero pressure gradient, a rough approximation, but the best available).

Measured head-loss = $\frac{0.0775}{12} \times 0.047 = 0.000303'$

$\therefore$ Loss due to the bend = 0.000303 - (0.000115 + 0.000113) = 0.000075'

$\therefore$ 0.00184 K = 0.000075

i.e., K = 0.04

The values of K for non-uniform velocity distributions have been tabulated in Table 10.

However, it should be observed that the measurement of head-loss in a bend should, strictly speaking, be done by extrapolating energy gradients towards the bend from stations sufficiently upstream and downstream. But owing to the limited facilities in the laboratory, in the present work the pressure tappings had to be located no further than a distance of 1½ feet downstream from the bend and 6 inches upstream from the bend at the centre line of each end plate. The average of the centre

* represents the surface area on one side of each guide vane. The width of the guide vane is of course equal to 1 foot.

line pressures on the four sides was approximated to by the weighted average over the cross section (In a theoretically more accurate approach,the total head should perhaps have been evaluated by integration of stagnation pressures measured at various points across the downstream cross section,but it is in fact, very doubtful whether under the present experimental conditions of low velocity head and high average pressure, this approach would,in fact, have given improved results.

It may be worthwhile also to mention at this point that as far as the breakaway is concerned, the present tests were conducted under adverse conditions, seeing that laminar boundary layers are not frequently found in practice*. However it should also be recalled that friction in a turbulent boundary layer may be 6 or more times higher than those in a laminar one,for a given velocity in the main stream.

It is always desirable to avoid separation of the fluid from the walls,since it is accompanied by

---

* In the mathematical analysis of this problem,the flow is assumed to be laminar,and head losses due to a laminar boundary layer are taken into consideration when analysing the experimental results. When considering the practical applications of this work,e.g. in industrial ducts,it should be noted that laminar boundary layers are rarely found.

considerable energy loss. Laminar boundary layers can support only very small adverse pressure gradients (retarded flows) without separation as compared to turbulent ones (Ref.12). However, existence of adverse pressure gradients favours the transition from laminar to turbulent flows. The easiest method of controlling separation is to arrange the pressure gradients to remain below the limit for which separation occurs. Other possible methods include suction or by injecting fluid into the boundary layer or by the addition of aerodynamic guide vanes. The first method of boundary layer control is used here and with constant velocity along the intrados, the pressure must remain theoretically constant(the intrados, a line of constant pressure).

8. CONCLUSIONS

A general analysis for the design of an inner-curved wall and internal guide vanes for a right-angled elbow has been described using free streamline theory. The effectiveness of such a design in reducing the head-losses and its efficiency in providing an undisturbed velocity distribution after the bend was determined experimentally for three different velocity conditions. The design of internal guide vanes was checked by an electrical analogy.

8.1. EXPERIMENTAL

8.1.1.

With a uniform velocity distribution, the head-loss coefficient due to the bend was reduced from 0.52 to 0.47 when the inner-curved wall was substituted for the mitre head. When internal guide vanes were employed these were reduced further from 0.47 to 0.04. These figures are quoted after subtracting skin friction losses within the bend.

The guide vanes were able to maintain approximately the same velocity distribution after the bend as that before the bend - this was not the case when the guide vanes were removed.

8.1.2.

Even with trapezoidal velocity distributions, the inner-curved wall and internal guide vanes are still advantageous.

With the maximum velocity along the extrados, the head loss coefficient was reduced from 3.3 to 2.3, when the inner-curved wall was used instead of the mitre bend. The internal guide vanes reduced it further to 1.5.

With the maximum velocity along the intrados, the inner-curved wall proved its efficiency by reducing the head-loss coefficient from 2.1 to 0.64 when it was used instead of the sharp mitre bend. But the internal guide vanes presented only a minor supplemental advantage by reducing the head-loss coefficient to 0.57.

The velocity distribution after the bend in both trapezoidal velocity conditions does not approach the velocity pattern before the bend, even when internal guide vanes were employed.

8.1.3.

Owing to limitations in the laboratory facilities, the limited time available and the considerable difficulties in carrying out these tests, the experiments could not be conducted in the best way. Quite a lot of improvements could have been made (as mentioned at appropriate places) if circumstances had allowed.

The guide vanes were found to be efficient in reducing the turbulence and eddy effects to a measurable degree.

8.2. THEORETICAL

(i) The form of the streamlines and equipotentials was well defined by the theory.

(ii) The theoretical solution could be adopted to cases for which $x_o \neq b$, viz. for different two-dimensional flows, by substituting suitable values to 'x_o' in terms of 'b'.

8.3. INFERENCE

The effect of the internal guide vanes could not be predicted under non-uniform velocity conditions. But it can be assumed from the results of the two trapezoidal velocity distribution tests that its effect is always to reduce head-losses and to increase the efficiency of the bend, even though the improvement may not be very appreciable in all cases.

Allowing for the fact that the internal guide vanes used were probably much longer than necessary, it is clear that the curved intrados with guide vanes give a very small loss of head indeed for a uniform inlet velocity distribution. Bends so designed may be useful in industrial application where high performance (i.e., very low head-losses) is required, e.g., dump tanks for heavy water atomic reactors. Use of only one curved-wall may facilitate construction.

APPENDIX 1

COMPUTER PROGRAMME USED IN I.B.M.360

I. To calculate the value of λ from equation (47) with x_o=a and

$$V/U = \frac{\sqrt{\lambda+1} + \sqrt{\lambda-1}}{\sqrt{2}}$$

FORTRAN SOURCE STATEMENT LIST

```
    IMPLICIT REAL*8(A-H,O-Z)
    DIMENSION DIFF(1000)
    AL=1.001 DO
    DO 200 I=1,1000
    ALHS=(DSQRT(AL+1.0DO)+DSQRT(AL-1.0DO))/DSQRT(2.0DO)
    ALA=(DSQRT(AL+1.0)+DSQRT(2.0DO))/(DSQRT(AL+1.0DO)-DSQRT(2.0DO))
    ALB=(2.0DO*AL)/3.1415926535897932
    ALC=(DSQRT(AL+1.0DO))/(AL*DSQRT(2.0DO))
    ALD=(DSQRT(2.0DO))/(AL*DSQRT(2.0DO))
    ALE=(DSQRT(2.0DO))/(DSQRT(AL-1.0DO))
    ARHS=ALB*((ALC*DLOG(ALA))-(ALD*DATAN(ALE)))
    DIFF(1)= ALHS-ARHS
    DIFR=DABS(DIFF(I))
    IF(DIFR.LE.0.0DO)GO TO 100
    AL=AL+0.001DO
    GO TO 200
100 WRITE(6,20)AL,DIFF(I)
 20 FORMAT(20X,2D25.14)
    AL=AL+0.001DO
200 CONTINUE
    STOP
    END
```

II. <u>TO CALCULATE THE SHAPE OF THE INNER CURVED WALL FROM EQUATION (41) WITH $\lambda = 1.099$ AND</u>

$$V/U = \frac{\sqrt{\lambda + 1} + \sqrt{\lambda - 1}}{\sqrt{2}}$$

<u>FORTRAN SOURCE STATEMENT LIST</u>

```
   DIMENSION V(11),VAR(11),X(11)
   AL = 1.0993446116037O5DO
   PI = 3.14159265DO
   N  = 10
   RALP = SQRT(AL+1.0)
   RALM = SQRT(AL-1.0)
   R2   = SQRT(2.0)
   K    = N + 1
   DO 10 I = 1,K
   V(I)  = COS(PI/2 + PI/2/N - I*PI/2/N)
   VAR(I) = 12/PI/(RALP + RALM) * (RALP*ALOG((RALP +R2 * V(I)))
  1-2*RALM*ATAN(R2*V(I)/RALM))
   X(I)  = VAR(I) - VAR(1)
10 CONTINUE
   WRITE(6,12)
12 FORMAT(20X,'X',20X,'Y',//////)
   WRITE(6,13) (X(I),X(K-I + 1),I = 1,K)
13 FORMAT (10X,2E 20.8,//)
   STOP
   END
```

APPENDIX-2

COMPUTER PROGRAMME USED IN I.B.M.360

I. To calculate the intersection point of the internal guide vanes and the complex line BF (or numerical integration of equation (56))

$$\frac{dz}{d\zeta} = \frac{aU}{\sqrt{2}\,\pi V}\left\{\frac{(\lambda+1) + (\lambda-1)\zeta}{\zeta\sqrt{(1-\zeta)\left[(\lambda+1)+(\lambda-1)\zeta\right]}} + i\,\frac{-(\lambda-1) - (\lambda+1)\zeta}{\zeta\sqrt{(1-\zeta)\left[-(\lambda-1)-(\lambda+1)\zeta\right]}}\right\}$$

for the range of ζ from -1 to $-e^{-i\beta}$

FORTRAN SOURCE STATEMENT LIST

```
      IMPLICIT REAL*8(A-H,O-Z)
      DIMENSION C(1000),RO(1000),THETA(1000),F(1000),
     1DELTA(10,40),AEAL(40),BNREAL(40),X(1000),Y(1000)
      AL = 1.099345DO
      DO 1000 NNN =1,8
      DO 5000 LLL =1,35
      LL = LLL * 5
      PI = 3.1415926DO
      M = LL * 2 + 1
      J = M - 10
      C(1) = 0.0DO
      GO TO (1,2,3,4,5,6,7,8),NNN
    1 DO I = J,M
      IF ( I.EQ.1) GO TO 11
      C(I) = C(I-1) + ((0.5DO*PI)/180.0DO)
   11 X(I) = (AL+1.0DO)+2.0DO*DCOS(C(I))+(1.0DO-AL)*
     1((DCOS(C(I)))**2-(DSIN(C(I)))**2)
      Y(I)=2.0DO*DSIN(C(I))+(AL-1.0DO)*2.0DO*DSIN(C(I))*
     1DCOS(C(I))
```

```
      RO(I)=DSQRT((X(I))**2 +(Y(I))**2)
      THETA(I)=DATAN2(Y(I)/X(I))
   10 F(I)=DSIN(THETA(I)/2.0D0)/DSQRT(RO(I)))
      GO TO 2000
    2 DO 20 I=J,M
      IF(I.EQ.1) GO TO 21
      C(I)=C(I-1)+((0.5D0*PI)/180.0D0)
   21 X(I)=(AL+1.0D0)+2.0D0*DCOS(C(I))+(1.0D0-AL)*((DCOS(C(I)))**2-
     1(DSIN(C(I)))**2)
      Y(I)=-2.0D0*DSIN(C(I))+(AL-1.0D0)*2.0D0*DSIN(C(I))*DCOS(C(I))
      RO(I)=DSQRT(X(I))**2 +(Y(I))**2)
      THETA(I)=DATAN2(Y(I)/X(I))
   20 F(I)=DCOS(THETA(I)/2.0D0)/DSQRT(RO(I))
      GO TO 2000
    3 DO 30 I=J,M
      IF(I.EQ.1) GO TO 31
      C(I)=C(I-1)+((0.5D0*PI)/180.0D0
   31 X(I)=(1.0D0-AL(+2.0D0*DCOS(C(I))+(1.0D0+AL)*((DCOS(C(I)))**2-
     1(DSIN(C(I)))**2)
      Y(I)=2.0D0*DSIN(C(I))+(AL+1.0D0)*2.0D0*DSIN(C(I))*DCOS(C(I))
      RO(I)=DSQRT((X(I))**2 +(Y(I))**2)
      THETA(I)=DATAN2(Y(I)/X(I))
   30 F(I)=DSIN(THETA(I)/2.0D0)/DSQRT(RO(I))
      GO TO 2000
    4 DO 40 I=J,M
      IF(I.EQ.1) GO TO 41
      C(I)=C(I-1)+((0.5D0*PI)/180.0D0)
   41 X(I)=(1.0D0-AL)+2.0D0*DCOS(C(I))+(1.0D0+AL)*((DCOS(C(I)))**2)
     1-(DSIN(C(I)))**2)
```

```
   Y(I)=2.0D0*DSIN(C(I))+(1.0D0+AL)*2.0D0*DSIN(C(I))*DCOS(C(I))
   RO(I)=DSQRT((X(I))**2 +(Y(I))**2)
   THETA(I)=DATAN2(Y(I)/X(I))
40 F(I)=DCOS(THETA(I)/2.0D0)/DSQRT(RO(I))
   GO TO 2000
 5 DO 50 I=J,M
   IF (I.EQ.1) GO TO 51
   C(I)=C(I-1)+((0.5D0*PI)/180.0D0)
51 X(I)=(1.0D0-AL)+2.0D0*DCOS(C(I))+(1.0D0+AL)*((DCOS(C(I)))**2-
  1DSIN(C(I)))**2)
   Y(I)=-2.0D0*DSIN(C(I))-(1.0D0+AL)*2.0D0*DSIN(C(I))*DCOS(C(I))
   RO(I)=DSQRT((X(I))**2 +(Y(I))**2)
   THETA(I)=DATAN2(Y(I)/X(I))
50 F(I)=DCOS(THETA(I)/2.0D0)/DSQRT(RO(I))
   GO TO 2000
 6 DO 60 I=J,M
   IF(I.EQ.1) GO TO 61
   C(I)=C(I-1)+((0.5D0*PI)/180.0D0)
61 X(I)=(1.0D0-AL)+2.0D0*DCOS(C(I))+(1.0D0+AL)*((DCOS(C(I)))**2
  1-(DSIN(C(I)))**2)
   Y(I)=2.0D0*DSIN(C(I))-(1.0D0+AL)*DSIN(C(I))*DCOS(C(I))
   RO(I)=DSQRT((X(I))**2 +(Y(I))**2)
   THETA(I)=DATAN2(Y(I)/X(I))
60 F(I)=DSIN(THETA(I)/2.0D0)/DSQRT(RO(I))
   GO TO 2000
 7 DO 70 I=J,M
   IF(I.EQ.1) GO TO 71
   C(I)=C(I-1)+((0.5D0*PI)/180.0D0)
```

```
71 X(I)=(1.0D0-AL)*((DCOS(C(I)))**2-(DSIN(C(I)))**2)+2.0D0*
  1DCOS(C(I))+(AL+1.0D0)
   Y(I)=(1.0D0-AL)*2.0D0*DSIN(C(I))*DCOS(C(I))+2.0D0*DSIN(C(I))
   RO(I)=DSQRT((X(I))**2+(Y(I))**2)
   THETA(I)=DATAN2(Y(I)/X(I))
70 F(I)=DCOS(THETA(I)/2.0D0)/DSQRT(RO(I))
   GO TO 2000
 8 DO 80 I=J,M
   IF(I.EQ.1) GO TO 81
   C(I)=C(I-1)+((0.5D0*PI)/180.0D0)
81 X(I)=(1.0D0-AL)*((DCOS(C(I)))**2-(DSIN(C(I)))**2)+2.0D0*
  1DCOS(C(I))+(AL+1.0D0)
   Y(I)=(1.0D0-AL)*2.0D0*DSIN(C(I))*DCOS(C(I))+2.0D0*DSIN(C(I))
   RO(I)=DSQRT((X(I))**2+(Y(I))**2)
   THETA(I)=DATAN2(Y(I)/X(I))
80 F(I)=DSIN(THETA(I)/2.0D0)/DSQRT(RO(I))
2000 FO=0.0D0
   FE=0.0D0
   K=LL-4
   DO 3000 I=K,LL
   NN=2*I
   FO=FO+F(NN-1)
3000 FE=FE+F(NN)
   FO=FO-F(J)
   DELTA(NNN,LLL)=((0.5D0*PI)/(3.0D0*1800D0))*(F(J)+F(M)+2.0D0
  1*FO+4.0D0*FE)
   IF(LLL.EQ.1) GO TO 5000
   DELTA(NNN,LLL)=DELTA(NNN,LLL)+DELTA(NNN,LLL-1)
```

```
5000 CONTINUE
1000 CONTINUE
     DO 4000 LLL=1,35
     AEAL(LLL)=(1.0DO/(PI*(DSQRT(AL+1.0)+DSQRT(AL-1.0DO))))*
    1(-(AL*1.0DO)*(DELTA(1,LLL))+(AL-1.0DO)*(DELTA(3,LLL))-
    2(AL-1.0DO)*(DELTA(5,LLL))+(AL+1.0DO)*(DELTA(7,LLL)))
     BNREAL(LLL)=(1.0DO/(PI*(DSQRT(AL+1.0DO)+DSQRT(AL-1.0DO))))
    1*(-(AL+1.0DO)*(DELTA(2,LLL))+(AL-1.0DO)*(DELTA(4,LLL))+
    2(AL-1.0DO)*(DELTA(6,LLL))-(AL+1.0DO)*(DELTA(8,LLL)))
     NDGREE=LLL*5
4000 WRITE (6,101)NDGREE,AEAL(LLL),BNREAL(LLL)
 101 FORMAT(10X,I4,2F26.14)
     STOP
     END
```

II TO CALCULATE THE SHAPE OF THE INTERNAL GUIDE VANES (OR NUMERICAL INTEGRATION OF EQUATION (56)

$$\int dz \doteq \frac{aU}{\sqrt{2}\, V\pi} \int \left\{ \frac{(\lambda+1) + (\lambda-1)\zeta}{\zeta\sqrt{(1-\zeta)[(\lambda+1)+(\lambda-1)\zeta]}} + i \, \frac{-(+\lambda-1) - (\lambda+1)\zeta}{\zeta\sqrt{(1-\zeta)[-(+\lambda-1)-(\lambda+1)\zeta]}} \right\}$$

for the range of ζ from $-e^{-i\beta}$ to $-re^{-i\beta}$

FORTRAN SOURCE STATEMENT LIST

```
      DIMENSION RO(2000),THETA(2000),F(2000),DELTA(2000),AEAL(2000),
     1BNREAL(2000),R(2000),X(2000),Y(2000)
      AL=1.09935
      PI=3.1415927
      C=(135.0*PI)/180.0
      DO 1000 NNN=1,8
      DO 5000 LLL=1,100
      LL=LLL*5
      M=LL*2+1
      J=M-10
      R(1)=1.0
      GO TO(1,2,3,4,5,6,7,8),NNN
    1 DO 10 I=J,M
      IF(I.EQ.1)GO TO 11
      R(I)=R(I-1)+0.2
   11 X(I)=(AL+1.0)+2.0*R(I)*COS(C)+(R(I)**2)*(1.0-AL)*((COS(C))**2-
     1(SIN(C))**2)
      Y(I)=-2.0*R(I)*SIN(C)+(R(I)**2)*(AL-1.0)*2.0*SIN(C)*COS(C)
      RO(I)=SQRT((X(I)**2)+(Y(I)**2))
      THETA(I)=ATAN2(Y(I)/X(I))
   10 F(I)=COS(THETA(I)/2.0)/(SQRT(RO(I)*R(I))
      GO TO 2000
```

```
  2 DO 20 I=J,M
    IF(I.EQ.1) GO TO 21
    R(I)=R(I-1)+0.2
 21 X(I)=(AL+1.0)+2.0*R(I)*COS(C)+(R(I)**2)*(1.0-AL)*((COS(C))**2
   1-(SIN(C))**2)
    Y(I)=-2.0*R(I)*SIN(C)+(R(I)**2)*(AL-1.0)*2.0*SIN(C)*COS(C)
    RO(I)=SQRT((X(I)**2)+(T(I)**2))
    THETA(I)=ATAN2(Y(I)/X(I))
 20 F(I)=SIN(THETA(I)/2.0)/(SQRT(RO(I))*R(I))
    GO TO 2000
  3 DO 30 I=J,M
    IF(I.EQ.1) GO TO 31
    R(I)=R(I-1)+0.2
 31 X(I)=(AL+1.0)*((COS(C)**2-(SIN(C))**2)+2.0*R(I)*COS(C)+(R(I)**2)
   1*(1.0-AL)
    Y(I)=(AL+1.0)*2.0*SIN(C)*COS(C)+2.0*R(I)*SIN(C)
    RO(I)=SQRT((X(I)**2)+(Y(I)**2))
    THETA(I)=ATAN2(Y(I)/X(I))
 30 F(I)=COS(THETA(I)/2.0)/SQRT(RO(I))
    GO TO 2000
  4 DO 40 I=J,M
    IF(I.EQ.1)+0.2
 41 X(I)=(AL+1.0)*((COS(C))**2-(SIN(C))**2)+2.0*(R(I)**2)*(1.0-AL)
    Y(I)=(AL+1.0)*2.0*SIN(C)*COS(C)+2.0*R(I)*SIN(C)
    RO(I)=SQRT((X(I)**2+(Y(I)**2))
    THETA(I)=ATAN2(Y(I)/X(I))
 40 F(I)=SIN(THETA(I)/2.0)/SQRT(RO(I))
```

```
      GO TO 2000
    5 DO 50 I=J,M
      IF(I.EQ.1) GO TO 51
      R(I)=R(I-1)+0.2
   51 X(I)=(1.0-AL)+2.0*R(I)*COS(C)+R(I)**2*(1.0+AL)*((COS(C))**2-
     1(SIN(C))**2)
      Y(I)=-2.0*R(I)*SIN(C)-(R(I)**2)*(1.0+AL)*2.0*SIN(C)*COS(C)
      RO(I)=SQRT((X(I)**2+(Y(I)**2))
      THETA(I)=ATAN2(Y(I)/X(I))
   50 F(I)=SIN(THETA(I)/2,0)/(SQRT(RO(I))*R(I))
      GO TO 2000
    6 DO 60 I=J,M
      IF(I.EQ.1) GO TO 61
      R(I)=R(I-1)+0.2
   61 X(I)=(1.0-AL)+2.0*R(I)*C)S(C)+(R(I)**2)*(1.0+AL)*((C)S(C))**2-
     1(SIN(C)**2)
      Y(I)=-2.0*R(I)*SIN(C)-(R(I)**2)*(1.0+AL)*SIN(C)*COS(C)*2.0
      RO(I)=SQRT((X(I)**2)+(Y(I)**2))
      THETA(I)=ATAN2(Y(I)/2.0)/(SQRT(RO(I))*R(I))
   60 F(I)=COS(THETA(I)/2.0)/(SQRT(RO(I))*R(I))
      GO TO 2000
    7 DO 70 I=J,M
      IF(I.EQ.1) GO TO 71
      R(I)=R(I-1)+0.2
   71 X(I)=(AL+1.0)*(R(I)**2)+2.0*R(I)*COS(C)+(1.0-AL)*((COS(C))**2-
     1(SIN(C))**2)
      Y(I)=2.0*R(I)*SIN(C)+(1.0-AL)*2.0*SIN(C)*COS(C)
      RO(I)=SQRT((X(I)**2+(Y(I)**2))
      THETA(I)=ATAN2(Y(I)/X(I))
```

```
   70 F(I)=SIN(THETA(I)/2.0)/SQRT(RO(I))
      GO TO 2000
    8 DO 80 I=J,M
      IF(I.EQ.1)GO TO 81
      R(I)=R(I-1)+0.2
   81 X(I)=(AL+1.0)*(R(I)**2)+2.0*R(I)*COS(C)+(1.0-AL)*((COS(C))**2
     1-(SIN(C))**2)
      Y(I)=2.0*R(I)*SIN(C)+(1.0-AL)*2.0*SIN(C)*COS(C)
      RO(I)=SQRT((X(I)**2)+(Y(I)**2))
      THETA(I)=ATAN2(Y(I)/X(I))
   80 F(I)=COS(THETA(I)/2.0)/SQRT(RO(I))
 2000 FO=0.0
      FE=0.0
      K=LL-4
      DO 3000 I=K,LL
      NN=2*I
      FO=FO+F(NN-1)
 3000 FE=FE+F(NN)
      FO=FO-F(J)
      DELTA(NNN,LLL)=(0.20/3.0)*(F(J)+F(M)+2.0*FO+4.0*FE)
      IF(LLL.EQ.1) GO TO 5000
      DELTA(NNN,LLL)=DELTA(NNN,LLL)+DELTA(NNN,LLL-1)
 5000 CONTINUE
 1000 CONTINUE
      DO 4000 LLL=1,100
      AEAL(LLL)=(1.0/(PI*(SQRT(AL+1.0)+SQRT(AL-1.0))))*((AL+1.0)*
     1(DELTA(1,LLL))-(AL-1.0)*(DELTA(3,LLL))-(AL-1.0)*(DELTA(5,LLL))
     2+(AL+1.0)*(DELTA(7,LLL)))
```

```
      BNREAL(LLL)=(1.0/(PI*(SQRT(AL+1.0)+SQRT(AL-1.0))))*(-(AL+1.0)*
     1(DELTA(2,LLL))+(AL+1.0)*(DELTA(4,LLL))-(AL-1.0)*(DELTA(6,LLL))+
     2(AL+1.0)*(DELTA(8,LLL)))
      AEAL(LLL)=AEAL(LLL)*12.0
      BNREAL(LLL)=BNREAL(LLL)*12.0
      XLL=LLL
      RADI=XLL*2.0+1.0
 4000 WRITE(6,101) RADI,AEAL(LLL),BNREAL(LLL)
  101 FORMAT(10X,3F18.5)
      STOP
      END
```

III. EXPLANATION OF COMPUTER SYMBOLS USED

AL = λ

C = The value of 'β' in radians

C(I) = The variable value of 'β' in radians

RO(I) = $\rho_{(I)}$

THETA(I) = $\theta_{(I)}$

X(I) = The real part of the particular function

Y(I) = The imaginary part of the particular function

M & J = The maximum and minimum ordinate of the trapezoid when integrating by Simpson's rule

PI = π

NDGREE = The value of 'β' at intervals af 5 degrees

DELTA(NNN, LLL) = Integrated result of the particular function

FO = Odd ordinate of the trapezoid when integrating by Simpson's rule

FE = Even ordinate of the trapezoid when integrating by Simpson's rule

AEAL(LLL) = Real part of the integration

BNREAL(LLL) = Imaginary part of the integration

RALP = $\sqrt{\lambda + 1}$

RALM = $\sqrt{\lambda - 1}$

R2 = $\sqrt{2}$

IV. NOTES ON PROGRAMMING

The programme was written in Fortran IV for use on the McGill University IBM 360 digital computer. In Appendix 2, Part I, the integral has been computed with the value of β increasing in steps of 5 degrees. Similarly, in Appendix 2, Part II, the integral has been evaluated with the value of r increasing in steps of 2. and the programme has been written with the value $\beta = 135^o$, Viz., $c/_a = \frac{1}{4}$. The same programme has been used for computing internal guide vanes at $\frac{1}{2}$ and 3/4 positions, by changing the value of β to 90^o and 45^o, respectively, instead of 135^o. In all the programmes better accuracy can be attained by changing the interval of integration. Tables 8-13 show the computer output tabulated in order.

APPENDIX 3

NUMERICAL INTEGRATION OF EQUATION (56) TO FIND THE SHAPE OF INTERNAL STREAMLINES

PART I

For the range of ζ from -1 to $-e^{-i\beta}$

By putting
$$\zeta = -e^{-i\beta}$$
$$d\zeta = i e^{-i\beta} d\beta$$

Equation (56) becomes

$$\int dz = \frac{-aU}{\sqrt{2}\,\pi V}\int_0^\beta \frac{(\lambda-1)\,d\beta}{\sqrt{(1+e^{-i\beta})\left[-(\lambda-1)+(\lambda+1)e^{-i\beta}\right]}}$$

$$+ \frac{aU}{\sqrt{2}\,\pi V}\int_0^\beta \frac{(\lambda+1)\,e^{-i\beta}\,d\beta}{\sqrt{(1+e^{-i\beta})\left[-(\lambda-1)+(\lambda+1)e^{-i\beta}\right]}}$$

$$- \frac{i\,aU}{\sqrt{2}\,\pi V}\int_0^\beta \frac{(\lambda+1)\,d\beta}{\sqrt{(1+e^{-i\beta})\left[(\lambda+1)-(\lambda-1)e^{-i\beta}\right]}}$$

$$+ \frac{aU}{\sqrt{2}\,\pi V}\int_0^\beta \frac{(\lambda-1)\,i\,e^{-i\beta}\,d\beta}{\sqrt{(1+e^{-i\beta})\left[(\lambda+1)-(\lambda-1)e^{-i\beta}\right]}}$$

$$= \frac{-i\,aU(\lambda+1)}{\sqrt{2}\,\pi V}\int_0^\beta \frac{d\beta}{\sqrt{\left[(\lambda+1)+2\cos\beta+(1-\lambda)\cos 2\beta\right]-i\left[2\sin\beta+(1-\lambda)\sin 2\beta\right]}}$$

$$+ \frac{i\,aU(\lambda-1)}{\sqrt{2}\,\pi V}\int_0^\beta \frac{d\beta}{\sqrt{\left[(1-\lambda)+2\cos\beta+(1+\lambda)\cos 2\beta\right]+i\left[2\sin\beta+(\lambda+1)\sin 2\beta\right]}}$$

$$- \frac{aU(\lambda-1)}{\sqrt{2}\,\pi V}\int_0^\beta \frac{d\beta}{\sqrt{\left[(1-\lambda)+2\cos\beta+(1+\lambda)\cos 2\beta\right]-i\left[2\sin\beta+(1+\lambda)\sin 2\beta\right]}}$$

$$+ \frac{aU(\lambda+1)}{\sqrt{2}\,\pi V}\int_0^\beta \frac{d\beta}{\sqrt{\left[(1-\lambda)\cos 2\beta+2\cos\beta+(\lambda+1)\right]+i\left[(1-\lambda)\sin 2\beta+2\sin\beta\right]}}$$

For simplicity one can write

$$x_1 = x_4 = \left[(\lambda+1) + 2\cos\beta + (1-\lambda)\cos 2\beta\right]$$

$$x_2 = x_3 = \left[(1-\lambda) + 2\cos\beta + (1+\lambda)\cos 2\beta\right]$$

$$y_1 = -y_4 = \left[-2\sin\beta - (1-\lambda)\sin 2\beta\right]$$

$$y_2 = -y_3 = \left[2\sin\beta + (1+\lambda)\sin 2\beta\right]$$

Hence

$$\int dz = \frac{-iaU(\lambda+1)}{\sqrt{2}\,\pi V}\int_0^\beta \frac{d\beta}{\sqrt{\rho_1(\cos\Theta_1 + i\sin\Theta_1)}}$$

$$+ \frac{iaU(\lambda-1)}{\sqrt{2}\,\pi V}\int_0^\beta \frac{d\beta}{\sqrt{\rho_2(\cos\Theta_2 + i\sin\Theta_2)}}$$

$$- \frac{aU(\lambda-1)}{\sqrt{2}\,\pi V}\int_0^\beta \frac{d\beta}{\sqrt{\rho_3(\cos\Theta_3 + i\sin\Theta_3)}}$$

$$+ \frac{aU(\lambda+1)}{\sqrt{2}\,\pi V}\int_0^\beta \frac{d\beta}{\sqrt{\rho_4(\cos\Theta_4 + i\sin\Theta_4)}}$$

$$\left.\begin{aligned} \rho_i &= \sqrt{x_i^2 + y_i^2} \\ \Theta_i &= \operatorname{Arc\,Tan}\left(\frac{y_i}{x_i}\right) \end{aligned}\right| \quad i = 1, 2, 3, 4$$

$$\int dz = \frac{aU}{\sqrt{2}\,\pi V}\Bigg[-(\lambda+1)\left\{ i\int_0^\beta \frac{\cos(\Theta_1/2)}{\rho_1^{1/2}}\,d\beta + \int_0^\beta \frac{\sin(\Theta_1/2)}{\rho_1^{1/2}}\,d\beta\right\}$$

$$+ (\lambda-1)\left\{ i\int_0^\beta \frac{\cos(\Theta_2/2)}{\rho_2^{1/2}}\,d\beta + \int_0^\beta \frac{\sin(\Theta_2/2)}{\rho_2^{1/2}}\,d\beta\right\}$$

$$+ (\lambda-1)\left\{ -\int_0^\beta \frac{\cos(\Theta_3/2)}{\rho_3^{1/2}}\,d\beta + i\int_0^\beta \frac{\sin(\Theta_3/2)}{\rho_3^{1/2}}\,d\beta\right\}$$

$$+ (\lambda+1)\left\{ \int_0^\beta \frac{\cos(\Theta_4/2)}{\rho_4^{1/2}}\,d\beta - i\int_0^\beta \frac{\sin(\Theta_4/2)}{\rho_4^{1/2}}\,d\beta\right\}\Bigg]$$

PART II

For the range of ζ from $-e^{-i\beta}$ to $-re^{-i\beta}$

By putting $\qquad \zeta = re^{-i\beta}$

$$d\zeta = e^{-i\beta}dr$$

Equation (56) becomes

$$\int dz = \frac{aU}{\sqrt{2}\,\pi V}\int_{-1}^{-r}\frac{(\lambda+1)\,dr}{r\sqrt{(1-re^{-i\beta})[(\lambda+1)+(\lambda-1)\,re^{-i\beta}]}}$$

$$+\frac{aU(\lambda-1)}{\sqrt{2}\,\pi V}\int_{-1}^{-r}\frac{e^{-i\beta}dr}{\sqrt{(1-re^{-i\beta})[(\lambda+1)+(\lambda-1)\,re^{-i\beta}]}}$$

$$-\frac{iaU(\lambda-1)}{\sqrt{2}\,\pi V}\int_{-1}^{-r}\frac{dr}{r\sqrt{(1-re^{-i\beta})[-(\lambda-1)-(\lambda+1)\,re^{-i\beta}]}}$$

$$-\frac{iaU(\lambda+1)}{\sqrt{2}\,\pi V}\int_{-1}^{-r}\frac{e^{-i\beta}dr}{\sqrt{(1-re^{-i\beta})[-(\lambda-1)-(\lambda+1)\,re^{-i\beta}]}}$$

$$=\frac{aU(\lambda+1)}{\sqrt{2}\,\pi V}\int_{-1}^{-r}\frac{dr}{r\sqrt{[(\lambda+1)-2r\cos\beta+r^2(1-\lambda)\cos 2\beta]+i[2r\sin\beta-r^2(1-\lambda)\sin 2\beta]}}$$

$$+\frac{aU(\lambda+1)}{\sqrt{2}\,\pi V}\int_{-1}^{-r}\frac{dr}{\sqrt{[(\lambda+1)\cos 2\beta-2r\cos\beta+r^2(1+\lambda)]+i[(\lambda+1)\sin 2\beta-2r\sin\beta]}}$$

$$-\frac{iaU(\lambda-1)}{\sqrt{2}\,\pi V}\int_{-1}^{-r}\frac{dr}{r\sqrt{[(1-\lambda)-2r\cos\beta+r^2(1+\lambda)\cos 2\beta]+i[2r\sin\beta-r^2(1+\lambda)\sin 2\beta]}}$$

$$-\frac{iaU(\lambda+1)}{\sqrt{2}\,\pi V}\int_{-1}^{-r}\frac{dr}{\sqrt{[(1-\lambda)\cos 2\beta-2r\sin\beta+r^2(1+\lambda)]+i[(1-\lambda)\sin 2\beta-2r\sin\beta]}}$$

Let

$$x_5 = [(\lambda+1)-2r\cos\beta+r^2(1-\lambda)\cos 2\beta]$$

$$y_5 = [2r\sin\beta-r^2(1-\lambda)\sin 2\beta]$$

$$x_6 = \left[(\lambda+1)\cos 2\beta - 2\gamma\cos\beta + \gamma^2(1-\lambda)\right]$$

$$y_6 = \left[(\lambda+1)\sin 2\beta - 2\gamma\sin\beta\right]$$

$$x_7 = \left[(1-\lambda) - 2\gamma\cos\beta + \gamma^2(1+\lambda)\cos 2\beta\right]$$

$$y_7 = \left[2\gamma\sin\beta - \gamma^2(1+\lambda)\sin 2\beta\right]$$

$$x_8 = \left[(1-\lambda)\cos 2\beta - 2\gamma\cos\beta + \gamma^2(1+\lambda)\right]$$

$$y_8 = \left[(1-\lambda)\sin 2\beta - 2\gamma\sin\beta\right]$$

Hence

$$\int dz = \frac{aU}{\sqrt{2}\,\pi V}\left[(\lambda+1)\int_{-1}^{-\gamma}\frac{d\gamma}{\gamma\sqrt{\rho_5}\,(\cos\theta_5 + i\sin\theta_5)}\right.$$

$$+ (\lambda-1)\int_{-1}^{-\gamma}\frac{d\gamma}{\sqrt{\rho_6}\,[\cos\theta_6 + i\sin\theta_6]}$$

$$- i(\lambda-1)\int_{-1}^{-\gamma}\frac{d\gamma}{\gamma\sqrt{\rho_7}\,(\cos\theta_7 + i\sin\theta_7)}$$

$$\left.- i(\lambda+1)\int_{-1}^{-\gamma}\frac{d\gamma}{\sqrt{\rho_8}\,(\cos\theta_8 + i\sin\theta_8)}\right]$$

Where

$$\left.\begin{aligned} \rho_i &= \sqrt{x_i^2 + y_i^2} \\ \theta_i &= \operatorname{Arc\,Tan}(y_i/x_i) \end{aligned}\right| \quad i = 5, \cdots 8$$

$$\int dz = \frac{aU}{\sqrt{2}\,\pi V}\left[(\lambda+1)\left\{\int_{-1}^{-\gamma}\frac{d\gamma}{\gamma\,\rho_5^{1/2}}\cos(\theta_5/2) - i\int_{-1}^{-\gamma}\frac{\sin(\theta_5/2)\,d\gamma}{\gamma\,\rho_5^{1/2}}\right\}\right.$$

$$+ (\lambda - 1) \left\{ \int_{-1}^{-\gamma} \frac{\cos(\theta_6/2)}{\rho_6^{1/2}} \, d\gamma - i \int_{-1}^{-\gamma} \frac{\sin(\theta_6/2)}{\rho_6^{1/2}} \, d\gamma \right\}$$

$$+ (\lambda - 1) \left\{ -i \int_{-1}^{-\gamma} \frac{\cos(\theta_7/2)}{\gamma \, \rho_7^{1/2}} \, d\gamma - \int_{-1}^{-\gamma} \frac{\sin(\theta_7/2)}{\gamma \, \rho_7^{1/2}} \, d\gamma \right\}$$

$$+ (\lambda + 1) \left\{ - \int_{-1}^{-\gamma} \frac{\sin(\theta_8/2)}{\rho_8^{1/2}} \, d\gamma - i \int_{-1}^{-\gamma} \frac{\cos(\theta_8/2)}{\rho_8^{1/2}} \, d\gamma \right\} \Bigg] .$$

REFERENCES

1. Addison H. 'Hydraulic Measurements',Second Edition,John Wiley & Sons Inc., 440 Fourth Avenue,New York.

2. Rouse H. 'Engineering Hydraulics',John Wiley & Sons Inc.,New York.

3. Sedille M. 'Turbo machines hydrauliques et thermigues tome 1',Masson & Cie.,Paris,1966.

4. McNown J.S. Yih C.S. 'Free streamline analysis of transition flow and jet deflection',Studies in Engineering,Bulletin 35,State University of Iowa,Iowa City, U.S.A.

5. Birkhoff G. Plesset M.S. Simmons N. 'Wall effects in cavity flow', Q.Applied Mechanics,Vol.8, 1950,and vol 9,1952.

6. Plesset M.S. Shaffer P.A. 'Cavity drag in three dimensions',Journal of applied physics,Vol 19,1948.

7. McNown J.S. 'Mechanics of manifold flow', ASCE proceedings,Separate No. 258,Aug.1953.

8. Harr M.E. 'Ground water & seepage',McGraw-Hill Book Co.Inc.,New York.

REFERENCES(CONTINUED)

9. McNown J.S. 'Complexities of manifold flow', Proceedings of the second hydraulic conference, Washington State University, Pullman, Washington, U.S.A.

10. Tsakonas S. 'Divided flow through a divergent inlet conduit', Journal of Hydraulics division, ASCE, Vol.83, No.H.Y.6, Dec.1957.

11. McNown J.S., Hsu E.Y. 'Application of conformal mapping to divided flow', Proceedings First Midwestern conference on Fluid Mechanics, 1950, Ann Arbor, Michigan.

12. Schlichting H. 'Boundary layer theory', McGraw-Hill Book Co.Inc., New York.

13. Lamp H. 'Hydrodynamics', Dover Publications Inc., New York.

14. Milne Thomson L.M. 'Theoretical Hydrodynamics', Fifth Edition, McMillan & Co. Ltd., London.

15. Prandtl L., Tietjens O.G. 'Fundamentals of Hydro and Aeromechanics', Dover Publications Inc., New York.

REFERENCES(CONTINUED)

16. Seeger R.J. Temple G. 'Research Frontiers in Fluid Dynamics',InterScience Publishers,John Wiley & Sons Inc.,New York.

17. Sedov L.I. 'Two dimensional problems in Hydrodynamics and Aerodynamics, John Wiley & Sons Inc.,New York.

18. Birkhoff G. Zarantonello 'Jets Wakes & Cavities', Academic Press Inc.,Publishers, New York.

19. Comolet R. Bonnin 'Mechanique experimentale des fluids',Tome III,Recueil de Problems.

20. Gilbarg D. 'Jets and Cavities',Encyclopedia of Physics,Vol IX,Springer-Verlag,Berlin 1960.

21. Birkhoff G. 'Calculation of potential flows with free streamlines',Journal of Hydraulics division, Proceedings of the American Society of Civil Engineering, H.Y.6,November 1961.

22. Tinny E.R. Barnes W.E. Rechard O.W. 'Free streamline theory for segmental jet deflectors, Journal of Hydraulics Division, ASCE Proceedings,sept.1961, HY 5.

REFERENCES(CONTINUED)

23. Hawthorne W.R. 'Flow in bend pipes',Proceedings of seminar in Aeronautical Sciences,National Aeronautical laboratory,Bangalore,India.

24. Gibson A.H. 'Hydraulics and its applications', D.Van Nostrand Co.,Park Place, New York.

25. Binder R.C. 'Advanced Fluid Dynamics & Fluid Machinery',Prentice Hall Inc., 70 Fifth Ave,New York.

26. Rouse H. 'Fluid Mechanics For Hydraulic Engineers',McGraw Hill Book Company Inc.,New York.

27. Rosenhead L. 'Laminar Boundary Layers', University Press,Oxford,Amen House,London.E.C.4.

28. Rouse H. 'Elementary Mechanics of Fluids', John Wiley & Sons Inc., New York.

29. Ramsey A.S. 'A Treatise on Hydromechanics', G.Bell & Sons Ltd.,London.

30. Birkhoff G. 'Hydrodynamics',Dover Publications Inc.,New York.

31. Goldstein S. 'Modern Developement in Fluid Dynamics',University Press, Oxford,Amen House,London.

Table 2.

Table 2.1

HEAD LOSS MEASUREMENT WITH MAXIMUM VELOCITY ALONG THE INTRADOS WITH RIGHT ANGLE MITRE BEND

Expt. No.	Difference in level in the differential manometer corresponding to two points before and after the bend on the		
	Intrados	Sides	Extrados
1	0.95"	0.85"	1.15"
2	1.0"	0.90"	1.20"
3	1.0"	0.90"	1.20"
4	1.0"	0.90"	1.20"
5	1.0"	0.90"	1.20"

NB

The above readings have to be multiplied by $(\gamma - 1)$ to obtain the pressure difference in inches of water. γ = specific gravity of the manometer liquid = 1.047.

Table 2.2

HEAD LOSS MEASUREMENT WITH MAXIMUM VELOCITY ALONG THE EXTRADOS WITH RIGHT-ANGLE MITRE BEND

Expt. No.	Difference in level in the differential manometer corresponding to two points before and after the bend on		
	Intrados	Sides	Extrados
1	1.6"	1.35"	1.65"
2	1.7"	1.40"	1.70"
3	1.75"	1.45"	1.70"
4	1.75"	1.45"	1.70"
5	1.75"	1.45"	1.70"

NB

The above readings have to be multiplied by $(\gamma - 1)$ to obtain the pressure difference in inches of water. γ, specific gravity of the manometer liquid = 1.047.

Table 2.3

HEAD LOSS MEASUREMENT WITH UNIFORM VELOCITY DISTRIBUTION WITH RIGHT-ANGLE MITRE BEND

Expt. No.	Difference in level in the differential manometer corresponding to two points before and after the bend on the		
	Intrados	Sides	Extrados
1	0.15"	0.15"	0.55"
2	0.20"	0.15"	0.60"
3	0.20"	0.15"	0.60"
4	0.20"	0.15"	0.60"
5	0.20"	0.15"	0.60"

NB

The above readings have to be multiplied by $(\gamma - 1)$ to obtain the pressure difference in inches of water.

γ = specific gravity of the manometer liquid = 1.047.

TABLE 3

Table 3.1

HEAD LOSS MEASUREMENT WITH MAXIMUM VELOCITY ALONG THE INTRADOS

(i) WITH INNER-CURVED WALL ALONE

Expt. No.	Difference in level in the differential manometer corresponding to two points before and after the bend on the		
	Intrados	Sides	Extrados
1	0.25"	0.25"	0.55"
2	0.25"	0.25"	0.55"
3	0.25"	0.25"	0.55"
4	0.25"	0.25"	0.55"
5	0.25"	0.25"	0.55"

(ii) WITH INNER-CURVED WALL AND INTERNAL GUIDE VANES

Expt. No.	Difference in level in the differential manometer corresponding to two points before and after the bend on the		
	Intrados	Sides	Extrados
1	0.15"	0.40"	0.35"
2	0.15"	0.40"	0.35"
3	0.15"	0.40"	0.35"
4	0.15"	0.40"	0.35"

The above readings have to be multiplied by $(\gamma - 1)$ to obtain the pressure difference in inches of water. γ = specific gravity of the manometer liquid = 1.047.

Table 3.2

HEAD LOSS MEASUREMENT WITH MAXIMUM VELOCITY ALONG THE EXTRADOS

(i) WITH INNER-CURVED WALL ALONE

Expt. No.	Difference in level in the differential manometer corresponding to two points before and after the bend on the		
	Intrados	Sides	Extrados
1	1.1"	1.10"	1.15"
2	1.1"	1.1"	1.15"
3	1.1"	1.1"	1.15"
4	1.1"	1.1"	1.15"

(ii) WITH INNER-CURVED WALL AND INTERNAL GUIDE VANES

Expt. No.	Difference in level in the differential manometer corresponding to two points before and after the bend on the		
	Intrados	Sides	Extrados
1	0.7"	0.8"	0.8"
2	0.7"	0.8"	0.8"
3	0.7"	0.8"	0.8"
4	0.7"	0.8"	0.8"

The above readings have to be multiplied by ($\gamma - 1$) to obtain the pressure differences in inches of water. γ = specific gravity of the manometer liquid = 1.047.

Table 3.3

HEAD LOSS MEASUREMENT WITH UNIFORM VELOCITY DISTRIBUTION WITH INNER-CURVED WALL ALONE

(i)

Expt. No.	Difference in level in the differential manometer corresponding to two points before and after the bend on the		
	Intrados	Sides	Extrados
1	0.15"	0.25"	0.35"
2	0.15"	0.25"	0.35"
3	0.15"	0.25"	0.35"
4	0.15"	0.25"	0.35"
5	0.15"	0.25"	0.35"

(ii) WITH INNER-CURVED WALL AND INTERNAL GUIDE VANES

Expt. No.	Difference in level in the differential manometer corresponding to two points before and after the bend on the		
	Intrados	Sides	Extrados
1	0.00"	0.05"	0.2"
2	0.01"	0.05"	0.2"
3	0.01"	0.05"	0.2"
4	0.00"	0.05"	0.2"

The above readings have to be multiplied by $(\gamma - 1)$ to obtain the head loss in inches of water. γ = specific gravity of the manometer liquid = 1.047.

THE OUTPUT OF THE COMPUTER PROGRAMME AS PER APPENDIX 1 and 2

Table 4

I

The value of λ	The difference between computed value & 1 foot
1.0980	- 0.0068
1.0990	- 0.0017
1.1000	+ 0.0033
1.1010	+ 0.0083

HENCE λ = 1.0993

II THE SHAPE OF THE INNER-CURVED WALL

Table 5

x (inches)	y (inches)
0.0	12.0
0.130	10.708
0.662	8.497
1.466	6.546
2.448	4.939
3.595	3.595
4.939	2.448
6.546	1.466
8.497	0.662
10.708	0.130
12.00	0.0

The shape of the inner-curved wall has been plotted in figure 21.

III TO CALCULATE THE SHAPE OF THE INTERNAL GUIDE VANES

(a) Calculation of the point on the line BF(Fig.3)

(The output of the numerical integration for the range of ζ from -1 to $-e^{-i\beta}$)

Table 6

Value of	Real part (in feet)	Imaginary part (in feet)
5	0.01593	-0.01593
10	0.03226	-0.03226
15	0.04898	-0.04898
20	0.06611	-0.06611
25	0.08366	-0.08366
30	0.10164	-0.10165
35	0.12008	-0.12008
40	0.13898	-0.13898
45	0.15836	-0.15836
50	0.17824	-0.17824
55	0.19865	-0.19865
60	0.21961	-0.21961
65	0.24114	-0.24114
70	0.26327	-0.26327
75	0.28604	-0.28604
80	0.30948	-0.30948
85	0.33364	-0.33364
90	0.34855	-0.34855
95	0.38429	-0.38429
100	0.41091	-0.41091
105	0.43848	-0.43848
110	0.46710	-0.46710
115	0.49686	-0.49686
120	0.52710	-0.52710

(continued)

125	0.55726	-0.55726
130	0.58880	-0.58880
135	0.62192	-0.62192
140	0.65692	-0.65692
145	0.69416	-0.69416
150	0.73414	-0.73414
155	0.77760	-0.77760
160	0.82565	-0.82565
165	0.88016	-0.88016
170	0.94481	-0.94481
175	1.02905	-1.02905

IV <u>TO CALCULATE THE SHAPE OF THE INTERNAL GUIDE VANES (THE OUTPUT OF THE NUMERICAL INTEGRATION FOR THE RANGE OF ζ FROM $-e^{-i\beta}$ TO $-re^{-i\beta}$).</u>

(a) For $c/_a = 3/4$ or $\beta = 45^0$

<u>Table 7</u>

Radius	Real part (in inches)	Imaginary part (in inches)
1.50	0.86003	0.09495
2.0	1.55612	1.87644
2.5	2.03049	2.61780
3.0	2.37788	3.23439
5.0	3.17568	4.99518
7.0	3.57588	6.16991
9.0	3.8130	7.05136
11.0	3.98053	7.75725
13.0	4.09606	8.34651
15.0	4.18190	8.85272
17.0	4.24773	9.29690

(continued)

19.0	4.29951	9.69198
21.0	4.34109	10.05065
23.0	4.37508	10.37689
25.0	4.40331	10.67693
27.0	4.42707	10.95476
29.0	4.44732	11.21351
31.0	4.46476	11.45568
33.0	4.47993	11.68330
35.0	4.49324	11.89802
37.0	4.50501	12.10125
39.0	4.51548	12.19418
41.0	4.52487	12.47780
43.0	4.53332	12.65298
45.0	4.54097	12.82045
47.0	4.54793	12.98086
49.0	4.55429	13.13480
51.0	4.56012	13.28276

(b) For $^{c}/_{a} = 1/2$ or $\beta = 90^{o}$

Table 8

Radius	Real part (in inches)	Imaginary part (in inches)
1.5	1.25883	1.45323
2.0	2.04327	2.61580
2.5	2.56137	3.54068
3.0	2.93900	4.32403
5.0	3.74230	6.43567
7.0	4.12874	7.80619
9.0	4.35912	8.81597
11.0	4.51301	9.61400

(continued)

13.0	4.62339	10.27326
15.0	4.70653	10.83472
17.0	4.77142	11.32361
19.0	4.82348	11.75654
21.0	4.86617	12.14502
23.0	4.09181	12.49734
25.0	4.93200	12.81968
27.0	4.95789	13.11676
29.0	4.98035	13.39225
31.0	5.0000	13.64911
33.0	5.01735	13.88967
35.0	5.03276	14.11591
37.0	5.04655	14.32944
39.0	5.05896	14.53162
41.0	5.07019	14.72358
43.0	5.08039	14.90632
45.0	5.08970	15.08069
47.0	5.09823	15.24742
49.0	5.10608	15.40715
51.0	5.11331	15.45044
53.0	5.12002	15.70782
55.0	5.12623	15.84969
57.0	5.13202	15.98647
59.0	5.13741	16.11850
61.0	5.14246	16.24612
63.0	5.14719	16.36961
65.0	5.15164	16.48921
67.0	5.15582	16.60519
69.0	5.15975	16.71773
71.0	5.16347	16.82704
73.0	5.16698	16.93332
75.0	5.17031	17.03671

(continued)

77.0	5.17347	17.13737
79	5.17647	17.23544
83	5.18204	17.42433
87	5.18709	17.60431
91	5.19170	17.77617
95	5.19592	17.94063
99	5.19981	18.09828
103	5.20340	18.24986
107	5.20671	18.39531
111	5.20979	18.53558
115	5.21265	18.67087
119	5.21532	18.80153
123	5.21781	18.92786
127	5.22016	19.05016
131	5.22235	19.16864
135	5.22442	19.28357
139	5.22637	19.39513
143	5.22820	19.50351
147	5.22994	19.60890
151	5.23158	19.71147
155	5.23314	19.81136
159	5.23462	19.90869
163	5.23603	20.00360
167	5.23737	20.09621
171	5.23865	20.18663
175	5.23987	20.27495
181	5.24159	20.40372
185	5.24268	20.48721
189	5.24372	20.56892
193	5.24422	20.64893
197	5.24567	20.72726
201	5.24650	20.80405

(c) For $^{c}/_{a} = 1/4$ or $\beta = 135^{0}$

Table 9

Radius	Real part (in inches)	Imaginary part (in inches)
3.0	3.16775	5.94243
5.0	3.75179	8.52136
7.0	4.00577	10.10204
9.0	4.15114	11.23433
11.0	4.24634	12.11397
13.0	4.31394	12.83212
15.0	4.36461	13.43836
17.0	4.40410	13.96260
19.0	4.43578	14.42424
21.0	4.46180	14.83653
23.0	4.48356	15.20896
25.0	4.50204	15.54850
29	4.53176	16.14899
33	4.55463	16.66815
37	4.57279	17.12531
43	4.59396	17.72264
47	4.60520	18.07466
51	4.61474	18.39700
55	4.62229	18.69462
59	4.63006	18.97009
63	4.63631	19.22736
71	4.64676	19.69510
79	4.65514	20.11180
87	4.66202	20.48749
95	4.66778	20.82953
103	4.67265	21.14343
111	4.67683	21.43350
119	4.68045	21.70308
127	4.68363	21.95490

(continued)

135	4.68643	22.19110
143	4.68892	22.41357
151	4.69115	22.62378
159	4.69316	22.82301
167	4.69497	23.01237
175	4.69662	23.19278
183	4.69813	23.36504
191	4.69951	23.52988
199	4.70078	23.68787
201	4.70108	23.72638

Table 10

Average Velocity $V_2 = 0.344$ ft/sec

	V_1	$\frac{(V_1-V_2)^2}{2g}$	Measured Head loss	Head Loss in feet of water	Head Loss due to Laminar Boundary layer	$\Delta H = (4)-(5)$	$(6)/(2)$	$K = \frac{(6)}{V_2^2/2g}$
Mitre bend	(1)	(2)	(3)	(4)	(5)	(6)	(7)	(8)
(i) Uniform Velocity	0.544	0.00062	0.275"	0.00107	0.000115	0.00096	1.55	0.52
(ii) Maximum along intrados	0.90	0.00475	1.0"	0.00391	0.000115	0.0038	0.8	2.1
(iii) Maximum along extrados	0.60	0.00101	1.585"	0.00621	0.000115	0.0061	6	3.3
Inner-Curved wall								
(i) Uniform Velocity	0.544	0.00062	0.25"	0.00097	0.000115	0.00086	1.391	0.47
(ii) With maximum along intrados	0.70	0.00196	0.325"	0.00127	0.000115	0.00115	0.6	0.64
(iii) With maximum along extrados	0.6	0.00101	1.1125"	0.00436	0.000115	0.00425	4	2.3
Inner-Curved wall and Internal Guide Vanes								
(i) Uniform Velocity	-	-	0.0775"	0.00030	0.00023	0.00007	-	0.04
(ii) With maximum along intrados	-	-	0.325"	0.00127	0.00023	0.00104	-	0.57
(iii) With maximum along extrados	-	-	0.775"	0.00304	0.00023	0.0028	-	1.5

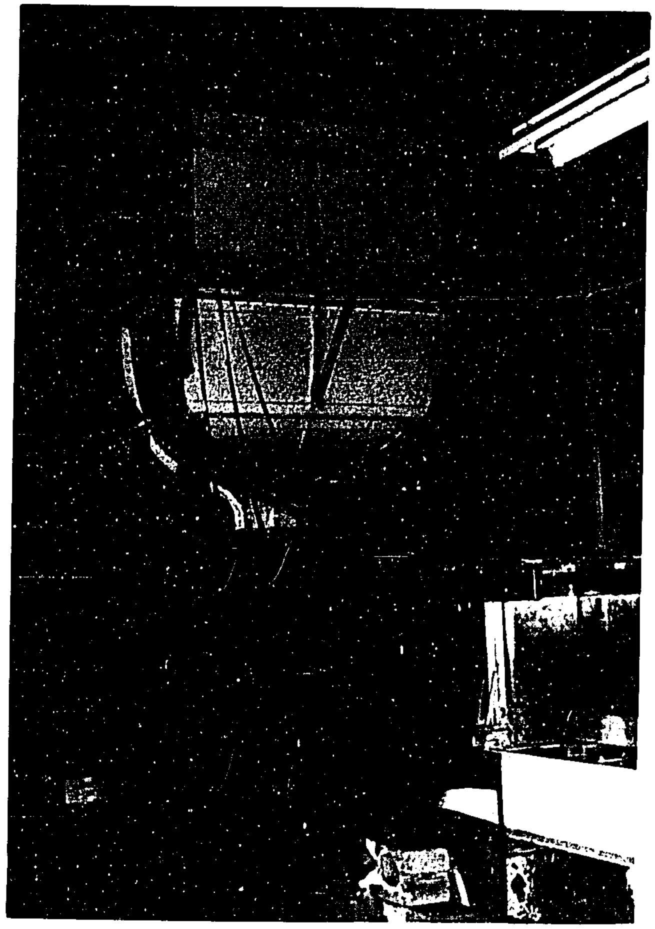

Plate No.1. Photograph of the Experimental Set up

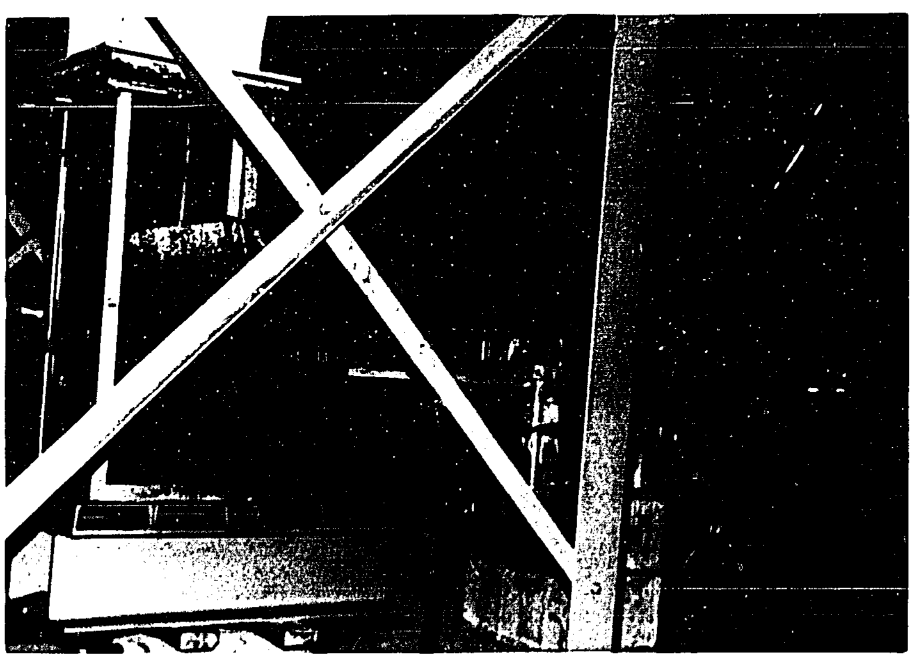

Plate No.2. Lucite Duct Covered with Aluminum Frame.

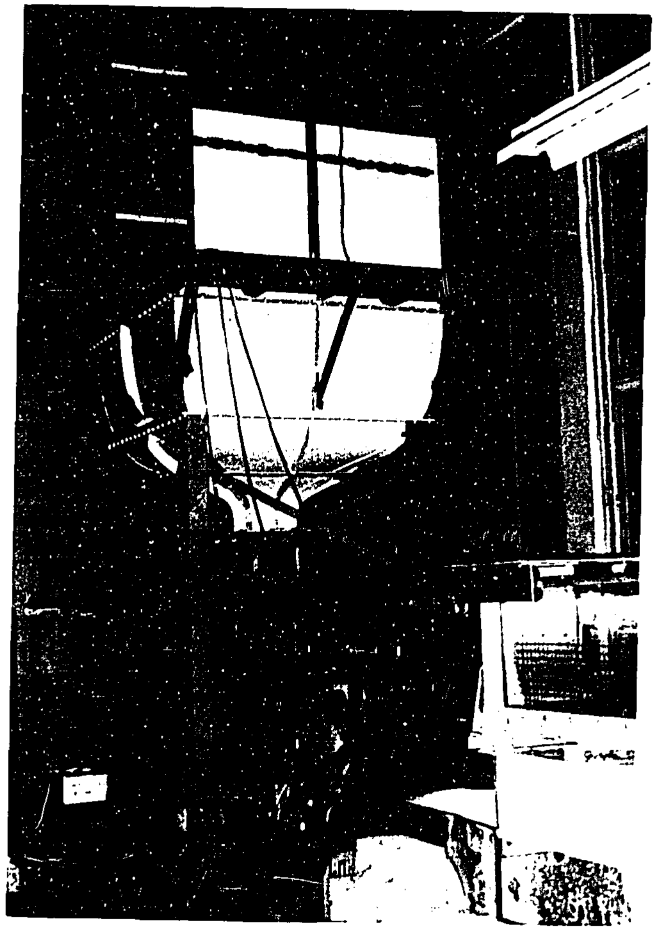

Plate No.1. Photograph of the Experimental Set up

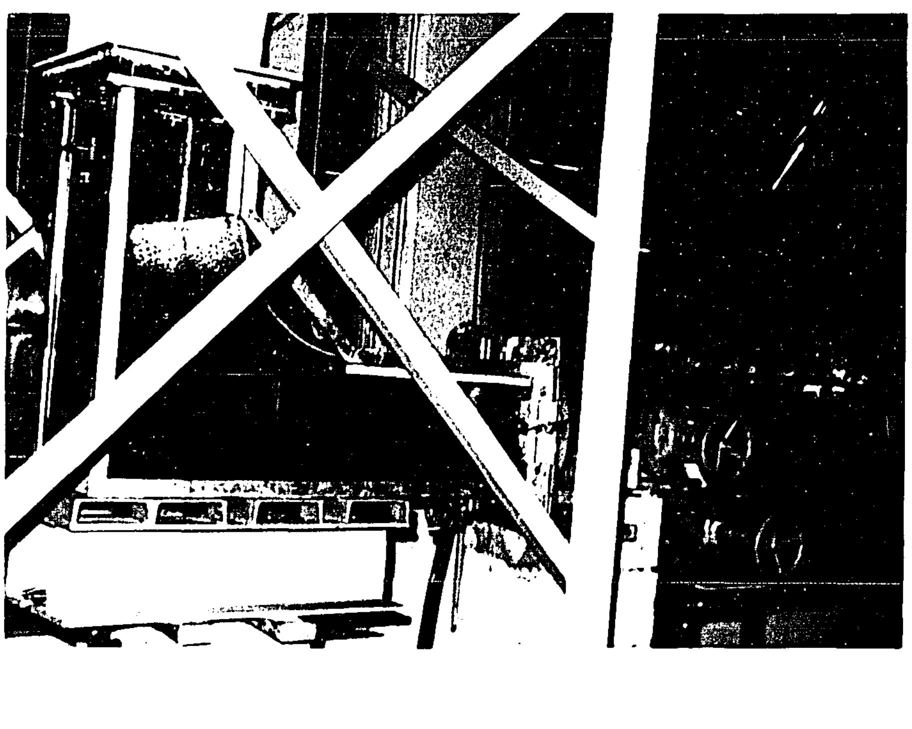

Plate No.2. Lucite Duct Covered with Aluminum Frame.

Plate No.3. The Differential Manometer

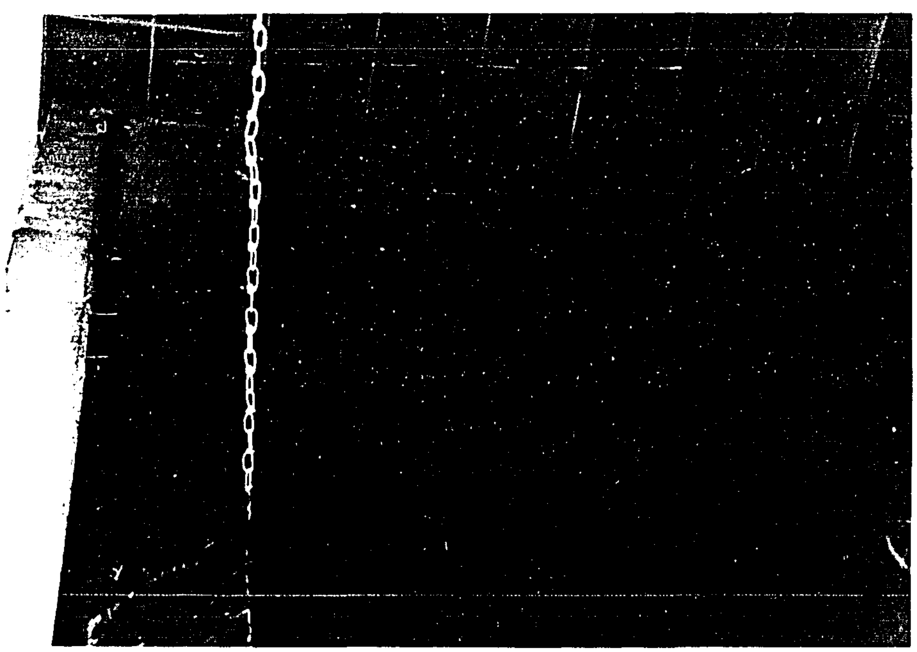

Plate 4. The Weir Construction at the top of the tank

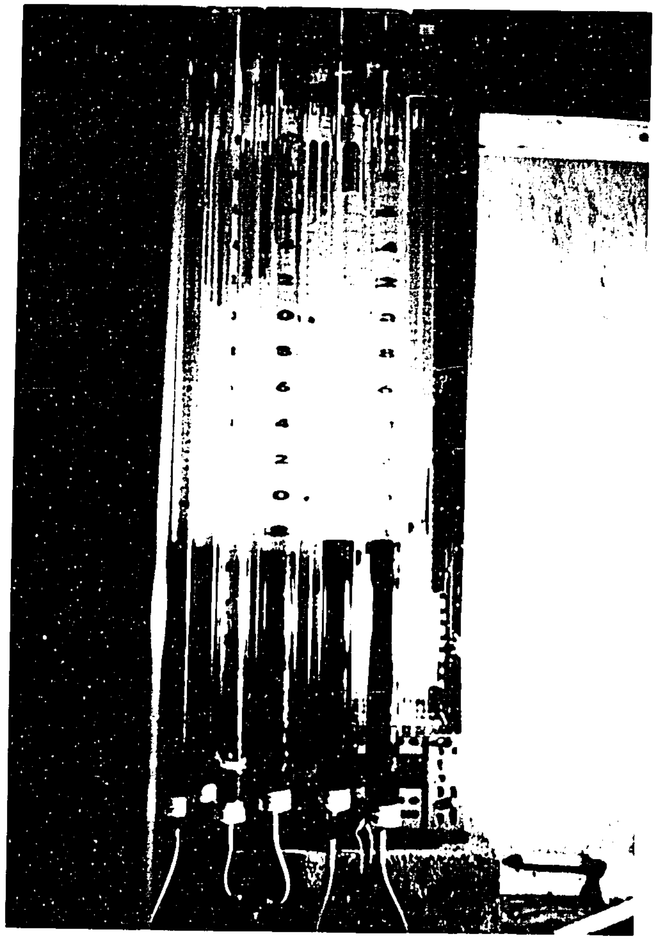

Plate No.3. The Differential Manometer

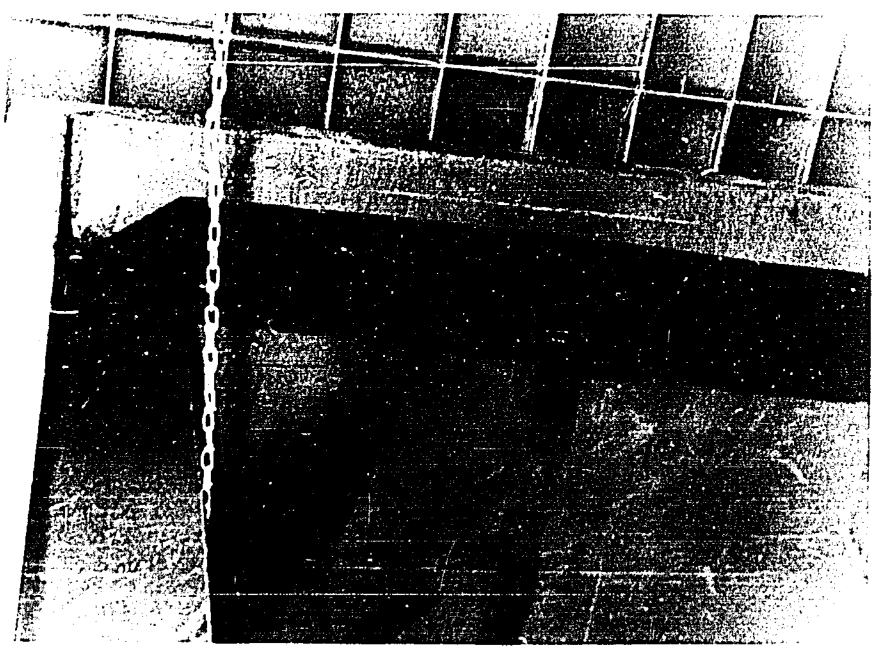

Plate 4. The Weir Construction at the top of the tank

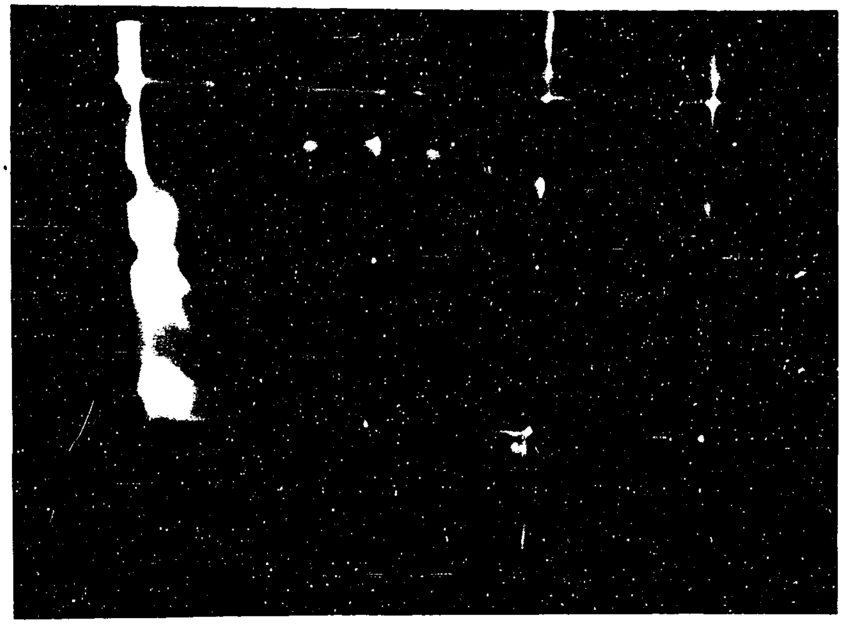

(a) Velocity Measurements in the Horizontal portion of the duct

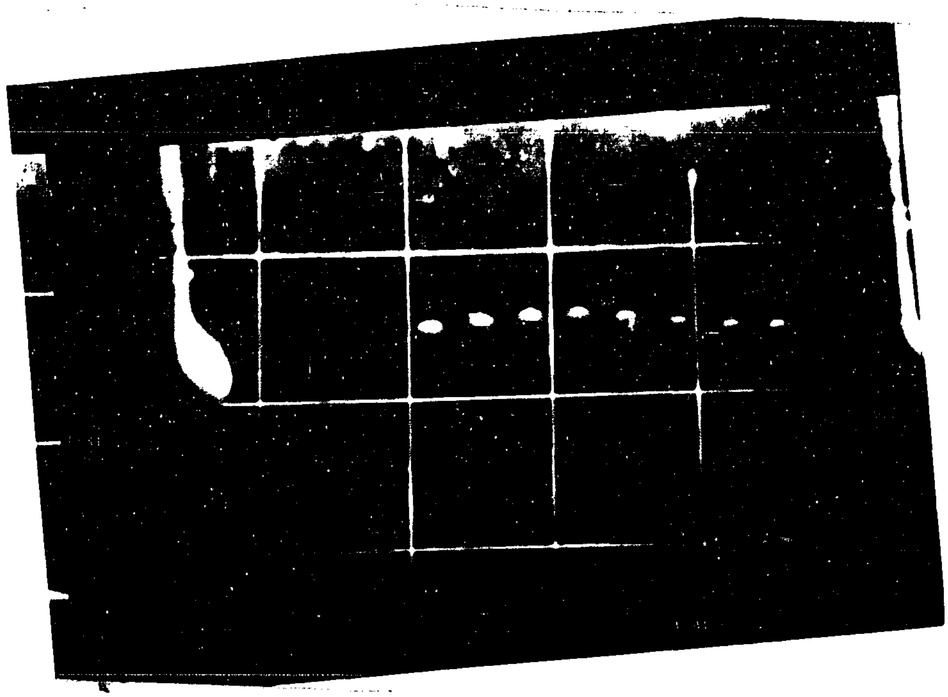

Plate.No.5.(b) Velocity Measurements in the horizontal portion of the duct

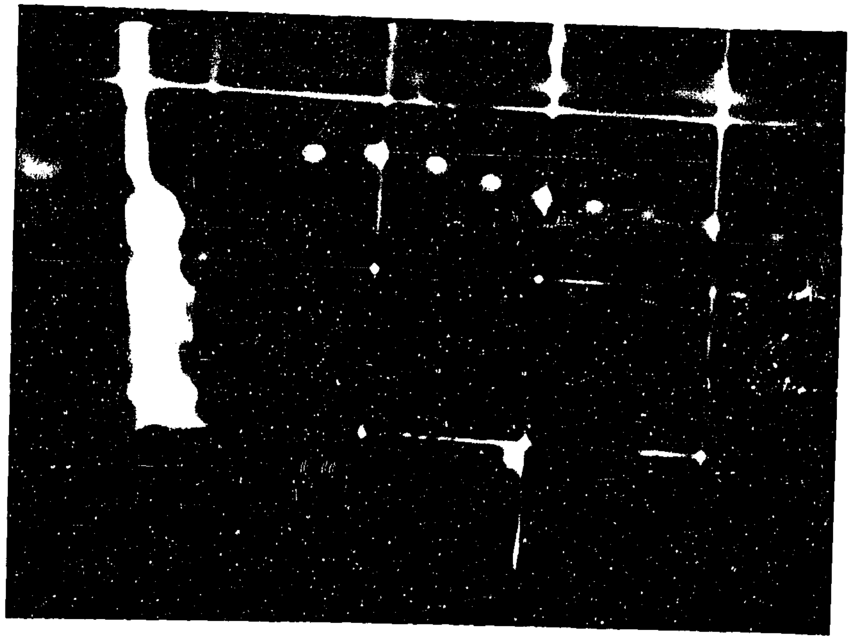

(a) Velocity Measurements in the Horizontal portion of the duct

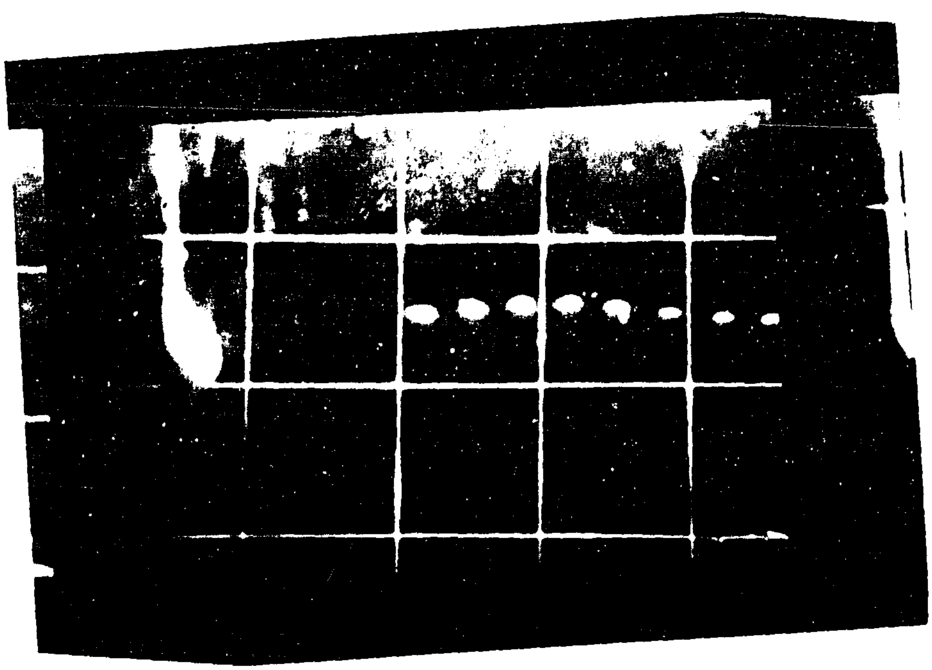

Plate.No.5.(b) Velocity Measurements in the horizontal portion of the duct

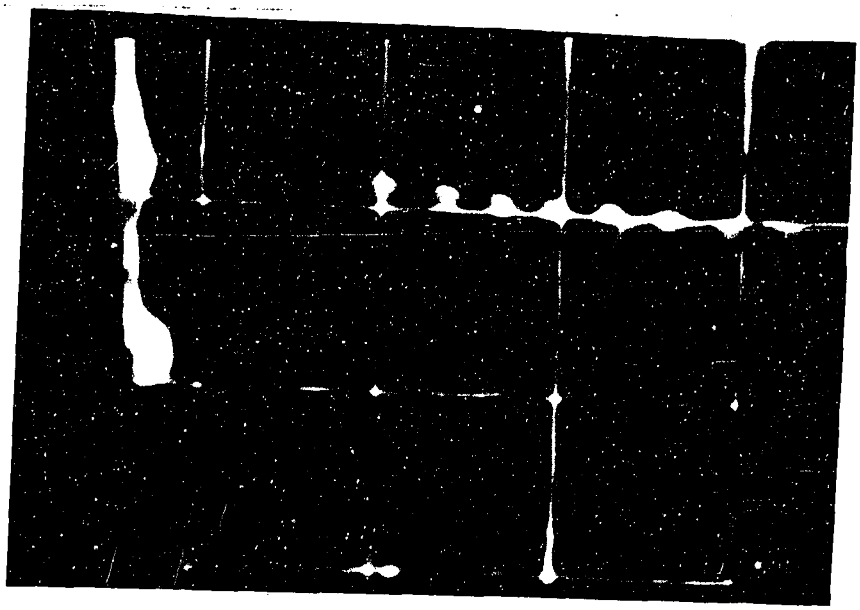

Plate No.6.(a) Velocity Measurements in the horizontal portion of the duct

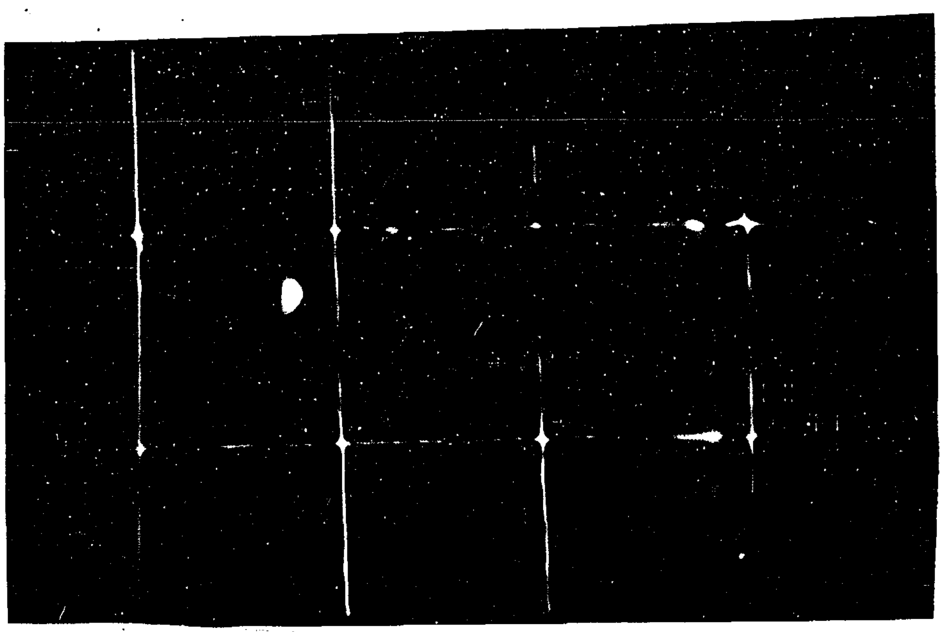

Plate No.6.(b) Velocity Measurements in the vertical portion of the duct

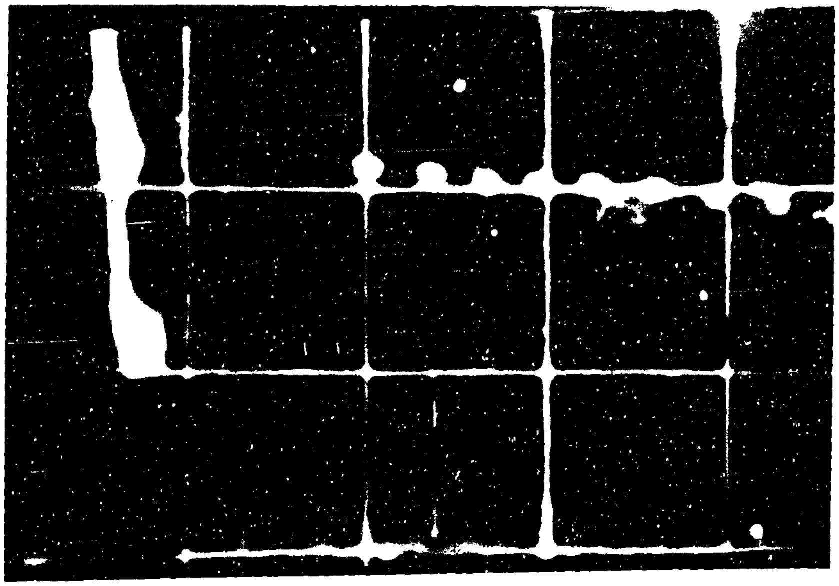

Plate No.6.(a) Velocity Measurements in the horizontal portion of the duct

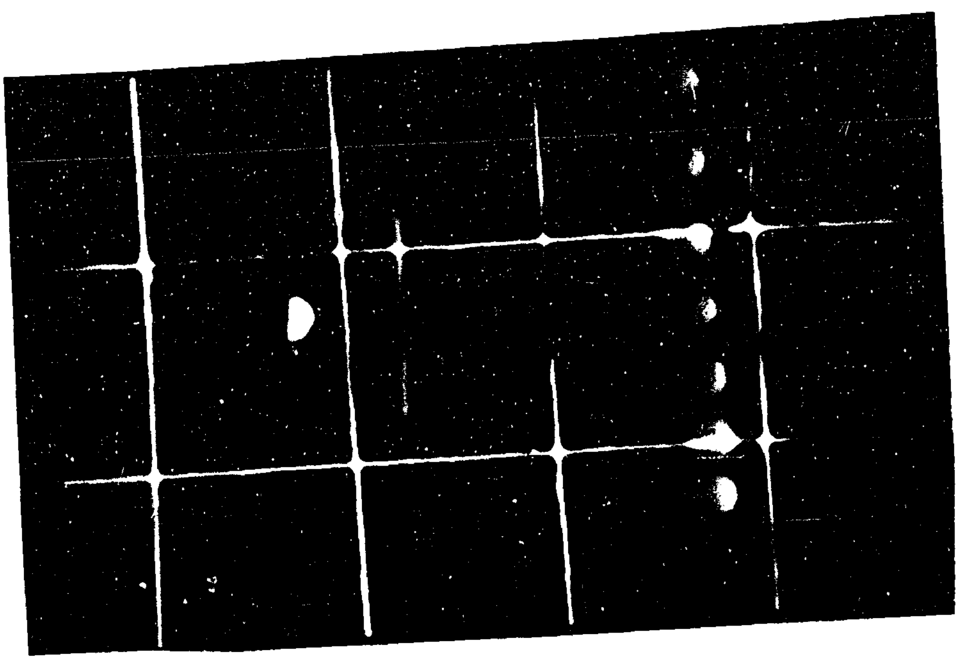

Plate No.6.(b) Velocity Measurements in the vertical portion of the duct

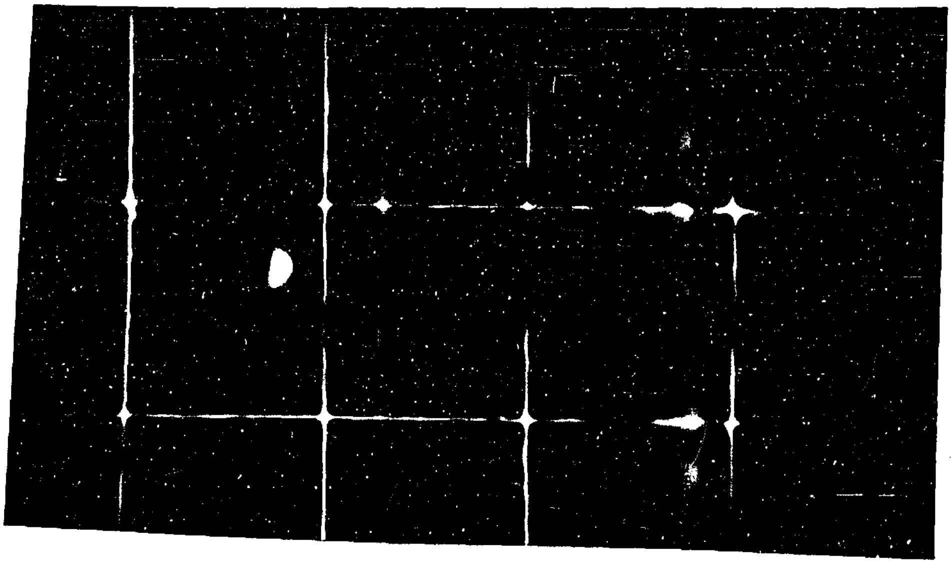

Plate No.7.(a) Velocity Measurements in the vertical portion of the duct

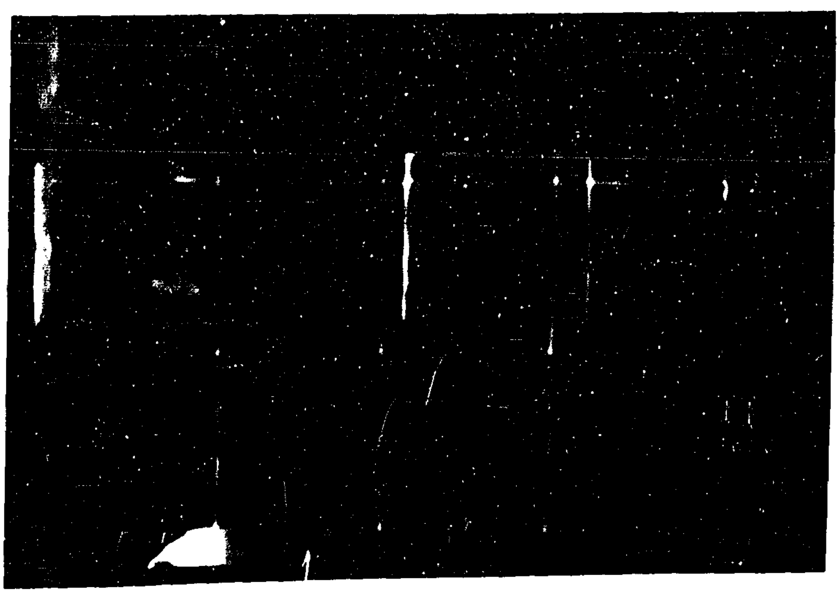

Plate No.7.(b) Velocity Measurements in the vertical portion of the duct.

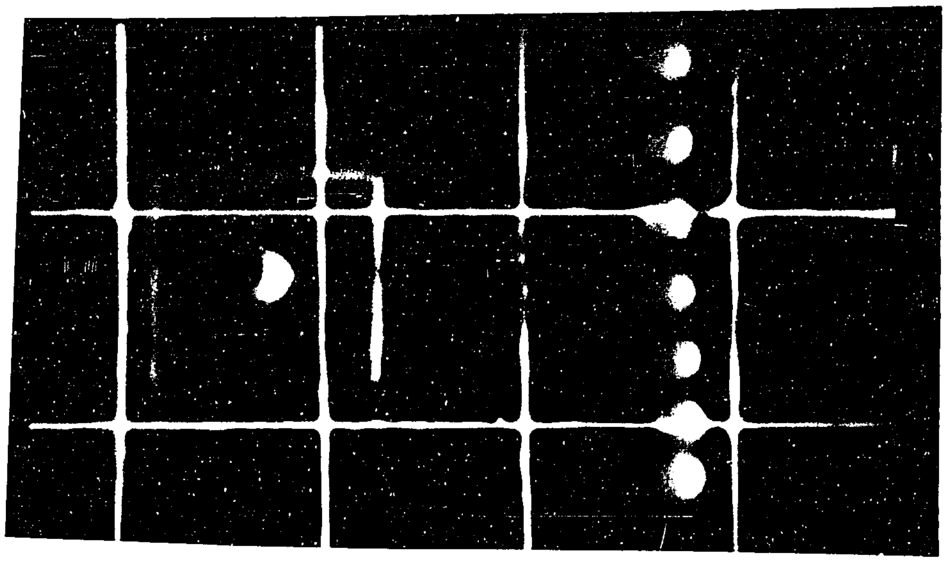

Plate No.7.(a) Velocity Measurements in the vertical portion of the duct

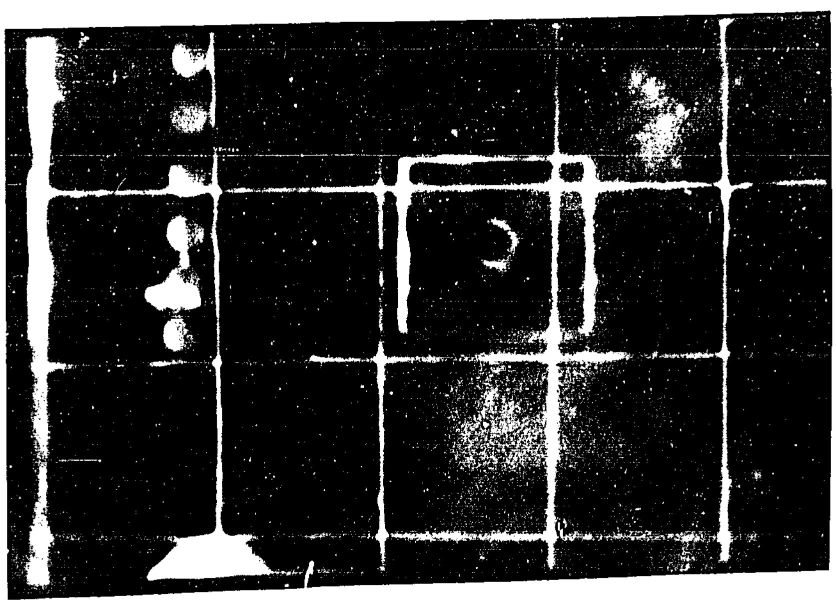

Plate No.7.(b) Velocity Measurements in the vertical portion of the duct.

Plate No.8. Lucite Duct Covered with frames all around

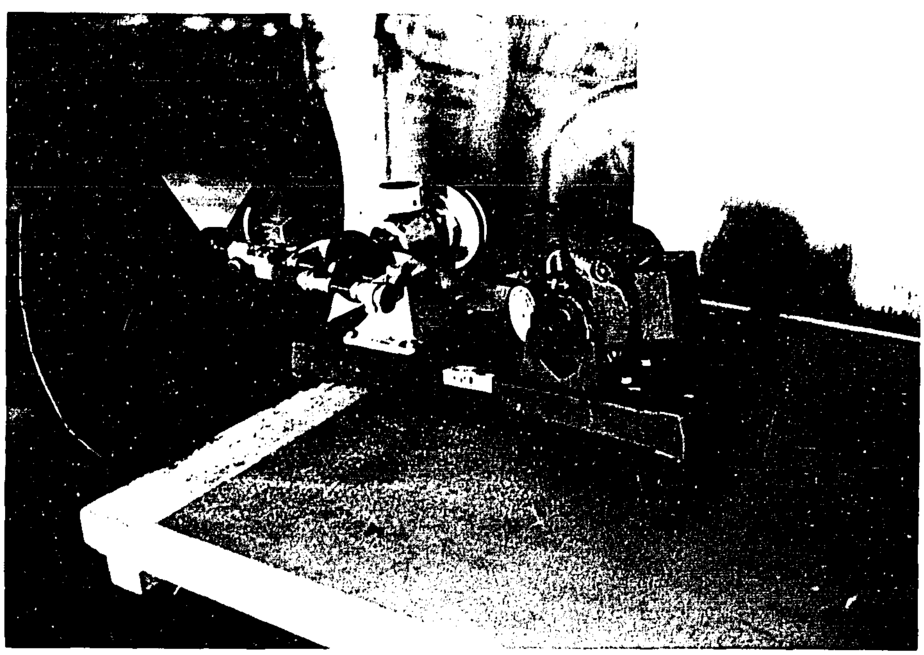

Plate No.9. The Equipment used for velocity measurement

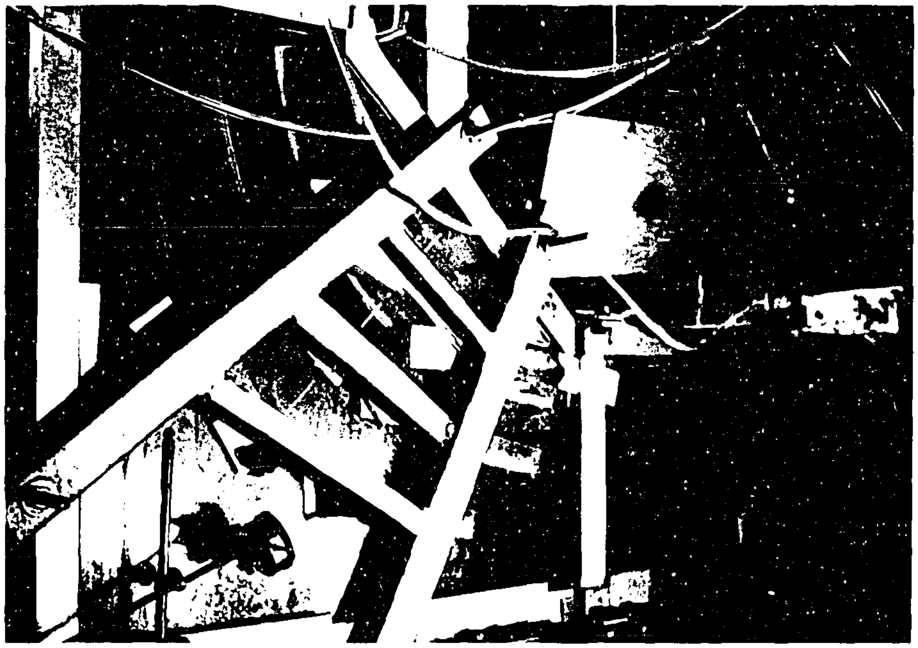

Plate No.8. Lucite Duct Covered with frames all around

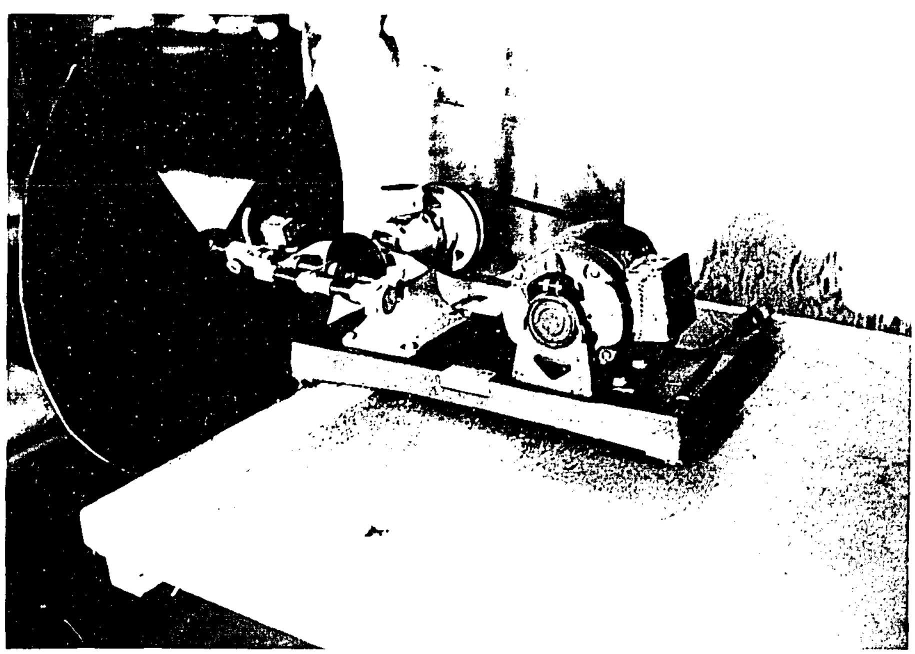

Plate No.9. The Equipment used for velocity measurement

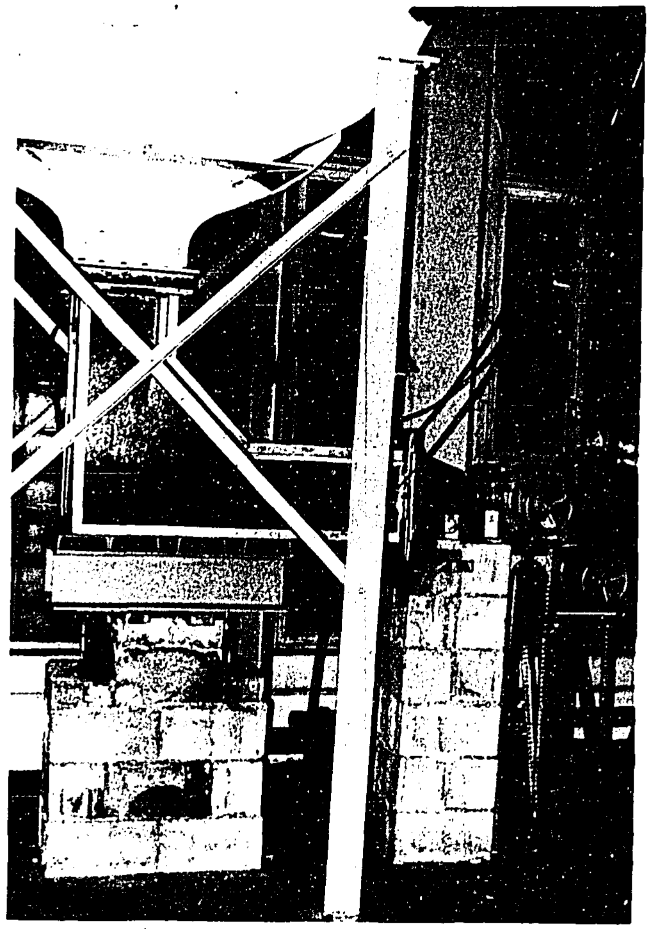

Plate No.10. Lucite Duct, Supporting Platform & Jacks

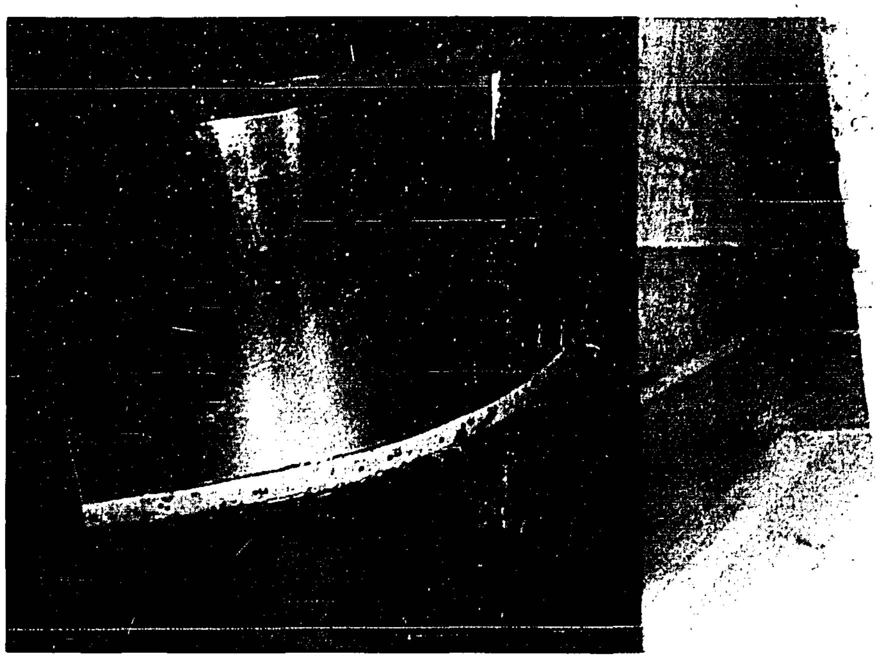

Plate No.11. An outside View of the Internal Guide Vanes

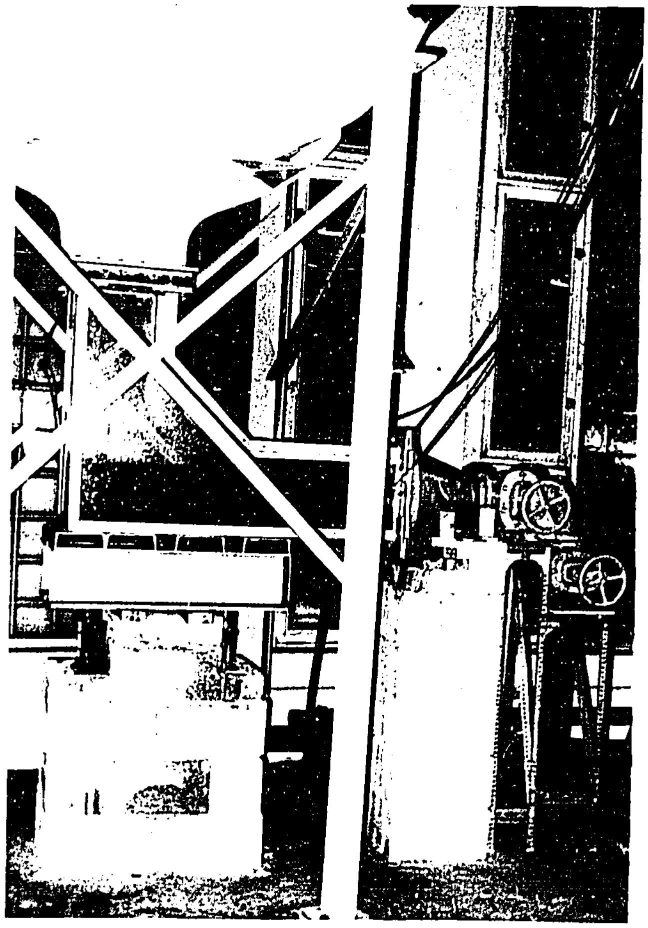

Plate No.10. Lucite Duct,Supporting Platform & Jacks

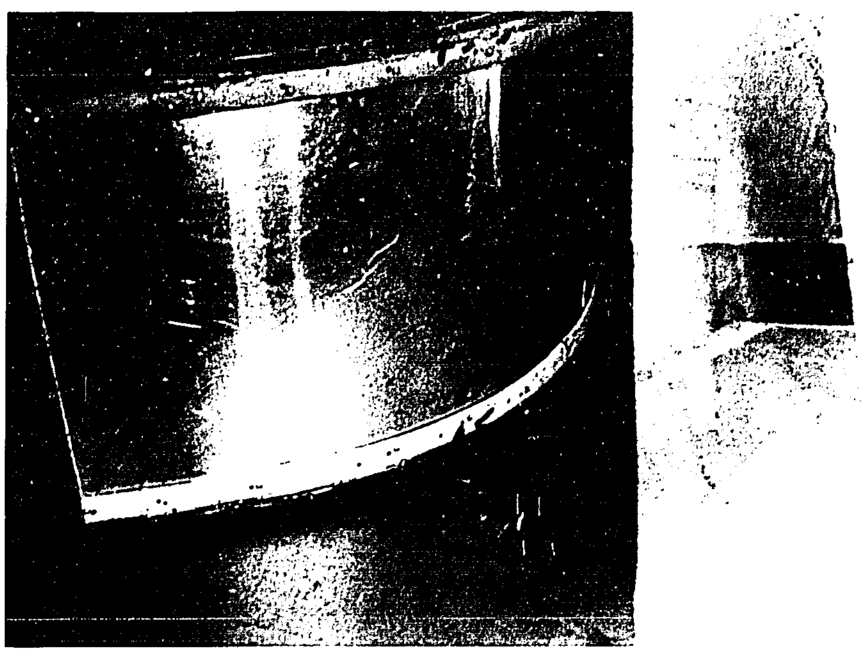

Plate No.11. An outside View of the Internal

Guide Vanes

Plate No.12. The Lucite Duct in Open Position

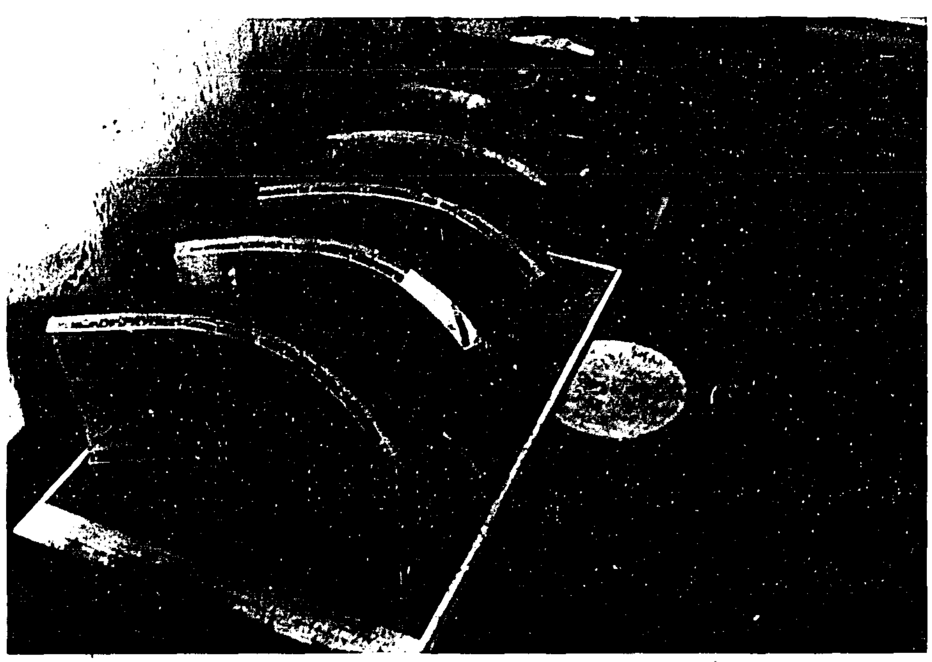

Plate No.13. An Inside View of the Guide Vanes

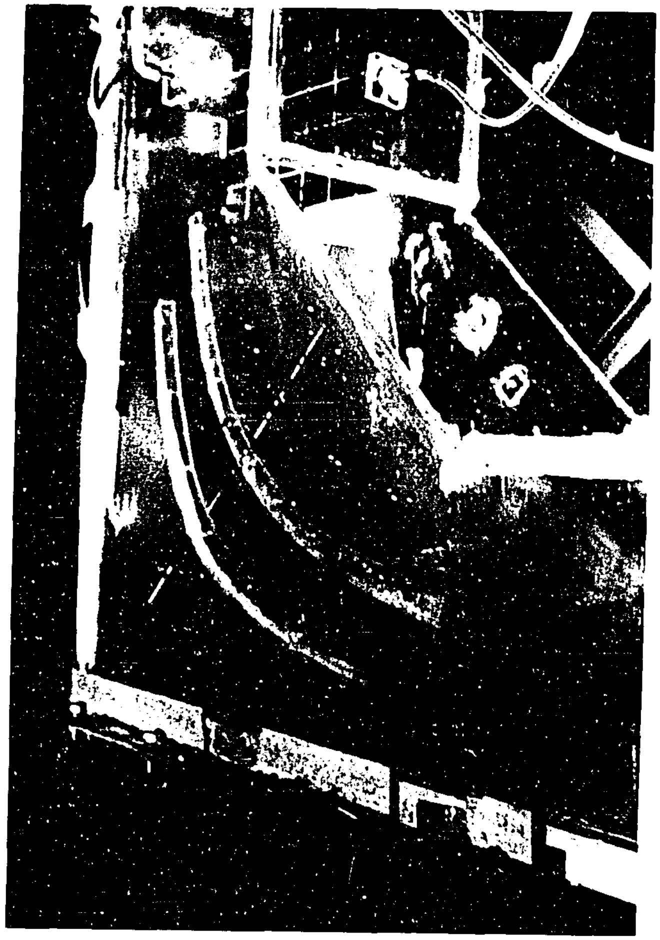

Plate No.12. The Lucite Duct in Open Position

Plate No.13. An Inside View of the Guide Vanes

WORKING SECTION IN POSITION

(The ladder, supporting frames
for the tank, and platform
not shown in this figure)

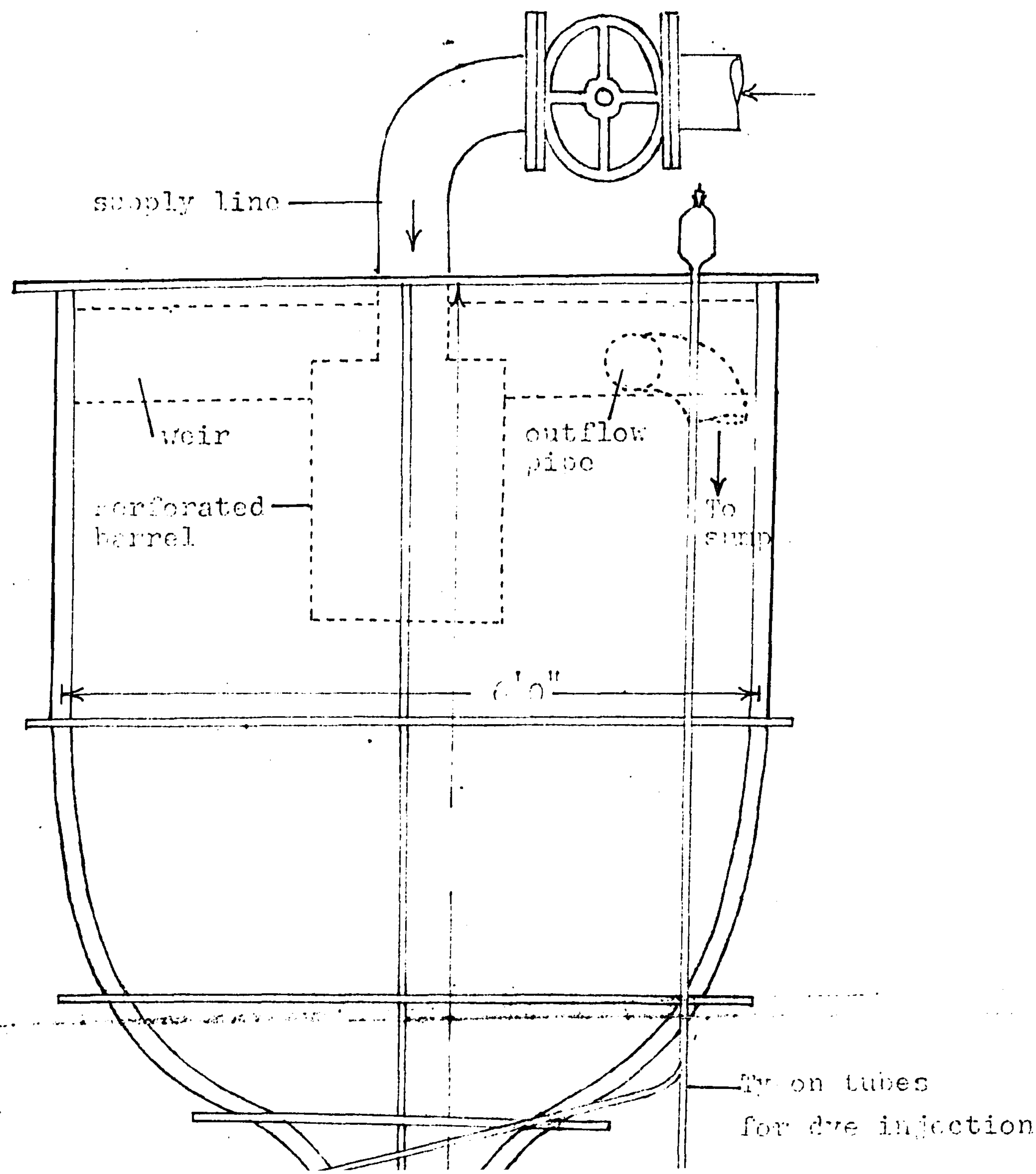

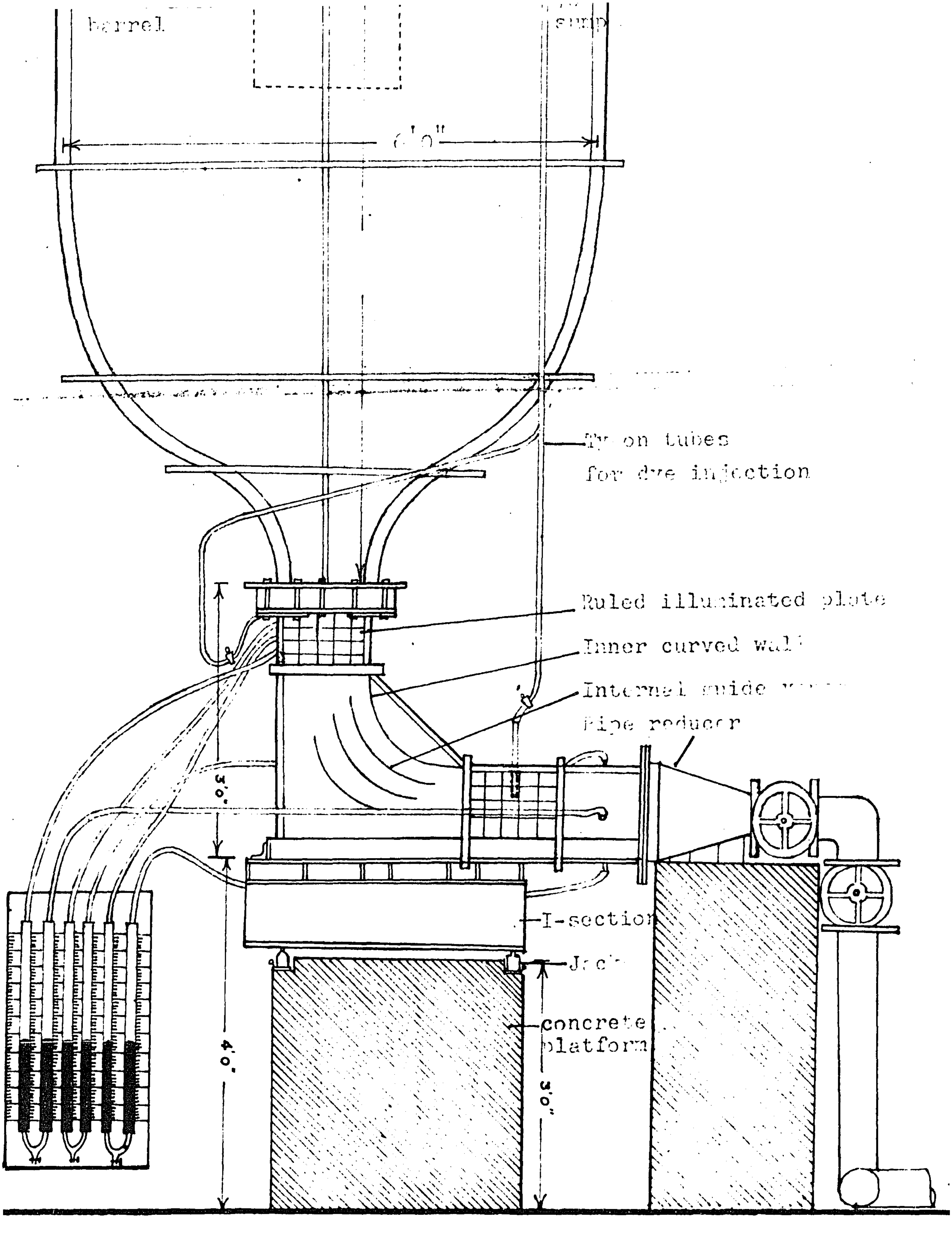
barrel
sump
6'0"
on tubes
for dye injection
Ruled illuminated plate
Inner curved wall
Internal guide
Pipe reducer
3'0"
I-section
concrete
platform
4'0"
3'0"

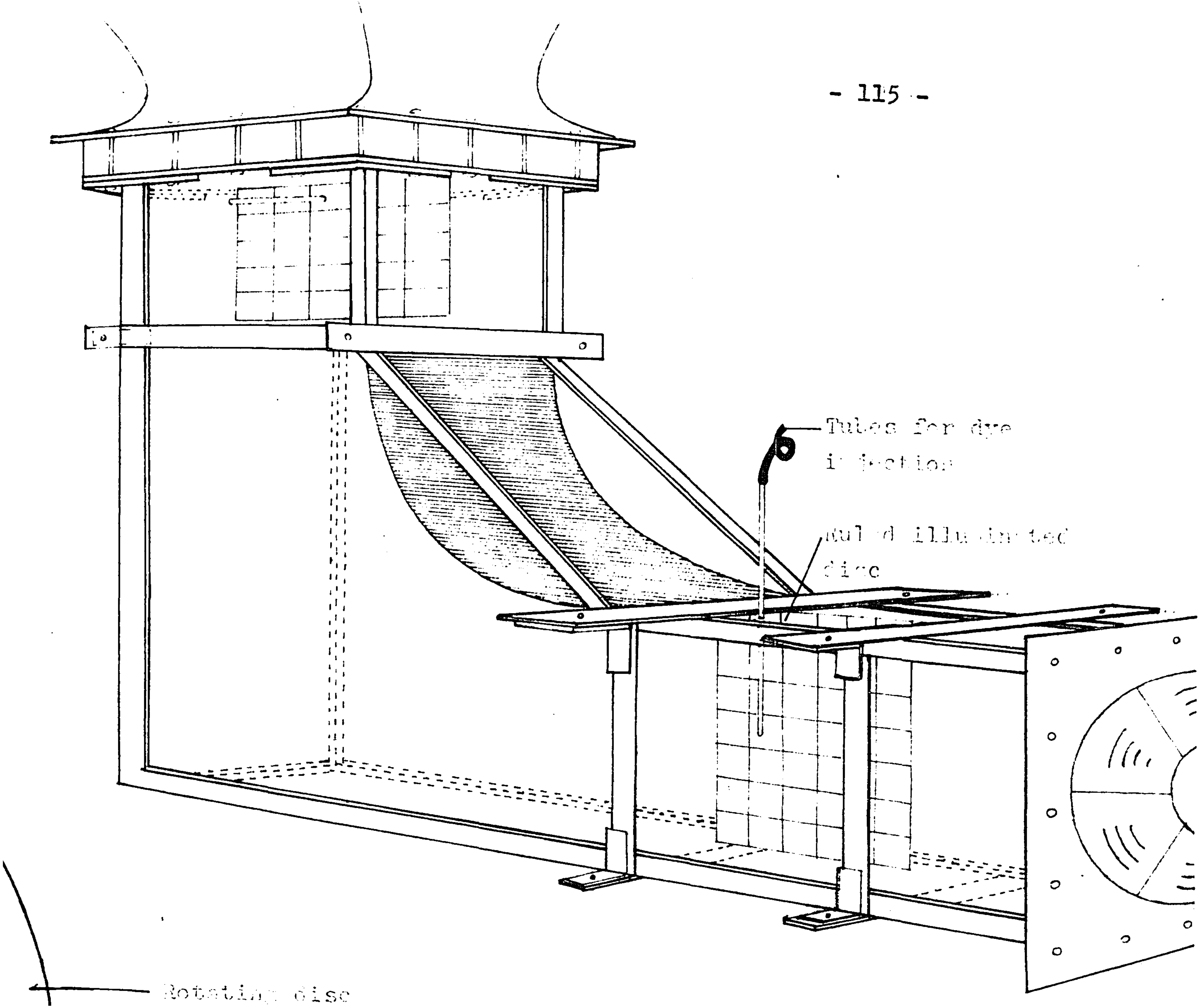
Tubes for dye
injection
Ruled illuminated
disc
Rotating disc

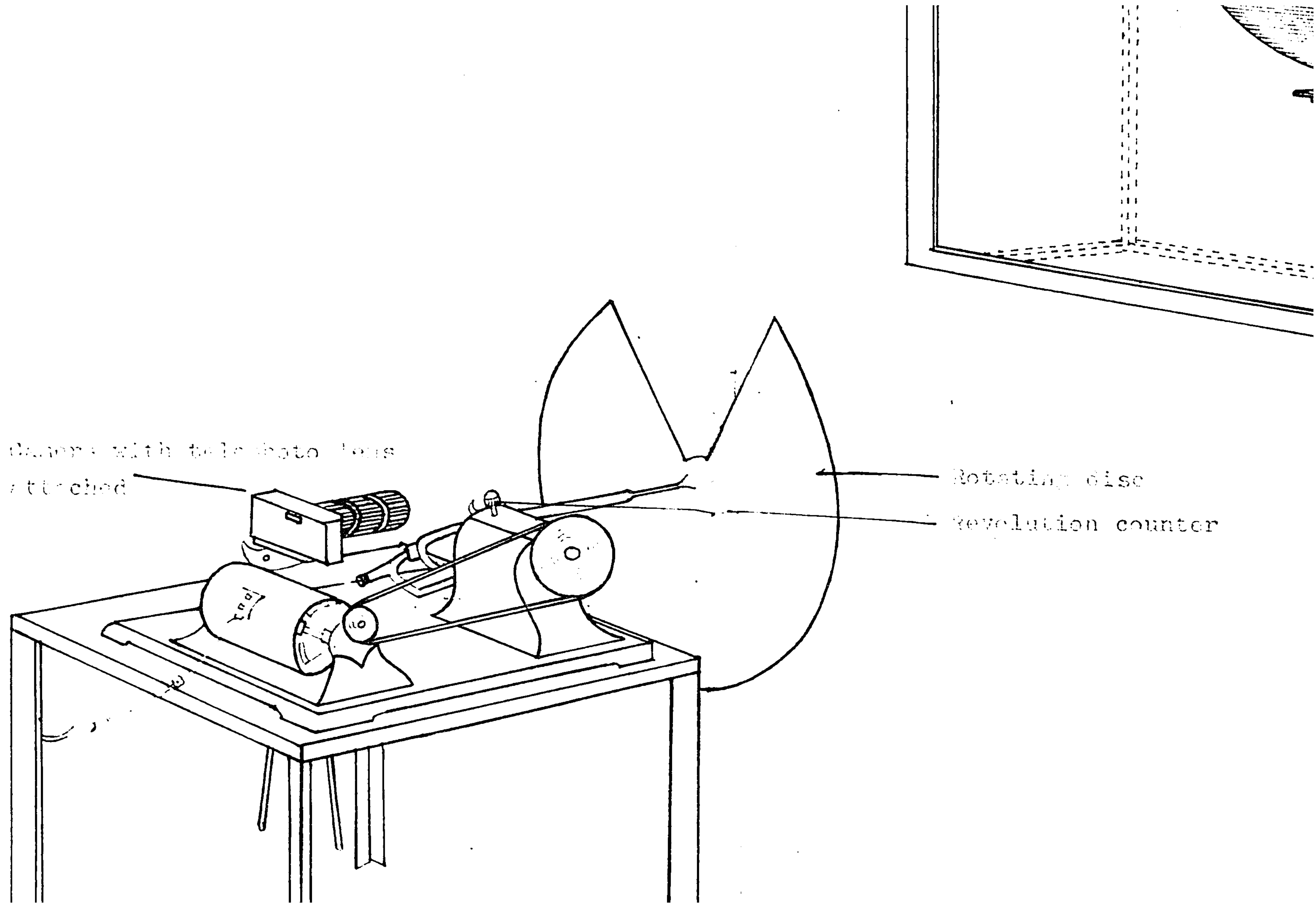
Camera with telephoto lens attached
Rotating disc
Revolution counter

RIGHT ANGLED DUCT WITH INNER CURVED WALL DESIGNED FOR CONSTANT VELOCITY

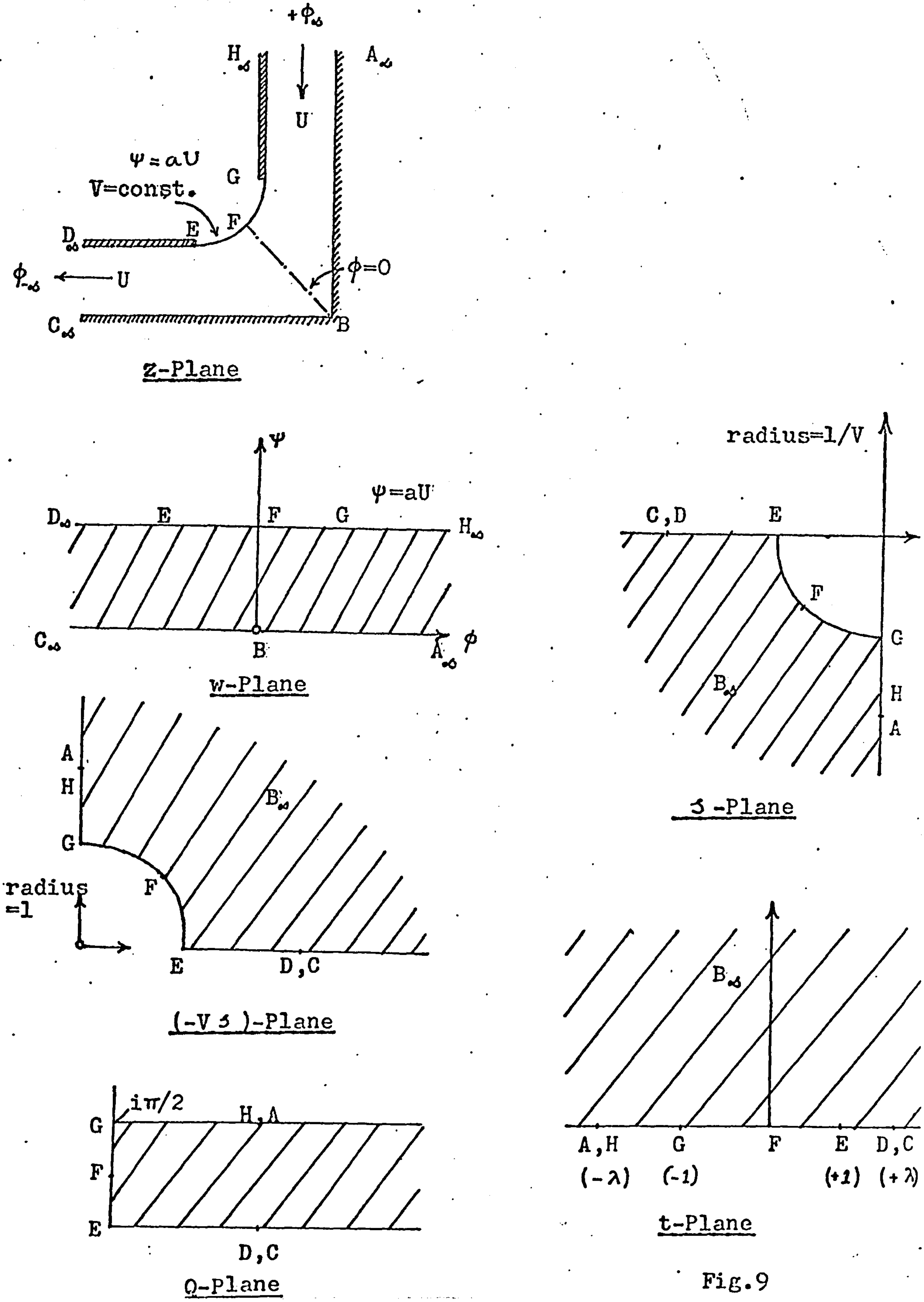

Fig.9

RIGHT ANGLED MITRE BEND

TRANSFORMATIONS USED

GRAPHICAL PRESENTATION

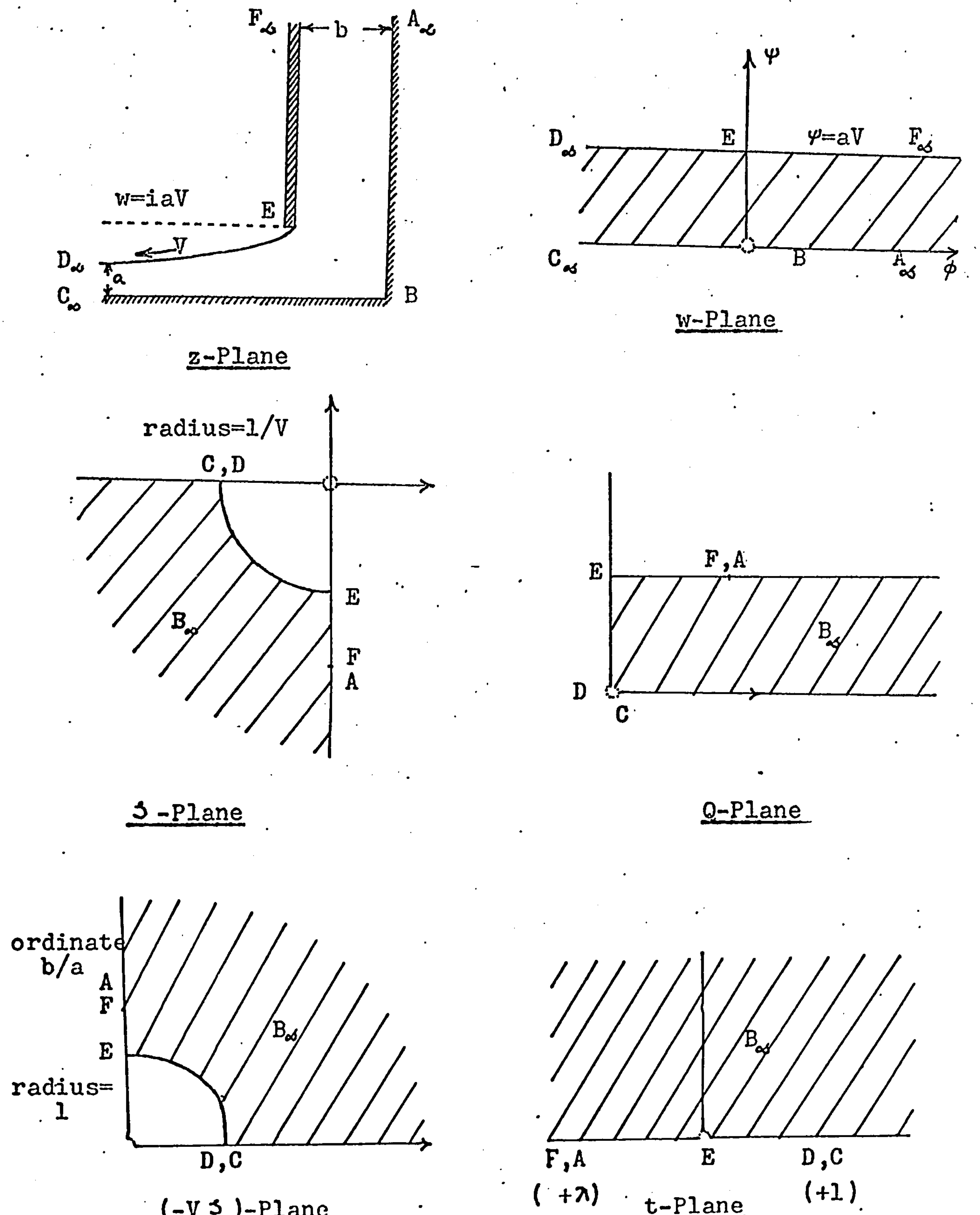

Fig.10.

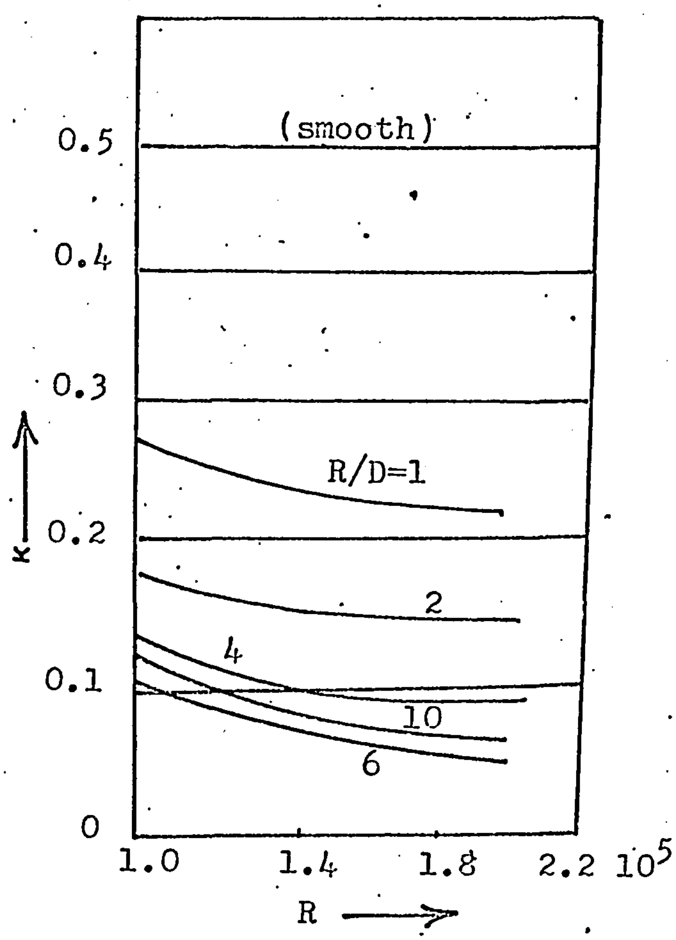

FIG.11. HEAD LOSS COEFFICIENTS FOR SMOOTH 90° BENDS

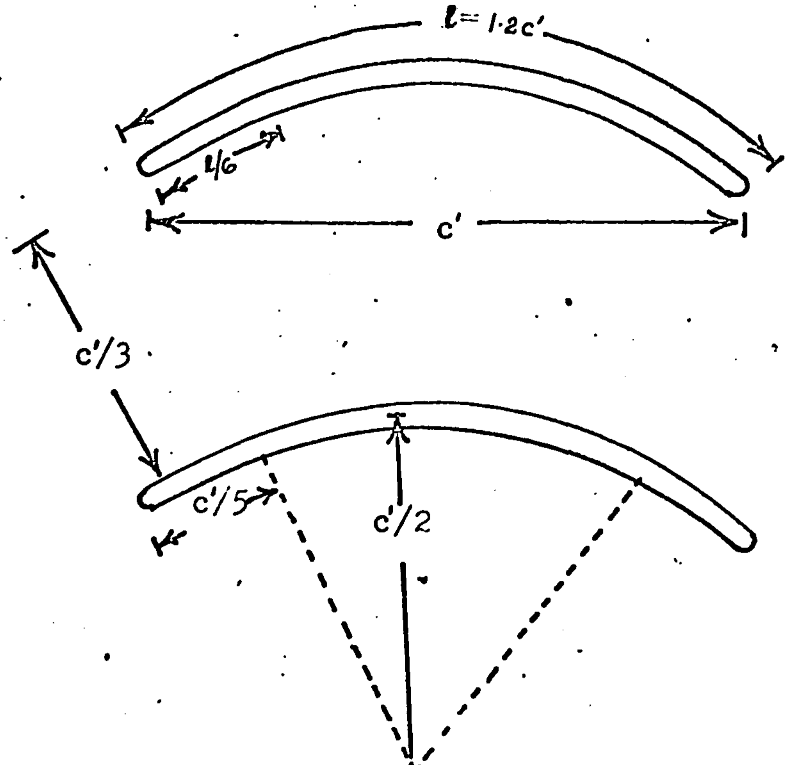

FIG. 12. DIMENSIONS OF DEFLECTING VANES FOR MITRE BENDS

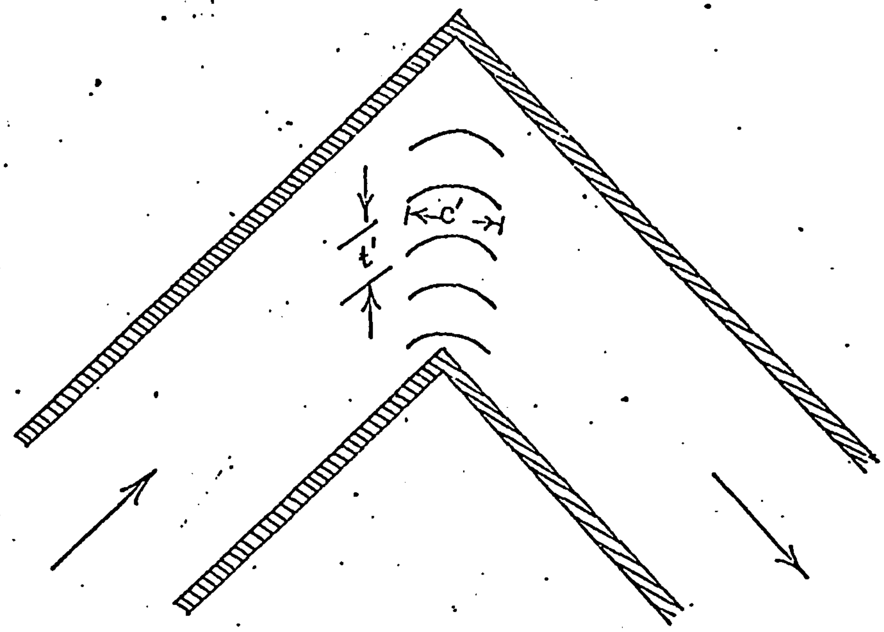

FIG. 13. SIMPLE VANE INSTALLATION FOR A 90° MITRE BEND

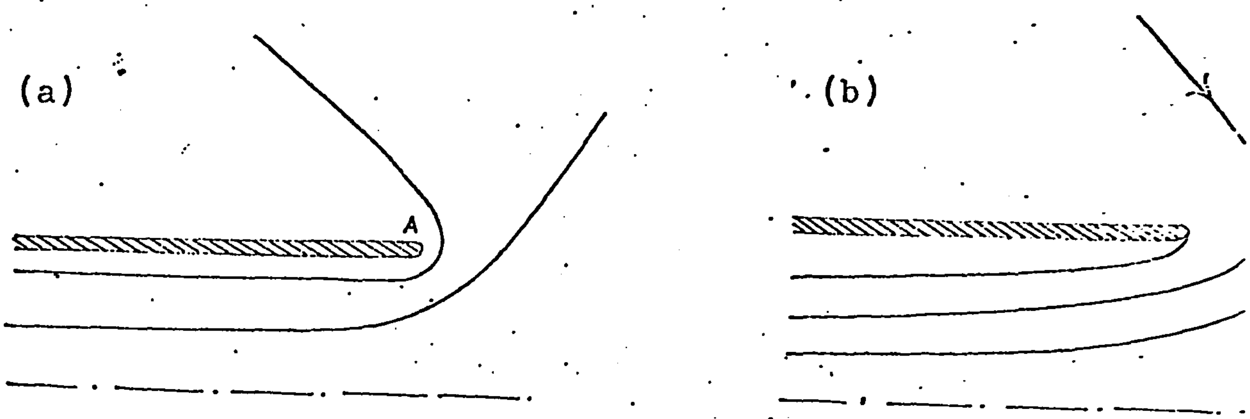

FIG. 14. COMPARISON OF ENTRANCE CONDITIONS

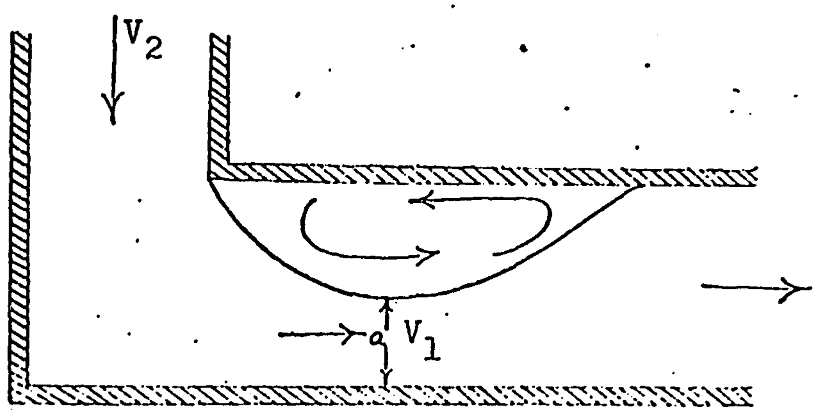

FIG. 15. LINE OF SEPARATION FOR MITRE BEND

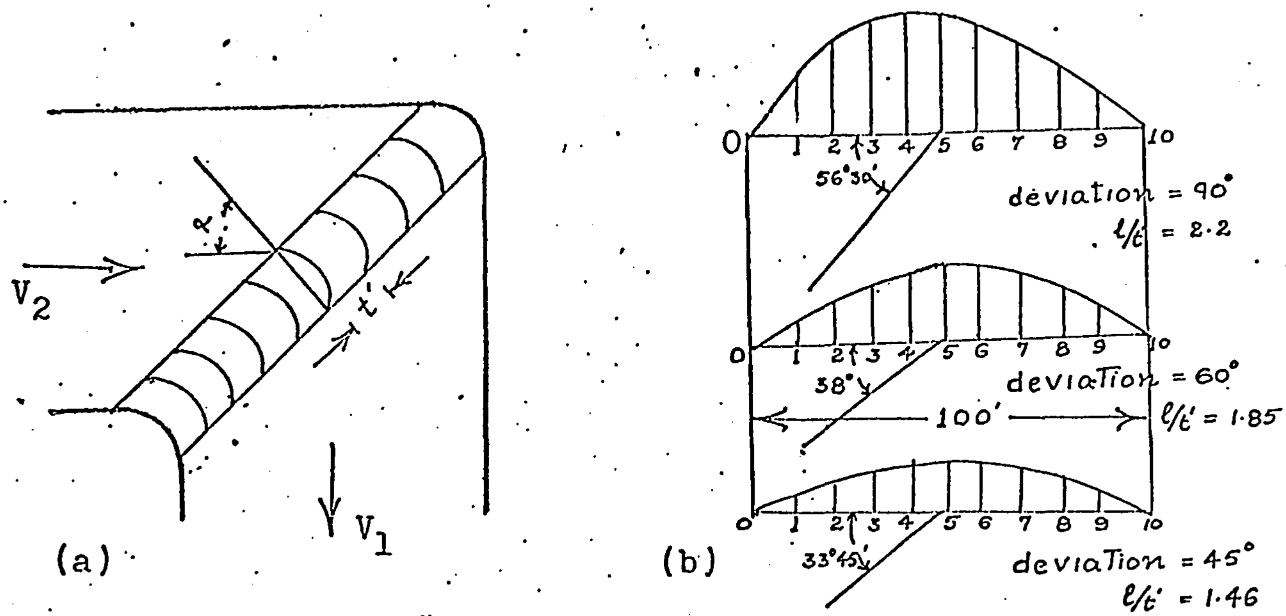

FIG. 16. KRÖBER PROFILES FOR DEFLECTING VANES

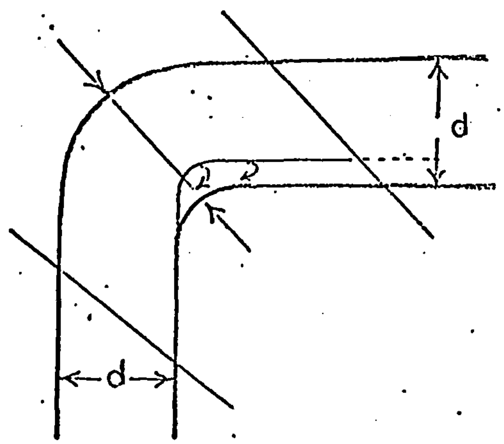

FIG.17 THE LINE OF SEPARATION FOR A 90° BEND

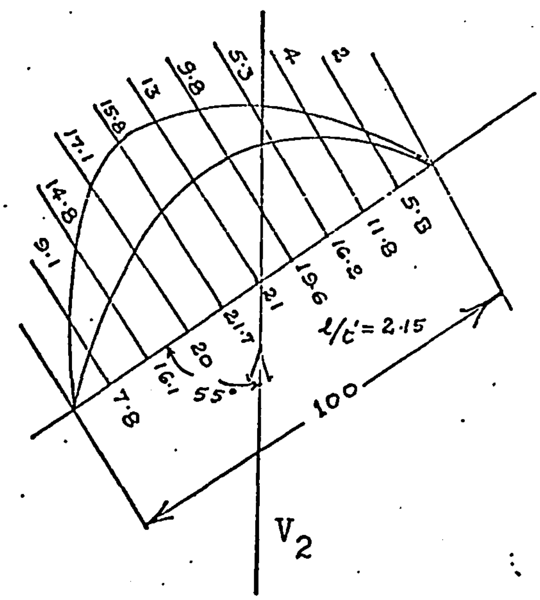

FIG. 18 .DEFLECTING VANES BY SOCIETE RATEAU

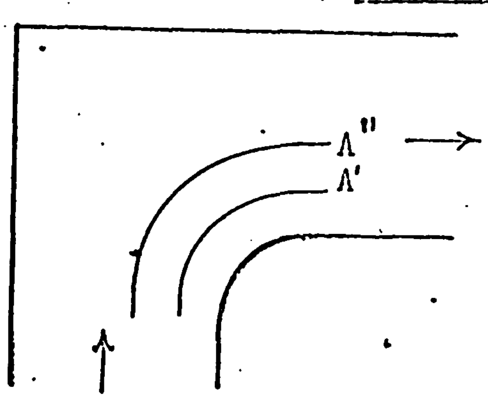

FIG.19 . ROUNDING THE INNER CORNER WITH AN ARC OF A CIRCLE

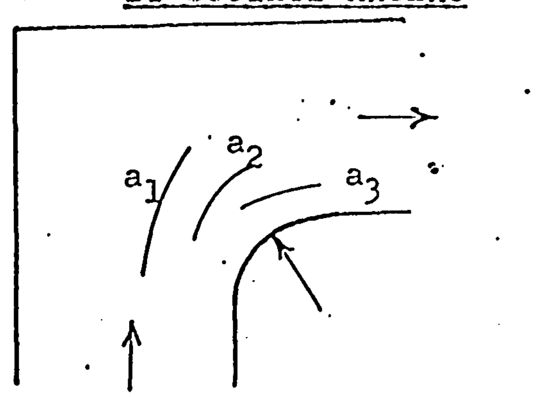

FIG. 20. ROUNDING THE INNER CORNER WITH AN ARC OF A CIRCLE ALONG WITH INTERNAL VANES

THE SHAPE OF THE INNER CURVED WALL

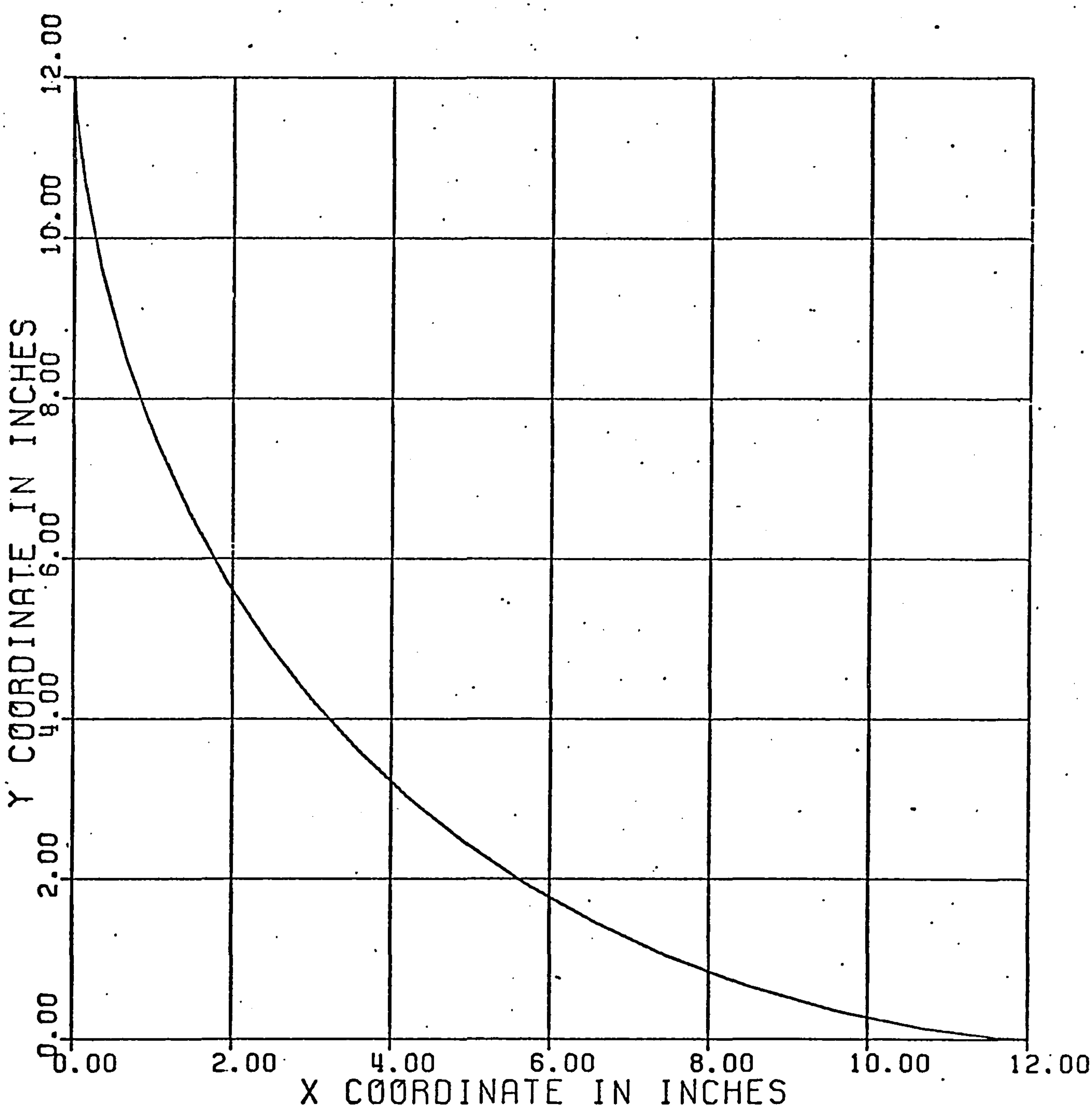

FIG. 21

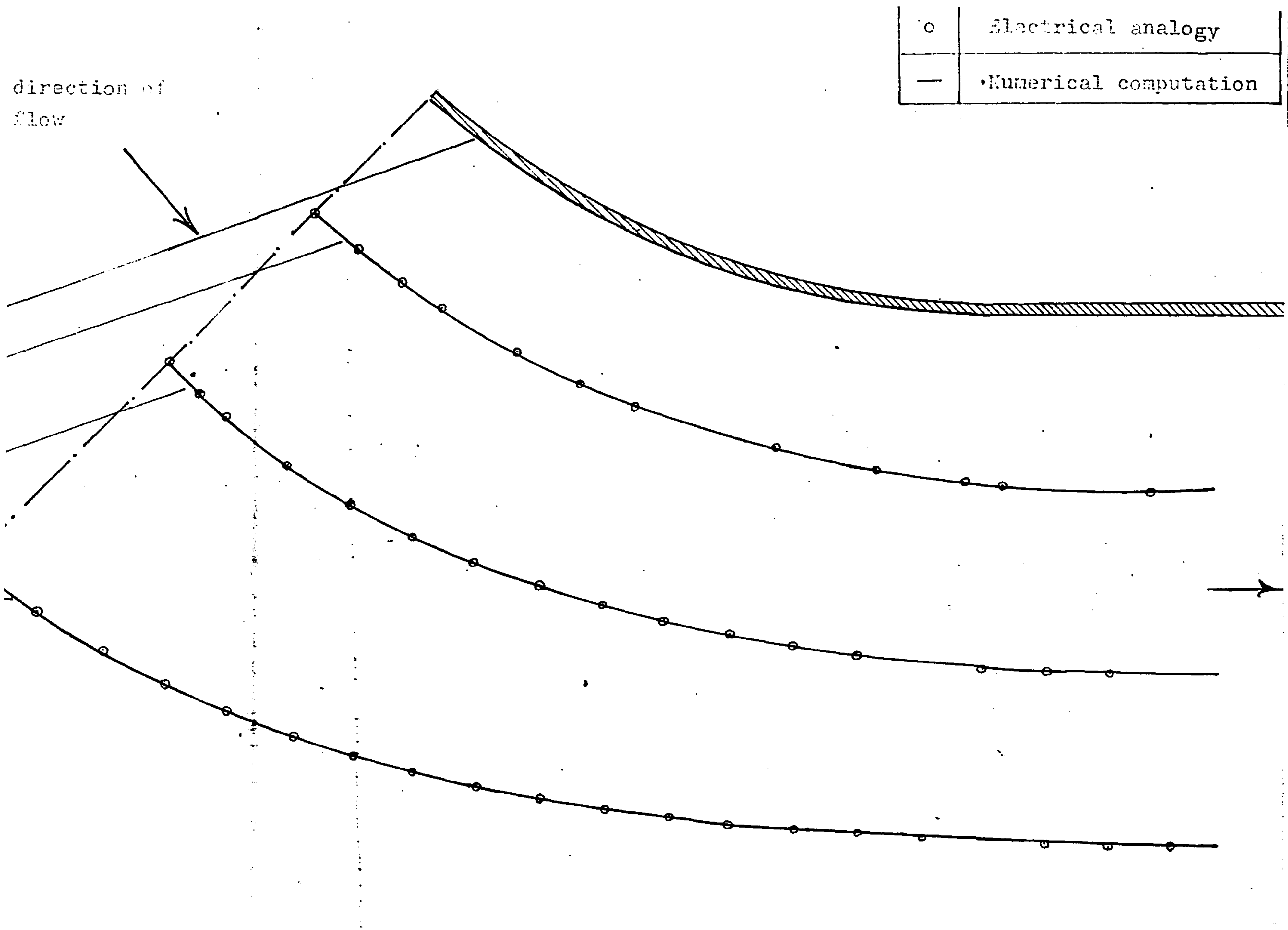

o Electrical analogy
— Numerical computation
direction of flow

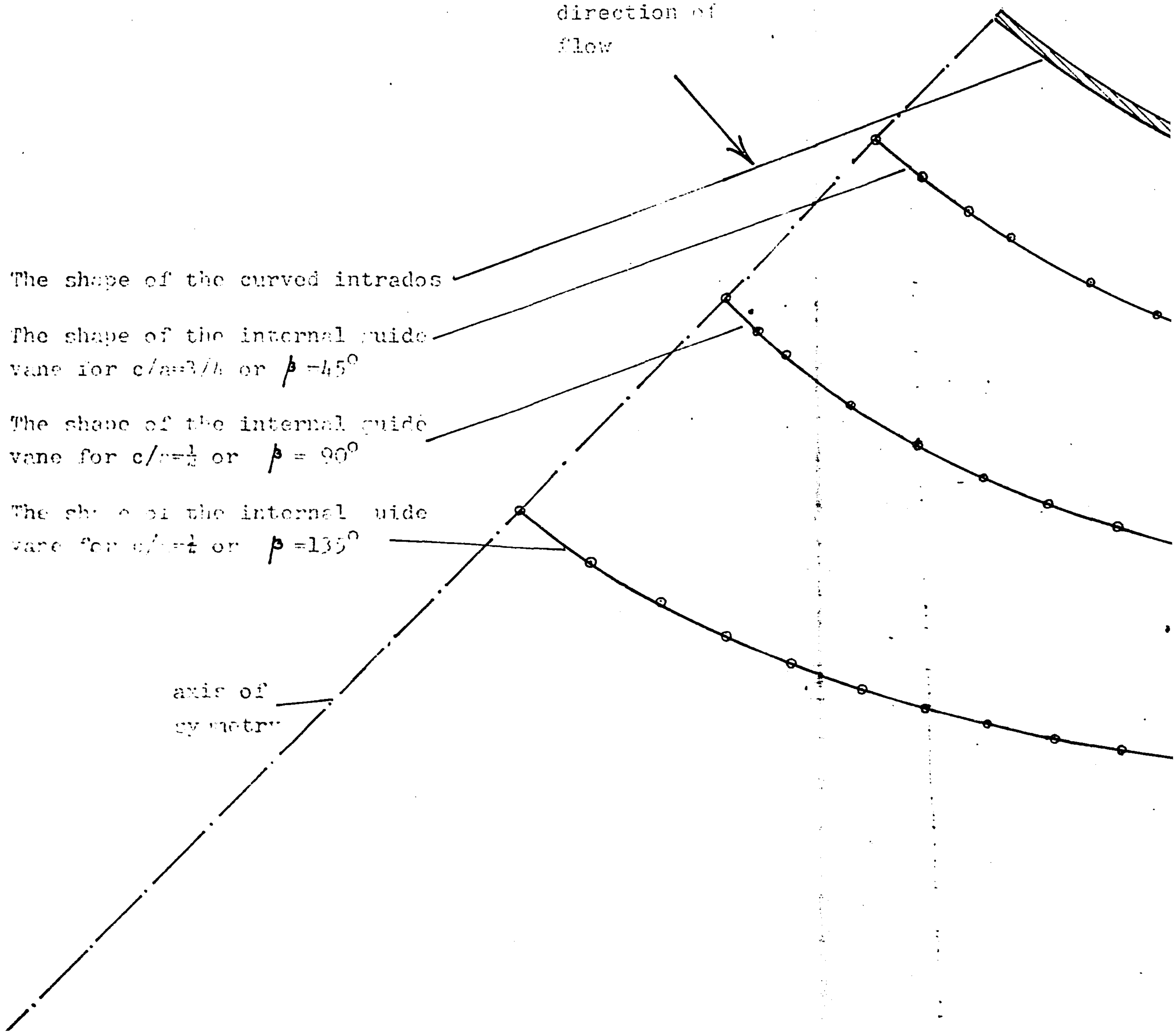
direction of flow
The shape of the curved intrados
The shape of the internal guide vane for c/a=3/4 or β =45°
The shape of the internal guide vane for c/a=½ or β = 90°
The shape of the internal guide vane for c/a=¼ or β =135°
axis of symmetry

INNER CURVED WALL WITH INTERNAL GUIDE VANES
VISUALIZATION OF FLOW BREAKAWAY USING
CONDENSED MILK

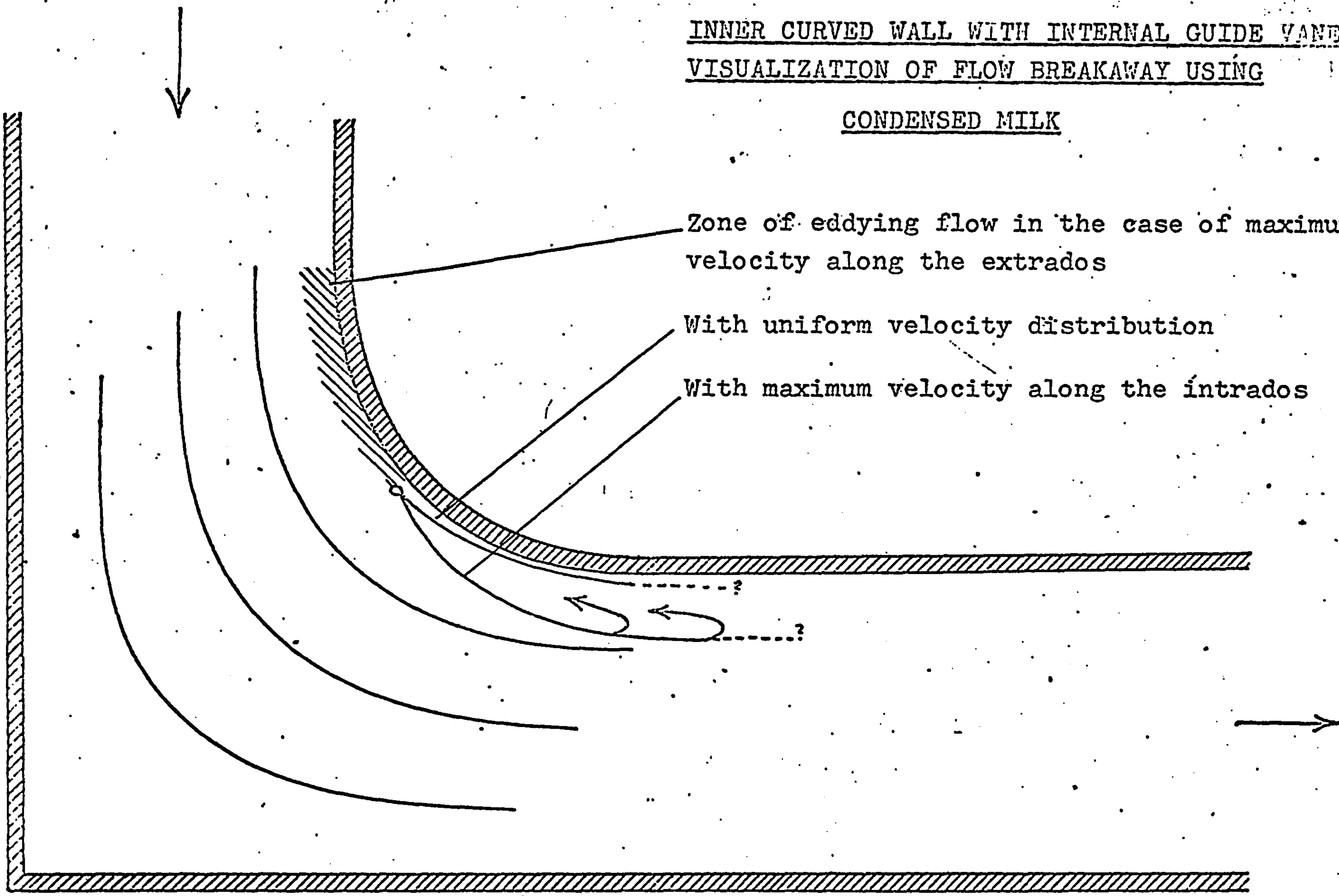

Fig. 23

INNER CURVED WALL ALONE

VISUALIZATION OF FLOW BREAKAWAY USING CONDENSED MILK

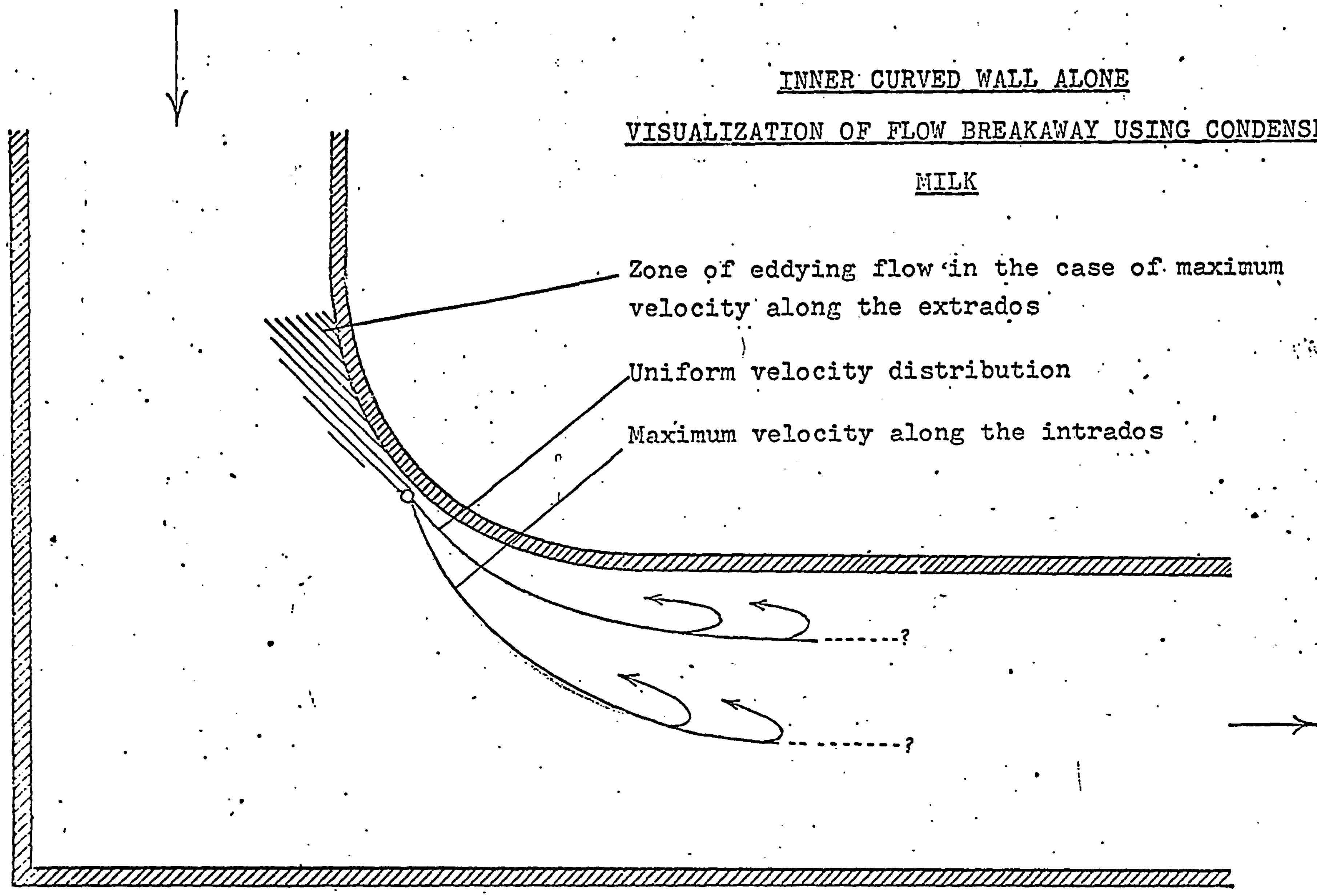

Fig. 24.

RIGHT ANGLED MITRE BEND

VISUALIZATION OF FLOW BREAKAWAY USING

CONDENSED MILK

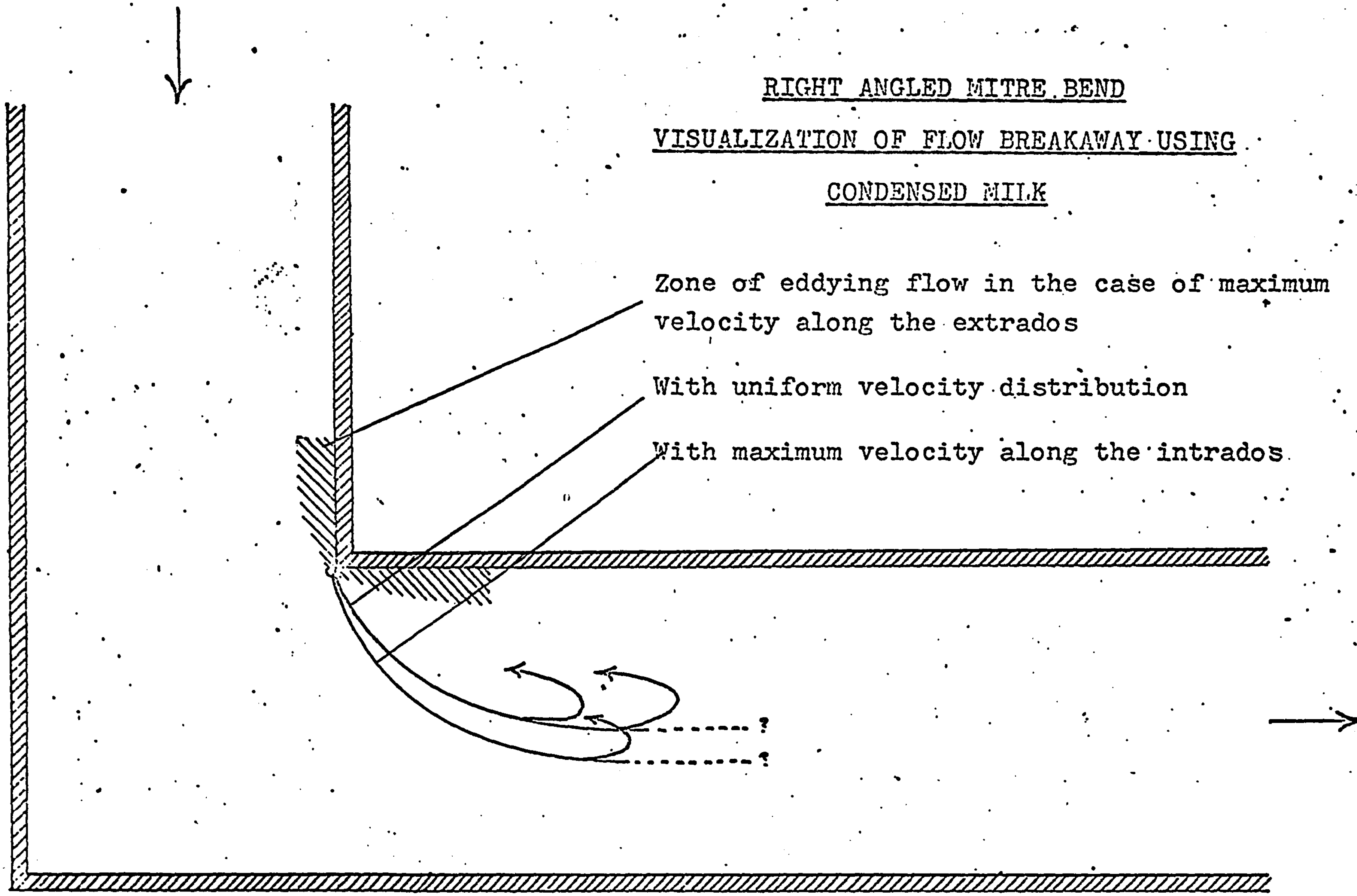

Fig. 25.

MEASUREMENT OF VELOCITY IN THE MITRE BEND(WITH MAXIMUM

VELOCITY ALONG INTRADOS

(i) In the vertical portion of the duct

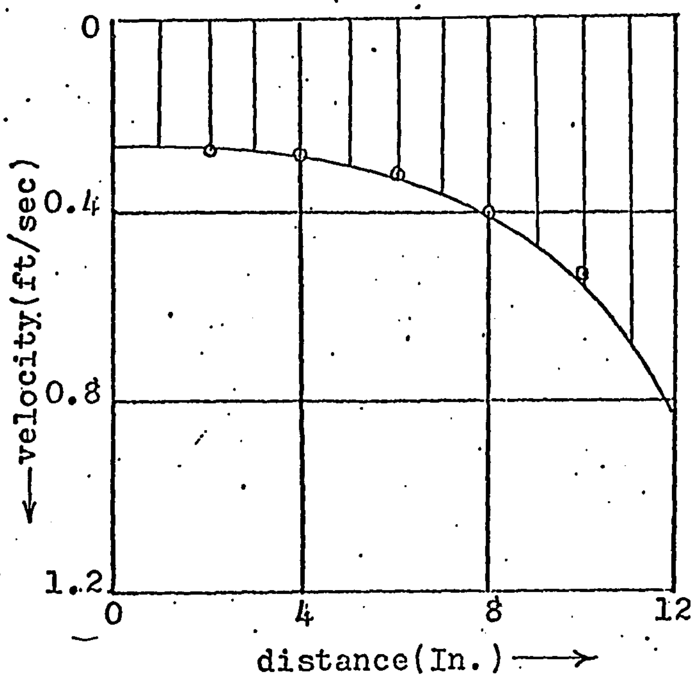

discharge=0.39cfs

(ii) In the horizontal portion of the duct

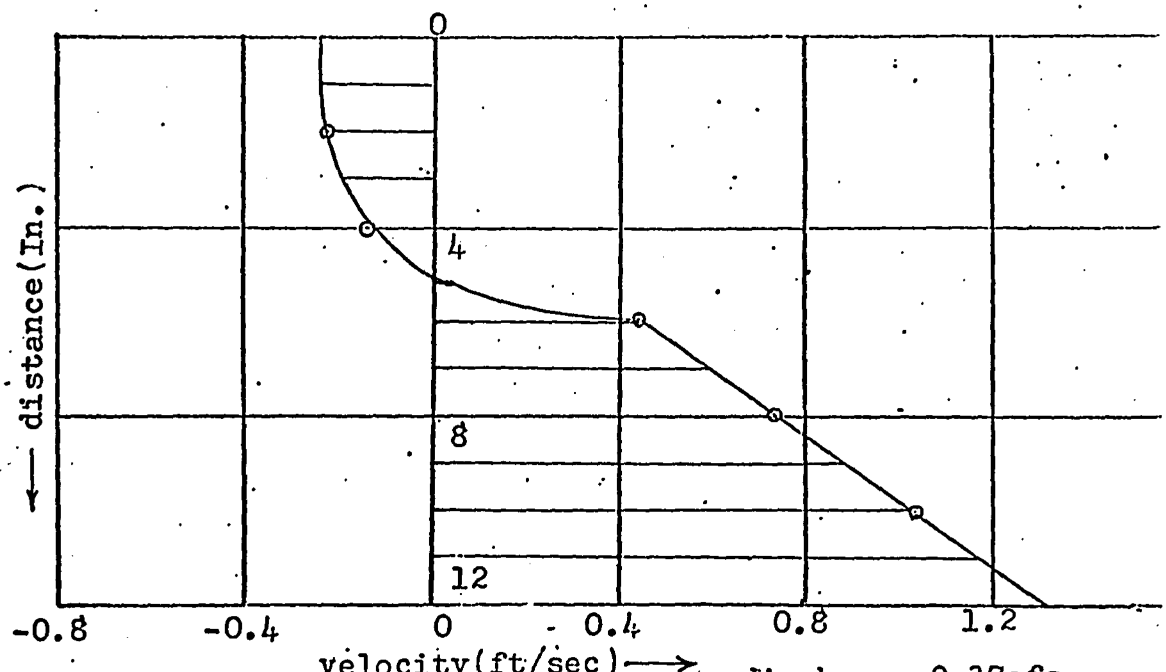

discharge=0.37cfs.

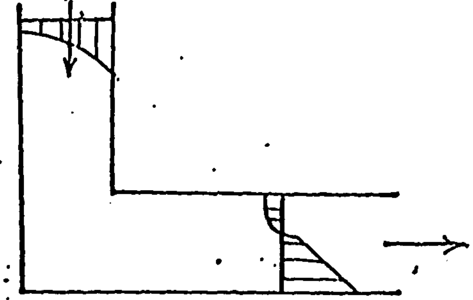

FIG. 26.

MEASUREMENT OF VELOCITY IN THE MITRE BEND (MAXIMUM

VELOCITY ALONG EXTRADOS

(i) In the vertical portion of the duct

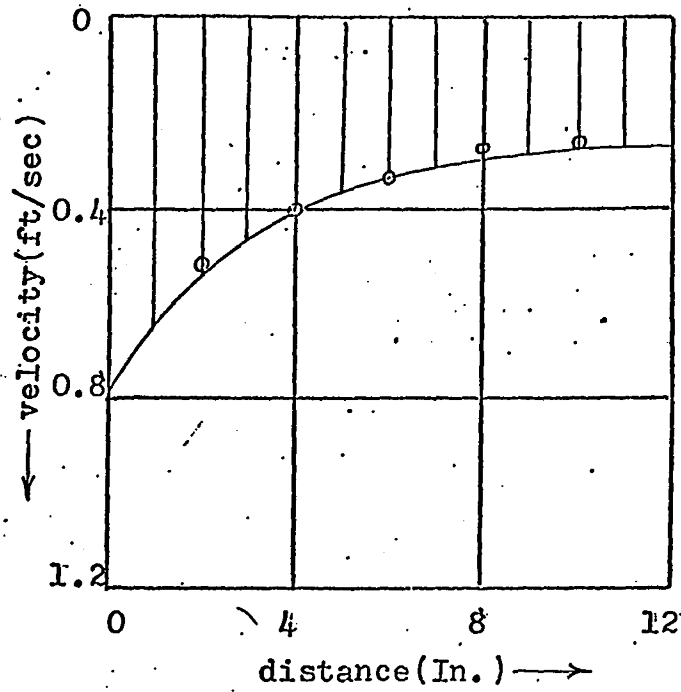

discharge=0.38cfs

(ii) In the horizontal portion of the duct

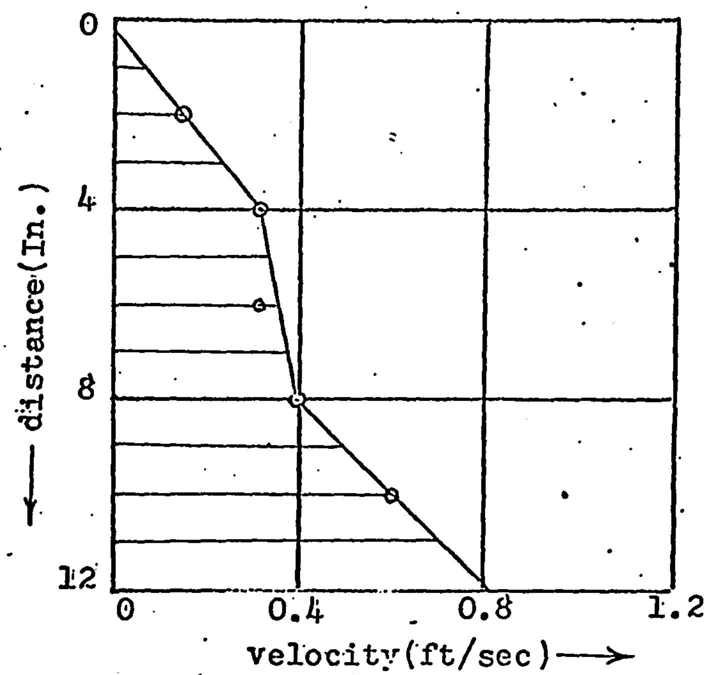

discharge=0.37cfs

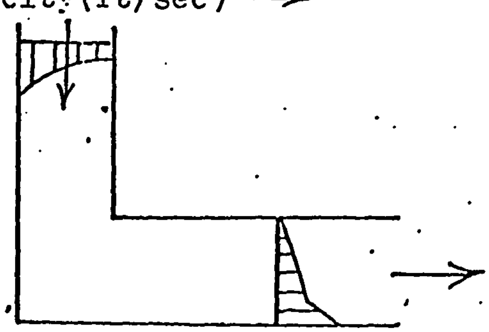

FIG. 27.

MEASUREMENT OF VELOCITY IN THE MITRE BEND WITH

UNIFORM VELOCITY DISTRIBUTION

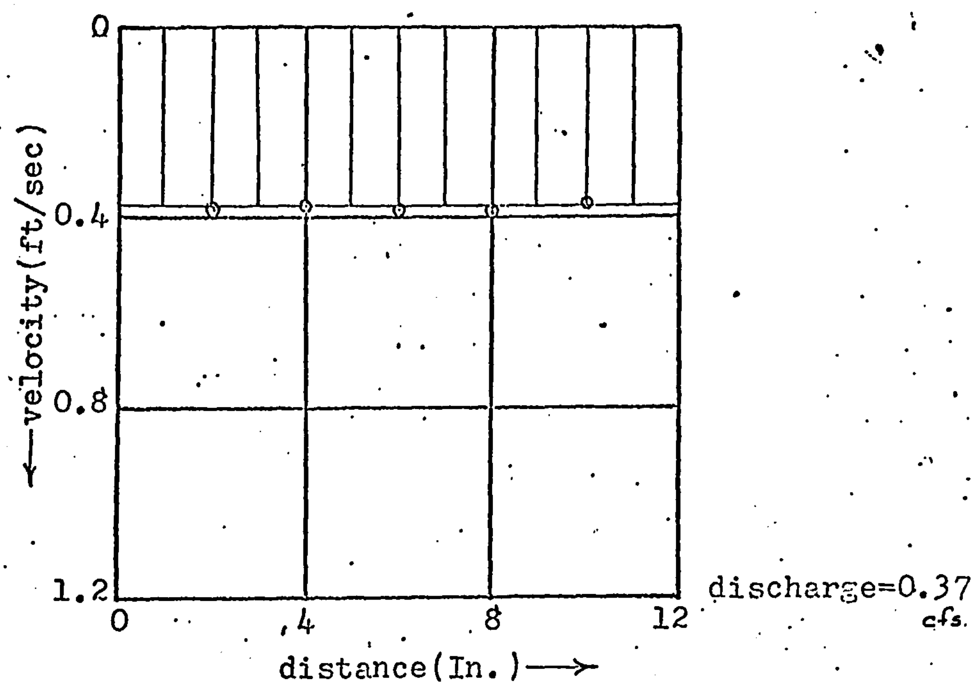

(ii) In the horizontal portion of the duct

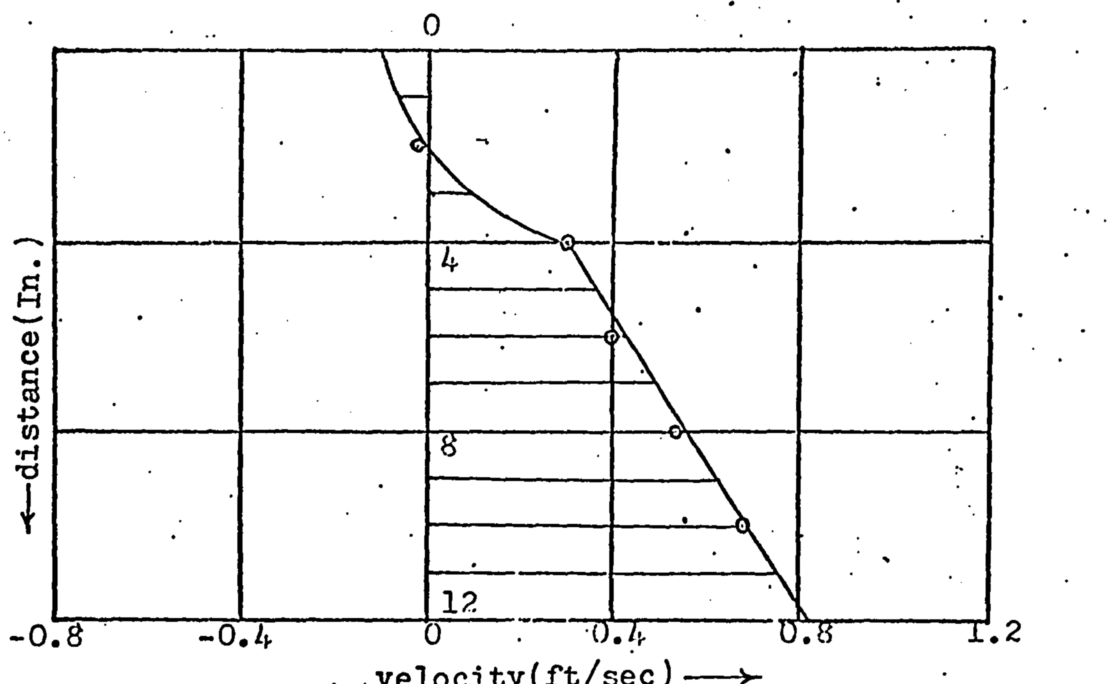

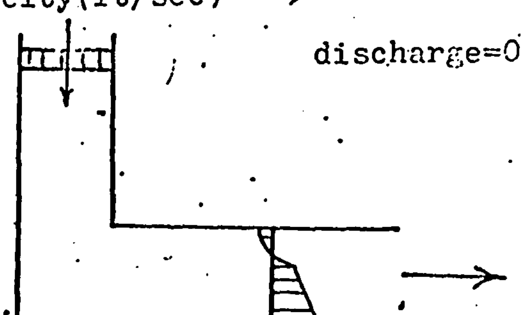

FIG.28.

MEASUREMENT OF VELOCITY WITH CURVED INTRADOS(WITH MAXIMUM VELOCITY ALONG INTRADOS)

(i) In the vertical portion of the duct

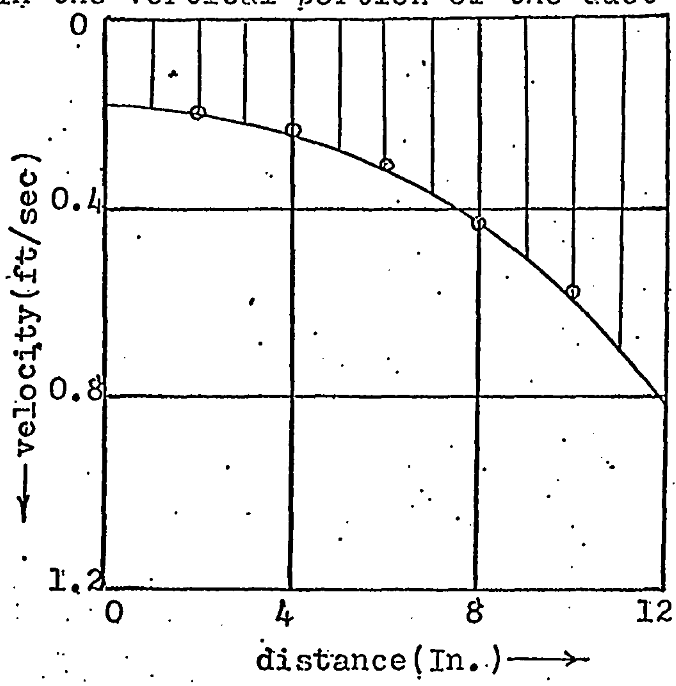

discharge=0.37cfs.

(ii) In the horizontal portion of the duct

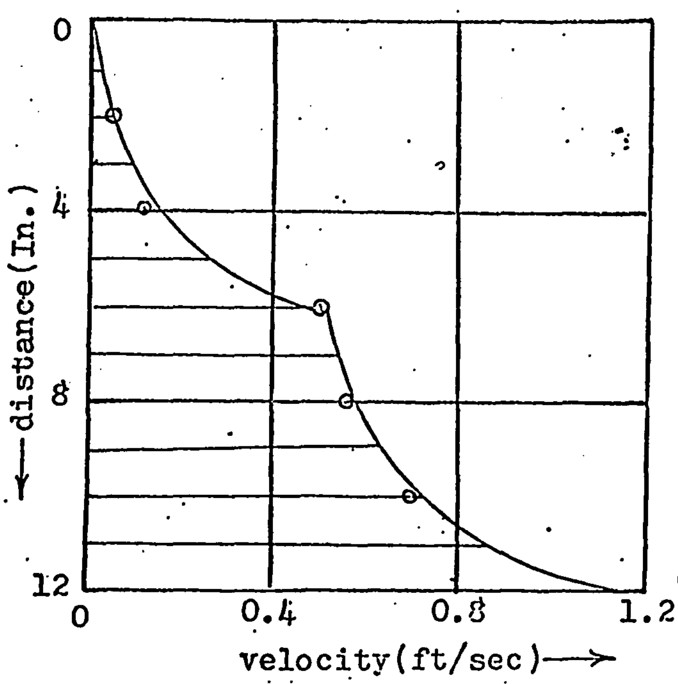

discharge=0.39cfs

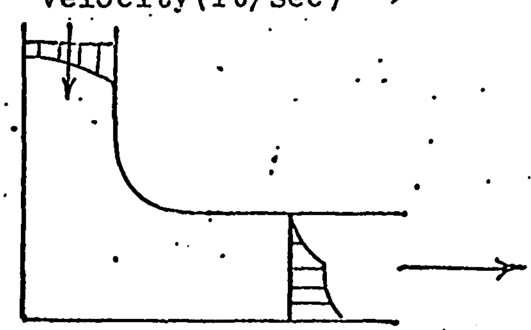

FIG.29.

MEASUREMENT OF VELOCITY WITH CURVED INTRADOS AND WITH

MAXIMUM VELOCITY ALONG THE EXTRADOS

(i) In the vertical portion of the duct

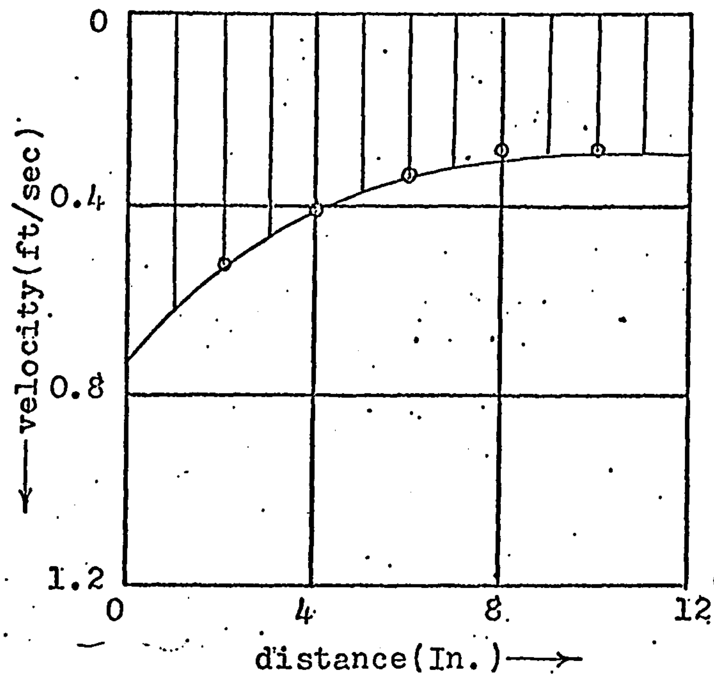

discharge=0.39cfs

(ii) In the horizontal portion of the duct

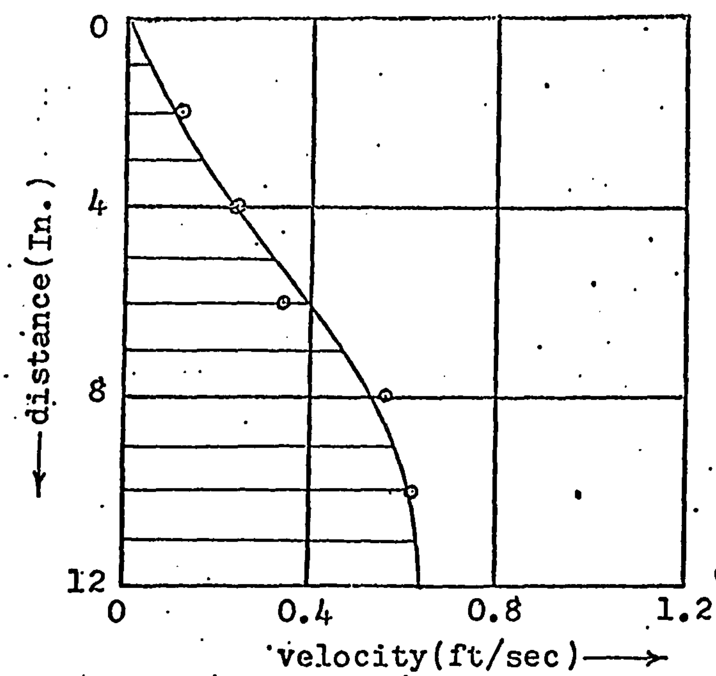

discharge=0.37cfs

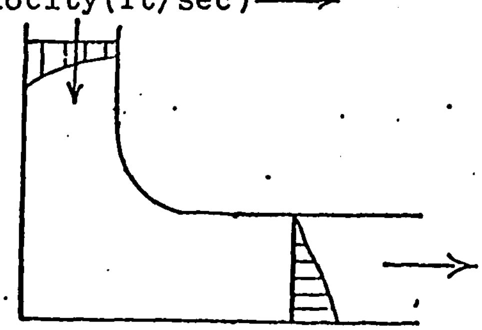

FIG.30.

MEASUREMENT OF VELOCITY WITH CURVED INTRADOS AND WITH UNIFORM VELOCITY DISTRIBUTION

(i) In the vertical portion of the duct

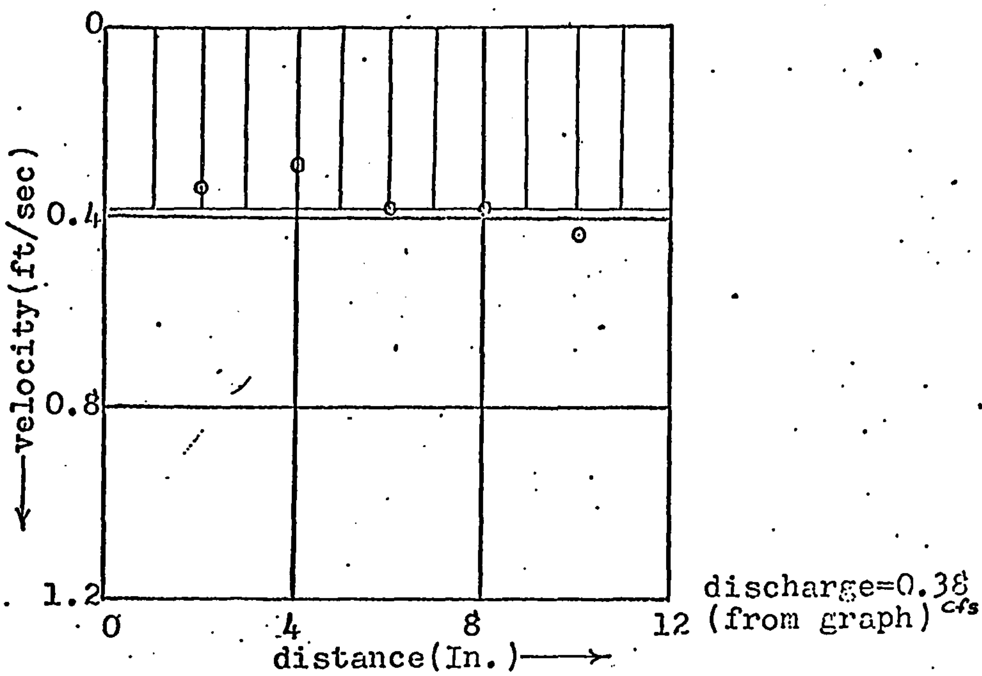

(ii) In the horizontal portion of the duct

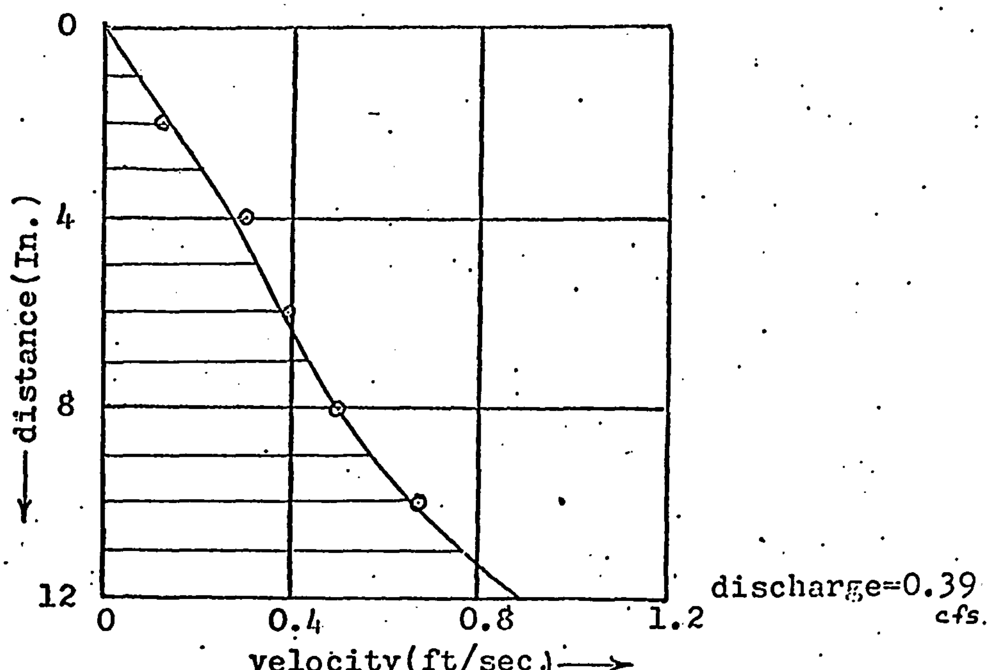

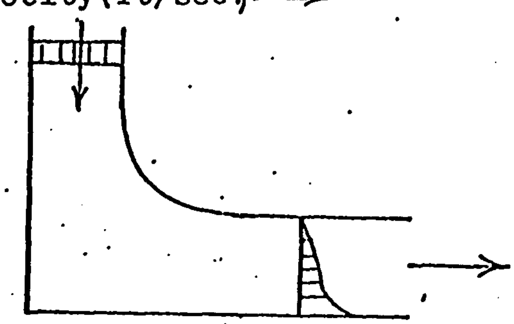

FIG.31.

MEASUREMENT OF VELOCITY WITH INTERNAL GUIDE VANES AND INNER CURVED WALL. (MAXIMUM VELOCITY ALONG INTRADOS)

(i.) In the vertical portion of the duct

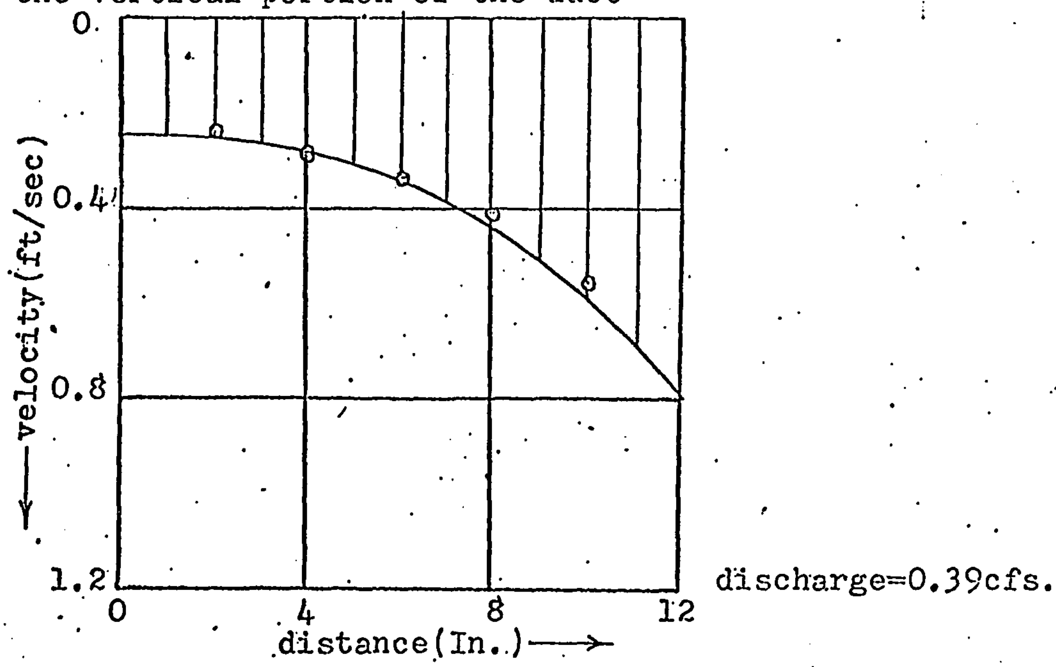

(ii) In the horizontal portion of the duct

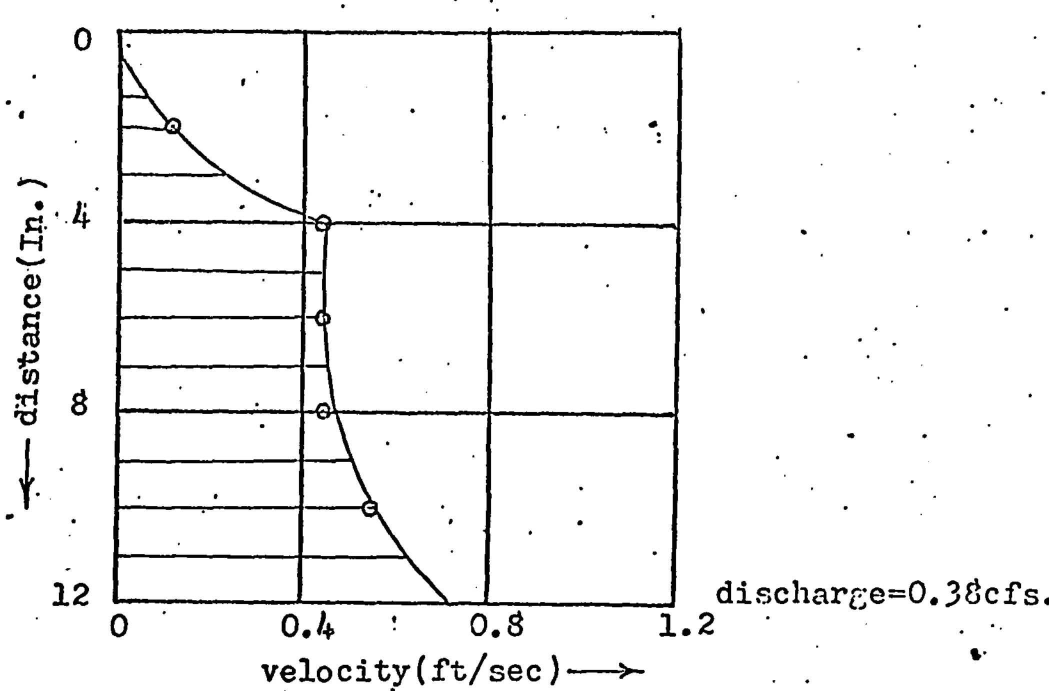

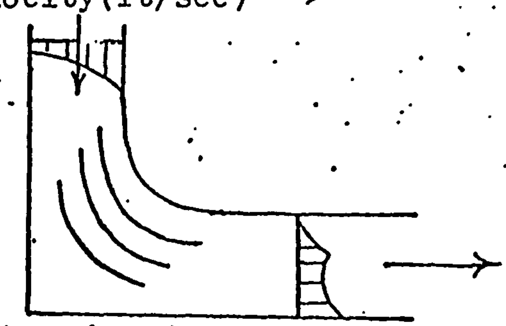

FIG.32.

MEASUREMENT OF VELOCITY WITH INTERNAL GUIDE VANES & INNER CURVED WALL. (MAXIMUM VELOCITY ALONG EXTRADOS)

(i) In the vertical portion of the duct

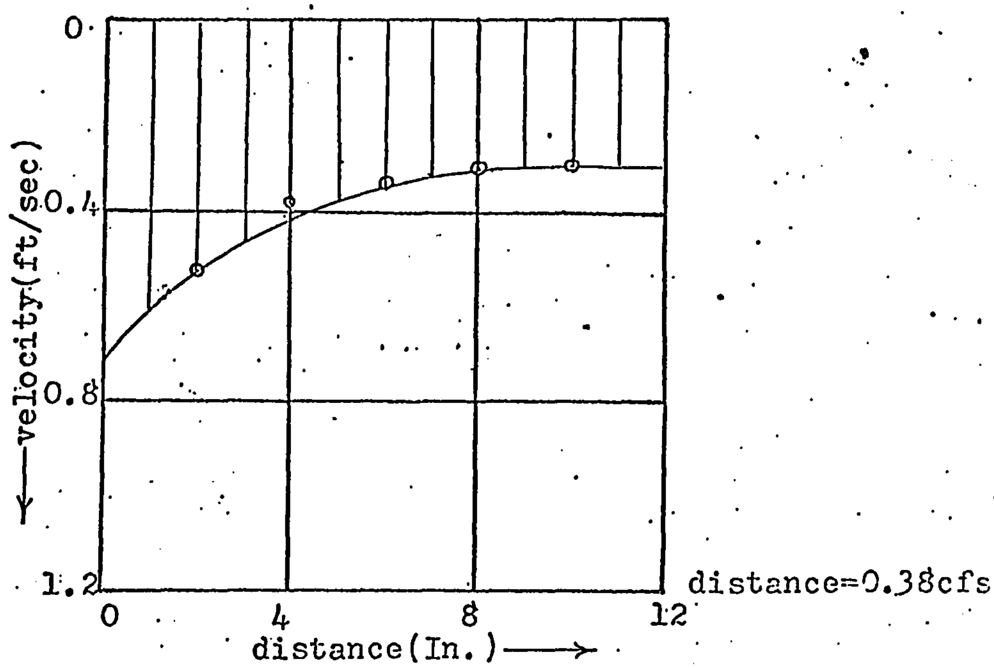

(ii) In the horizontal portion of the duct

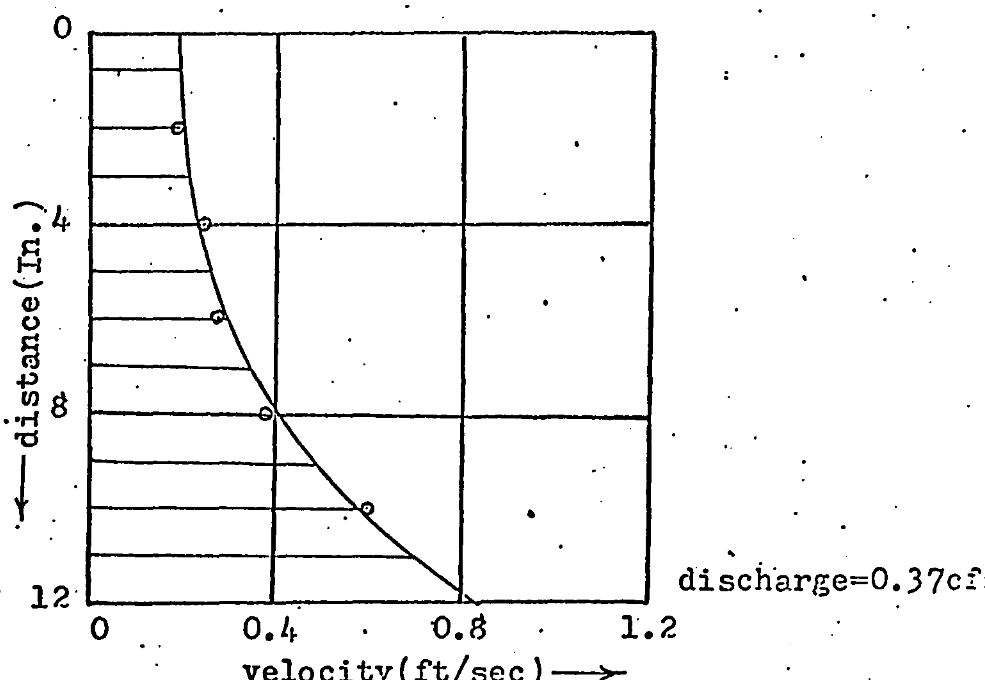

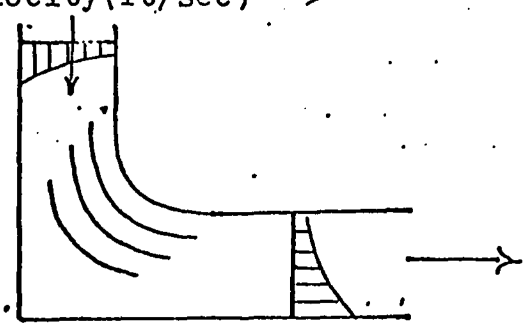

FIG.3.3.

MEASUREMENT OF VELOCITY WITH INTERNAL GUIDE VANES AND INNER CURVED WALL(UNIFORM VELOCITY DISTRIBUTION)

(i) In the verical portion of the duct

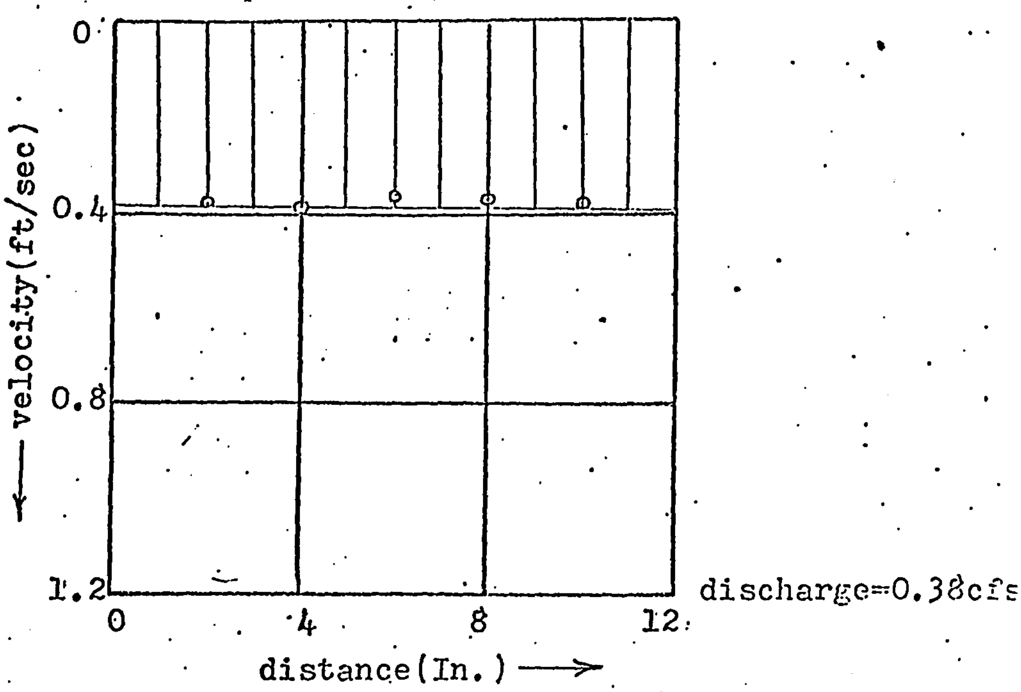

(ii) In the horizontal portion of the duct

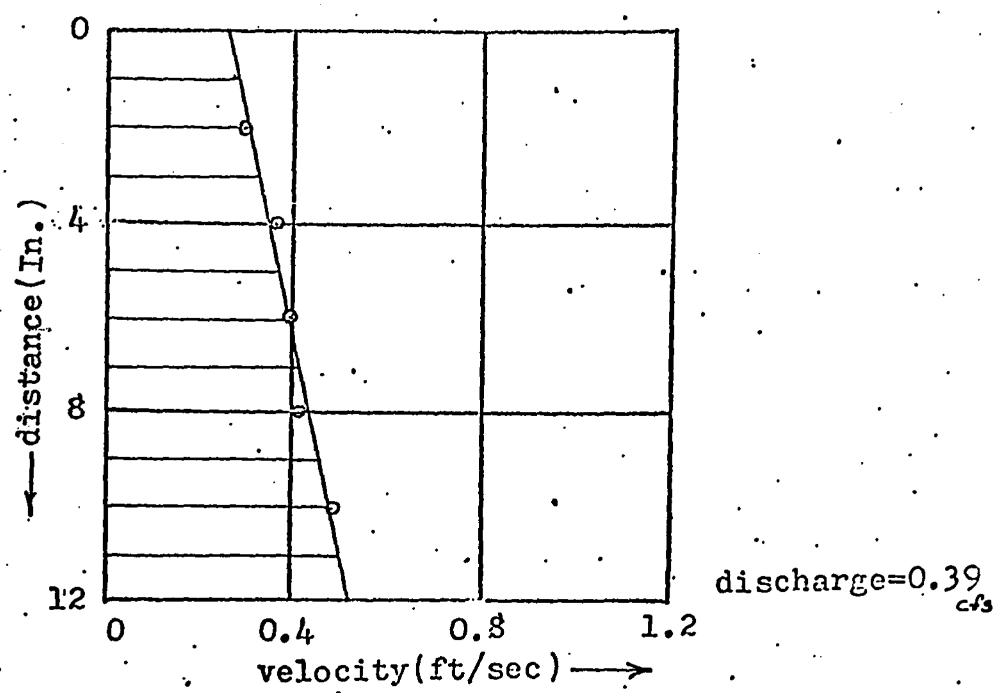

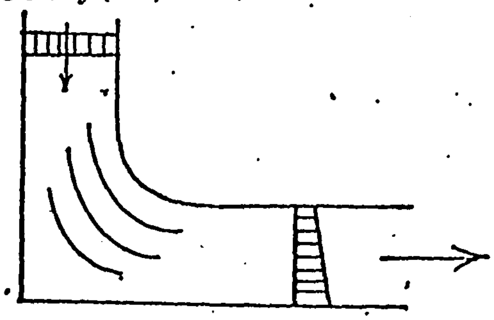

FIG.34.